EFFECT OF FINES AND GROUND ACCELERATION ON LIQUEFACTION RESISTANCE OF SILTY SAND: NUMERICAL STUDY

A Thesis Submitted to
the Graduate School of Engineering and Sciences of
İzmir Institute of Technology
in Partial Fulfillment of the Requirements for the Degree of

MASTER OF SCIENCE

in Civil Engineering

by
Batuhan TOZBURUN

June 2022
İzmir

ACKNOWLEDGMENTS

First, I would be grateful to my supervisor, Prof. Dr. Nurhan Ecemiş for her invaluable supervision, guidance, knowledge, and care throughout my thesis study and her scientific support during my thesis study.

I would like to thank the members of my dissertation committee; Asst. Prof. Volkan Isbuga, and Prof. Dr. Mehmet Murat Monkul for their attendance at my thesis defense seminar and for giving valuable suggestions and farsighted ideas for my thesis.

Finally, thanks to my family for their patience and their support. I could not have come to this point without my family that are Seyit Tozburun, Güler Tozburun and Serhat Tozburun. This thesis is dedicated to all of them. Mainly, I dedicate my thesis to my brother, Oğuzhan Tozburun, and his friends, who passed away at an early age.

ABSTRACT

EFFECT OF FINES AND GROUND ACCELERATION ON LIQUEFACTION RESISTANCE OF SILTY SAND: NUMERICAL STUDY

Liquefaction is a phenomenon that damages structures that have not been adequately studied during the design process. While improving the performance of the buildings under dynamic loading conditions, it is essential to evaluate the liquefaction behavior of soils under the dynamic load. In this thesis, the constitutive soil model (UBCSand Model), which can simulate liquefaction, is used within the finite difference methods (FDM). First, results are compared with the laboratory test results to verify numerical liquefaction simulations. The physical and mechanical tests performed at Izmir Institute of Technology (IZTECH) are used as an input for the soil model. Then, a series of constant volume cyclic direct simple shear results (CDSS) tests performed for the same silty sands were used to verify the numerical study (Tutuncu, 2021 and Monkul, 2021). CDSS tests were performed on mixtures of clean sands and three non-plastic silts at different contents of 0%, 5%, 15%, and 35% allowing for observing the liquefaction response of silty sands of different grades (Monkul, 2021). The laboratory tests performed at Yeditepe University and Izmir Institute of Technology were combined to study the effect of fines content and relative density on cyclic liquefaction resistance of silty sands. The aim of this thesis is to perform a numerical model to evaluate the effect of fines content (FC), ground acceleration (a_{max}) and relative density (D_r) on liquefaction resistance. The FDM model gives similar results to laboratory test results. Hence, the model can be used to assess the liquefaction with different soil models and conditions

ÖZET

SİLTLİ KUMLARDA YER İVMESİNİN VE İNCE DANENİN SIVILAŞMA DİRENCİNE ETKİSİ: SAYISAL ÇALIŞMA

Sıvılaşma, tasarım sürecinde yeterince çalışılmamış yapılara zarar veren bir olgudur. Binaların dinamik yükleme koşulları altında performansını iyileştirirken, dinamik yük altında zeminlerin sıvılaşma davranışlarının değerlendirilmesi esastır. Bu tezde, sıvılaşmayı simüle edebilen kurucu zemin modeli (UBCSand Model), sonlu farklar yöntemleri (FDM) içerisinde kullanılmaktadır. İlk olarak, sayısal sıvılaşma simülasyonlarını doğrulamak için sonuçlar laboratuvar test sonuçlarıyla karşılaştırılır. Zemin modeli için girdi olarak İzmir Yüksek Teknoloji Enstitüsü'nde (IYTE) yapılan fiziksel ve mekanik testler kullanılmıştır. Daha sonra, sayısal çalışmayı doğrulamak için aynı siltli kumlar için gerçekleştirilen bir dizi sabit hacimli çevrimsel doğrudan basit kesme sonuçları (CDSS) testleri kullanılmıştır (Tutuncu, 2021 ve Monkul, 2021). CDSS testleri, farklı derecelerdeki siltli kumların sıvılaşma tepkisini gözlemlemek için 0%, 5%, 15% ve 35% lik farklı içeriklerde temiz kum ve üç plastik olmayan silt karışımları üzerinde gerçekleştirilmiştir (Monkul, 2021). Yeditepe Üniversitesi ve İzmir Yüksek Teknoloji Enstitüsü'nde gerçekleştirilen laboratuvar testleri, ince tane içeriğinin ve bağıl yoğunluğun siltli kumların döngüsel sıvılaşma direnci üzerindeki etkisini incelemek için birleştirildi. Bu tezin amacı, ince tane içeriğinin (FC), yer ivmesinin (a_{max}) ve bağıl yoğunluğun (D_r) sıvılaşma direnci üzerindeki etkisini değerlendirmek için sayısal bir model gerçekleştirmektir. FDM modeli, laboratuvar test sonuçlarına benzer sonuçlar verir. Bu nedenle model, farklı zemin modelleri ve koşulları ile sıvılaşmayı değerlendirmek için kullanılabilir.

TABLE OF CONTENTS

LIST OF FIGURES

Figure **Page**

Figure **Page**

Figure **Page**

LIST OF TABLES

Table **Page**

CHAPTER 1

INTRODUCTION

1.1. General

Liquefaction can cause severe damage to structures, such as a loss in the foundation's bearing capacity, tilting, overturning the structures, and settlement problems. According to the Ministry of Land, Infrastructure, Transport and Tourism Japan (MLIT 2015), approximately 27.000 houses were damaged due to liquefaction on the Pacific coast of the Tohoku earthquake in Tokyo (2011). Liquefaction is one of the most significant engineering problems in which the strength and stiffness of the granular saturated soils are rapidly reduced by earthquake load or another type of dynamic load. Liquefaction is first observed after 1964 in Niigata. Researchers and engineers focused on understanding the reasons and conditions for this dangerous phenomenon. Therefore, they did many kinds of research using numerical simulation and experiments.

In this thesis, the liquefaction triggering conditions were evaluated using the software program FLAC-2D (Two Dimensional-Fast Lagrangian Analyses of Continua). Soils with different FC are modeled with the UBCSand model in FLAC-2D (ITASCA, FLAC Basics 2015). UBCSand Model is an effective stress plasticity model for advanced stress-deformation analyses of geotechnical structures and problems (UBCSand, 2011). The model was developed primarily for soils with potential liquefaction under dynamic loads.

Pore Water Pressure (PWP), Pore Water Pressure ratio (r_u), Y-Displacement (Y_{disp}), Shear Stress (τ), Shear Strain (γ), Cyclic Stress Ratio (CSR), and Number Cycles to Liquefaction (N_L) are determined with different soil properties and maximum acceleration levels in FLAC-2D. The liquefaction phenomenon is compared with different FC, D_r, and amax with the UBCSand model in FLAC-2D.

1.2. Problem Statement and Scope of the Study

In the past decades, engineers and researchers tried to understand conditions that cause liquefaction. Therefore, they did many kinds of research, including numerical studies and laboratory experiments on the liquefaction phenomenon. Several liquefaction approaches have been developed to evaluate the liquefaction. They include the cyclic stress approach (Seed and Idriss 1971, Seed et al. 1983), the cyclic strain approach (e.g., Dobry et al. 1982), the Arias intensity approach (Kayen and Mitchell 1997), the energy-based approach for sands (Nemat-Nasser and Shokooh 1979), and others. This thesis aims to investigate the liquefaction phenomenon at different FC and D_r . Pore Water Pressure (PWP), Pore Water Pressure ratio (r_u), Vertical Displacement (Y_{disp}), Shear Stress (τ), Shear Strain (γ), Cyclic Stress Ratio (CSR), Number Cycles to Liquefaction (N_L), Cyclic Resistance Ratio (CRR) results are determined liquefaction phenomenon in different conditions. In this thesis, the commercially available finite difference program FLAC-2D is used. FLAC is 2D numerical modeling software for advanced geotechnical analysis of soil, rock, groundwater, and ground support.

1.3. Organization of the Thesis

The thesis consists of seven chapters.

Chapter 1 represents a summary of this thesis. The contents of the study are put in order below.

Chapter 2 presents a literature review of fine content, ground acceleration effects and relative density effect of liquefaction phenomena.

Chapter 3 presents detailed information about numerical analysis of liquefaction phenomena. This chapter mentioned the background of the FDM method, model geometry, boundary conditions, and constitutive materials (Mohr-Coulomb and UBCSand model) used in the model.

Chapters 4 present a study of FLAC-2D model simulations. Detailed information about the numeric model is given in this chapter. Also, dynamic analysis results are mentioned.

Chapter 5 presents the conclusion of the study. In this chapter summary of the results and suggestions for future research are given.

At the end of these seven chapters, a list of references was given.

CHAPTER 2

FINE CONTENT AND ACCELERATION EFFECT ON LIQUEFACTION RESISTANCE

2.1. Introduction

The liquefaction potential is even more significant in saturated loose sand and silty sands. Many laboratory studies have been conducted to investigate the effect of fine grain (silt) content on the liquefaction resistance of soils. Moreover, determination methods are essential for estimating the initial state of the grain structure or the history of soil periodic loading and ground acceleration. This chapter includes a literature review of two main concepts: the effect of fines content and ground acceleration on liquefaction resistance.

2.2. Effect of Fines Content on Liquefaction Resistance

Many laboratory studies have been conducted to investigate the effect of fine grain (silt) content on the liquefaction resistance of soils. Recently, significant studies have been carried out on the factors affecting silty sands' liquefaction susceptibility, such as fine-grain content and ground acceleration (Bray, J. D, 2004, Arab, A., Belkhatir, 2012, Yassine, B., 2014, Bın Ye, 2007). Most earlier studies on the liquefaction phenomenon were on sands, and fine-grained soils such as silts, clayey silts, and even sands with fines were considered non-liquefiable. Ueng et al. (2010) used a biaxial laminar shear box mounted on a shaking table to study the settlements in saturated clean deposits of sand and related the volumetric strain in liquefied sand to the relative density for various shaking durations and earthquake magnitudes. Xenaki and Athanasopoulos, (2003) reported that sand's liquefaction resistance decreased with the fine grain content.

However, Dash and Sitharam, 2009 stated that the liquefaction resistance increases up to about 5% silt content at constant Dr, followed by a sharp decrease up to the boundary silt content, after which there is a constant resistance. Hazirbaba, K., Rathje,

E. M., (2009) and Carraro, J. A. H., Prezzi, M., Salgado, (2009) stated the liquefaction and post-liquefaction shear strength of soils decreased up to a certain fine content and then increased. With such relationships, it may be possible to evaluate the liquefaction trigger on a performance basis. Polito (2001) reported that the threshold silt content value of non-plastic silt sand mixtures ranged from $25<FC_{thr}<45$.

Figure 2.1. shows the CSR and N results with the different fine content soil. Based on the literature review, significant criteria which were applied to the study of liquefaction susceptibility considering fine content are Boulanger and Idriss (2006), Chinese Criteria, Andrews and Martin (2000) criteria, Polito (2001) criteria, Seed et al. (2003) criteria, Bray et al. (2004) criteria and Bray and Sancio (2006). Most studies on the liquefaction phenomenon were on sands, and fine content soils such as silts, silty sand, and even sands with fines were considered liquefiable. The liquefaction of soils under earthquake loadings (cyclic loading) has always been the main concern for geotechnical engineering practices.

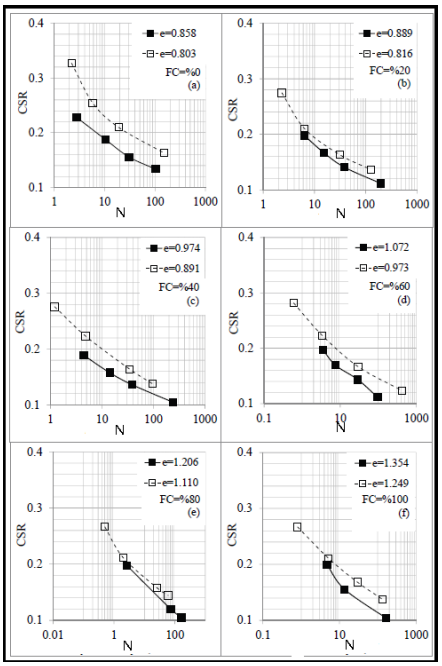

Figure 2.1. CSR-N Results with different Fine Content

(Source: Karakan, 2016)

Thus, liquefaction resistance and shear wave velocity were measured in the same laboratory samples, and then the data from this study were transferred to the field along with other available data and compared with the field performance curves proposed in

Figure 2.2. CSR is used to evaluate the seismic demand of a soil layer. It is given by (Seed and Idriss 1971);

$$CSR = \frac{\tau_{ave}}{\sigma'_{vo}} = 0.65 \frac{a_{max}}{g} \frac{\sigma_{vo}}{\sigma'_{vo}} r_d \quad (2.1)$$

Where CSR = cyclic stress ratio, τ_{ave} = average cyclic shear stress, a_{max} = peak horizontal acceleration at the ground surface, σ_{vo}' = initial vertical effective stress at depth D, σ_{vo} = initial vertical total stress at depth D, g = acceleration of gravity, and r_d = stress reduction coefficient depending on the depth (Youd and Idriss 1984).

$$r_d = \frac{(1 - 0.4113D^{0.5} + 0.04052D + 0.001753D^{1.5})}{1 - 0.4177D^{0.5} + 0.05729D - 0.006205D^{1.5} + 0.001210D^2)} \quad (2.2)$$

The relation between stress reduction coefficient (r_d) and depth is shown in Figure 2.2.

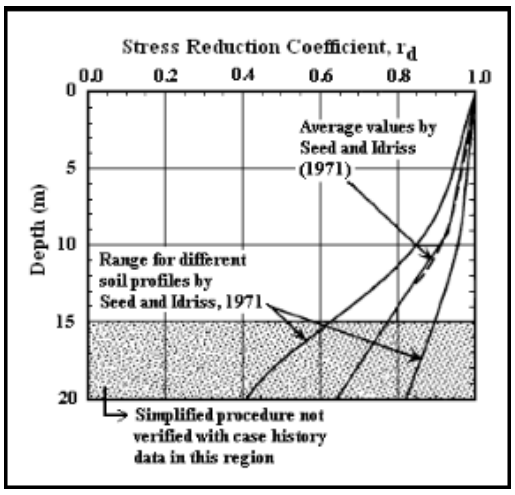

Figure 2.2. Depth and Stress Reduction Coefficient

(Source: Kramer,1996)

SPT, CPT or geophysical tests like measuring shear velocity are used to obtain strength results of soil. They are used to evaluate the soil with CSR. Cyclic triaxial and resonance column tests were performed on reconstituted samples of clean sand and sand-

silt mixtures prepared at different densities (Ning Liu et al., 2000, Huang et al., 2004). Capacity is the soil's resistance to liquefaction. The factor of safety is calculated as the capacity divided by the requisition. (According to Eurocode 8-98. FS > 1.25 and TBDY (Turkish Building Earthquake Regulation) FS>1.10) It can be obtained by using laboratory experiments or field tests. These tests are, respectively, the standard penetration test (SPT), cone penetration test (CPT), and shear wave velocity (Vs) test. The SPT was first used to develop liquefaction correlations and was the widespread in application up to the 1990s. CRR expresses the calculation of soil potential to liquefaction phenomenon.

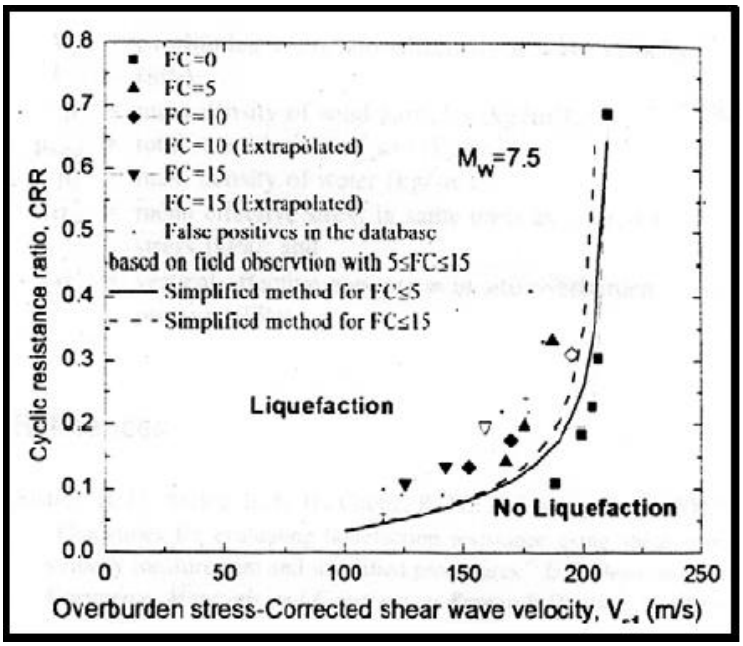

Figure 2. 3. Comparison of the CRRfield-Vs1 correlations developed in the laboratory with the field-based correlations (Source: Andrus and Stokoe, 2000)

The loosest possible density after deposition is a commonly used comparison basis for assessing the influence of fines content on the liquefaction potential of sands (Kuerbis et al. 1988; Vaid 1994; Zlatovic and Ishihara 1995; Lade and Yamamuro 1997; Georgiannou 2006; Bahadori et al. 2018). Especially Dr of the specimens formed by the loosest possible density after deposition might also help to explain the observed changes in liquefaction potential due to fines content. Table 2.1. shows the summary of a different literature review from Monkul (2010). Table 2.2. shows the summary of a different numerical study literature review. Issa and Mohsen et al. (2011) reported that liquefaction resistance of sands increases with increasing FC at constant or similar relative density from numerical study. Ali, Aliakbar and Mohsen (2014) performed numerical study for 4 different sands and silty sand in the range of 30-40 FC % and they stated that cyclic resistance ratio of sands decreases with increasing silt content at the same void ratio. Ronert Andrew Jaeger (2012) reported that clean sand has more resistant than silty sands with 10 % FC at the similar relative density from numerical study. silty sand is in the range of 30-40 FC % and liquefaction resistance decreases with increasing FC. Similarly, B.K. Maheshwari (2019) performed numerical study for silty sands 5 and 30 percent FC at the similar relative densities and reported that liquefaction resistance of sands decreases with increasing fines content. G.R Martin (2017) reported that liquefaction resistance of sands decreases with increasing fines content.

Table 2.1. Summary of some of the literature review for liquefaction with different fine content (Source: Monkul, 2010)

Reference No	Type of sand	D50 sand (mm)	Type of fines	Type of testing	Comparison basis	FC Range (%)	Effect of FC on liquefaction resistance or dilatancy
1	Ottawa sand	0,4	Silt	Cyclic triaxial	Same intergranular void ratio	0-20	Increase
2	Brenda mine tailings sand	0,25	Kamloops silt	Undrained triaxial	Similar intergranular void ratio	0-22,3	Increase
3	Ottawa sand	0,39	Crushed silica fines (angular)	Undrained triaxial	Similar initial void ratio	0-40	Increase
4	Ottawa sand	0,39	SilCoSil 106	Drained triaxial	Similar relative density	0-20	Increase
5	Old alluvium sand	0,73	Crushed quartz	Undrained triaxial	Same intergranular void ratio	0-9	Increase
6	Monterey sand	0,48	SilCoSil 52	Cyclic simple shear	Same void ratio, intergranular void ratio, relative density	0-20	Increase
7	Ottawa sand	0,6	SilCoSil 125	Cyclic triaxial	Same void ratio	0-30	Decrease
8	Toyoura sand	0,17	Toyoura silt	Undrained triaxial	Loosest possible density after deposition	0-30	Decrease
9	Nevada sand	0,16	Nevada fines	Undrained triaxial	Loosest possible density after deposition	0-30	Decrease
10	Ottawa sand	0,2-0,25	Kaolin silt	Undrained triaxial	Same void ratio	0-50 & 0-27	Decrease
11	Monterey sand	0,43-0,18	Yatesville silt	Cyclic triaxial	Relative density	0-40	Decrease (Depending on relative density)
12	Ham River sand	0,27	HPF-4 silt	Undrained triaxial	Loosest possible density after deposition	0-2,5	Increase
13	Ottawa sand	0,39	Silt-size mica SilCoSil 106	Undrained triaxial	-	0-2,5 & 0-15	Decrease
14	Firoozkuh sand	0,27	Firoozkuh silt	Hollow cylinder torsional shear	Loosest possible density after deposition	0-30	Decrease

Table 2.2. Summary of the literature review for numerical analysis the liquefaction with different fine content

Reference No	Author	Year	Type of fines	Type of Modeling	Comparison basis	FC Range (%)	Effect of FC on liquefaction resistance or dilatancy
1	Issa and Mohsen	2011	Silty Sand	FLAC 2D UBCSand Model	Similar relative density	0-20	Increase
2	Ali, Aliakbar and Mohsen	2014	Sand and Silty Sand	FLAC 2D UBCSand Model	Similar intergranular void ratio	30-40	Increase
3	Ronert Andrew Jaeger	2012	Silty sand and Clayey Sand	FLAC 2D Finn Model	Similar relative density	0-30	Decrease
4	Murat Tonaroglu	2006	Sand and Silty Sand	LASS III	Similar intergranular void ratio	0-20	Increase
5	B.K. Maheshwari	2019	Sand and Silty Sand	PLAXIS UBC3D-PLM Model	Similar relative density	0-35	Decrease
6	Jui-Ching Chou	2021	Silty Sand	FLAC 2D UBCSand and Finn Model	Same void ratio	5-20	Increase
7	Asskar Janalizadeh Choobbasti	2020	Sand and Silty Sand	FLAC 2D Finn Model	Similar relative density	0-40	Decrease
8	WJ Chang, SH Ni, AB Huang,	2011	Silty sand and Clayey Sand	FLAC 2D UBCSand Model	Similar intergranular void ratio	0-20	Increase
9	G.R Martin, K Arulmoli, L Yan	2017	Sand and Silty Sand	FLAC 2D UBCSand Model	Similar relative density	0-45	Decrease
10	K Mog, P Anbazhagan	2018	Silty Sand	FLAC 2D UBCSand Model	Similar intergranular void ratio	0-20	Increase

2.3. Effect of Acceleration on Liquefaction Resistance

The liquefaction analysis of these areas, whose ground accelerations (0.84g and 0.51g) are determined, cannot be done precisely with known techniques. Since the amplitudes of earthquake waves have very different values, the logarithmic scale was used. Accordingly, one unit of growth in size corresponds to a 10-fold increase in amplitude. In addition, since it is known that high-frequency vibrations occurring in a narrow range cause severe damage, the magnitude of the earthquake is inversely related

to the period of the wave motion (Celep, 2004). Also, since it is known that high-frequency vibrations occurring in a narrow range cause severe damage, the magnitude of the earthquake is inversely related to the period of wave motion.

Table 2.3. Earthquake magnitude scale

(Source: Celep, 2004)

Magnitude	Definition	Ground Acceleration (cm/s^2)	g (gravity acceleration)
I	It only detects sensitive instruments.	-1	0,001 g
II	In the upper floors, resting persons can feel, suspended objects may shake.	2-3	0,002-0,003 g
III	It can be felt in the building, shaking as if a truck has passed by a stationary vehicle.	3-7	0,003-0,007 g
IV	It feels majority in the building and few outside, utensils shake.	7-15	0,007-0,015 g
V	Everyone feels, plates, windows, etc. it breaks.	15-30	0,015-0,03g
VI	Everyone feels, many get scared and run out, chimney, plaster fall, slight damage.	30-70	0,03-0,07 g
VII	Everyone runs out, there is damage according to the strength of the structure, the people in the car feel it.	70-150	0,07-0,15 g
VIII	The walls are separated from the frames, the chimney, the wall can fall. Sand and mud gush out.	150-300	0,15-0,3 g
IX	The structure leaves the foundation, cracks, bends. Ground and underground pipes crack.	300-700	0,3-0,7 g
X	Most of the masonry and frame structures are destroyed, the ground cracks, the rails bend, landslides occur.	700-1500	0,7-1,5 g
XI	New types of structures can survive, bridges collapse, earth slides, rails bend.	1500-3000	1,5-3 g
XII	Almost everything is destroyed, ripples appear on the soil surface, objects are thrown into the air.	3000-7000	3 - 7 g

CHAPTER 3

LIQUEFACTION ANALYSIS WITH FINITE DIFFERENCE METHOD

3.1. Introduction

In this chapter, the dynamic numerical analysis for liquefaction phenomena is performed. The FDM examined pore pressure generation for liquefaction from the earthquake's ground acceleration. Within the content of this chapter, the details of these numerical simulations were presented. This thesis presents the results of parametric studies conducted using the explicit finite differences in FLAC 2D code to explore the influence of the fine content and dynamic load (ground acceleration) (N. Benmebarek, 2018). FLAC is a certain finite difference numerical program for geotechnical engineers. It was first developed in 1986 to make analyses on microcomputers operating on Microsoft Windows systems (ITASCA, FLAC Basics 2015). Different type of soil conditions is modeled with the UBCSand Model in FLAC-2D. UBCSand Model is an effective stress plasticity model for developed stress-deformation analyses of geotechnical structures and problems (UBCSand, 2011).

3.2. Background of FDM and FEM Method

The FDM is perhaps the oldest numerical technique used to solve sets of differential equations, given initial values or boundary values (Desai and Christian 1977). This method (also known as the finite volume method) is used in FLAC. The mistaken belief that finite differences and rectangular grids are inseparable. It is responsible for any statements about boundary shapes and the distribution of material properties. Using Wilkins' method, borders can be any shape, and any element, such as finite elements, can have any property value (ITASCA, FLAC Basics 2015). For instance, the lower box takes

the calculated velocities and computes new stresses for each element. The speeds are assumed to be frozen for the box to work. That is, the newly calculated stresses do not affect the velocities. The step of the calculation is expressed in Figure 3.1. The method calls the equations of motion to produce new velocities and displacements by using stresses and forces. After that, strains are derived from velocities and new stresses from strain rates. Loop takes time; that is called the time step, and the strains, velocities, and stresses are updated at every turn of the loop (ITASCA, FLAC Basics 2015).

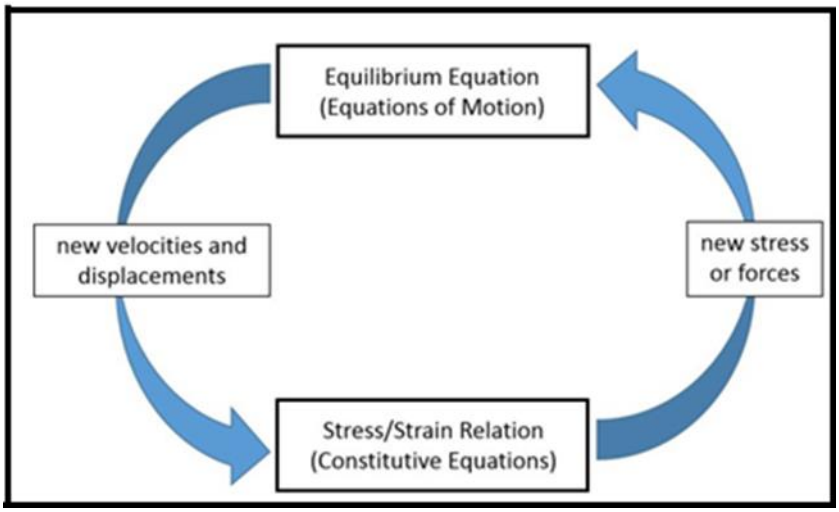

Figure 3. 1.Calculation cycle
(Source: ITASCA, FLAC Basics 2015)

The finite element method (FEM) is a widely used method for numerically solving differential equations arising from engineering and mathematical modelling. Typical problem areas include conventional structural analysis, heat transfer, fluid flow, mass transfer, and electromagnetic potential fields. FEM is a general numerical method for solving partial differential equations in two or three space variables (i.e. some boundary value problems). To solve a problem, FEM breaks up a large system into smaller, simpler parts called finite elements. This is achieved by a certain space discretization in space dimensions implemented by creating a mesh of the object: numerical space with a finite number of points for solution. The finite element method formulation of a boundary value problem eventually results in a system of algebraic equations. The method approaches the unknown function over the domain. The simple equations that model these finite

elements are then combined into a larger system of equations that models the entire problem. Dividing an entire domain into simpler parts has several advantages:

- Accurate representation of complex geometry
- Incorporation of different material properties
- Easy representation of the total solution
- Capturing local effects

Dividing the domain of the problem into a collection of subdomains with each subdomain represented by a set of element equations to the original problem. Systematically recombining all element equation sets into a global equation system for the final calculation. The system of spherical equations has known solution techniques and can be calculated from the initial values of the original problem to obtain a numerical answer. In the first step above, the element equations are simple equations that locally approximate the original complex equations to be studied, where the original equations are usually partial differential equations (PDE). To explain the approach in this process, the finite element method is often introduced as a special case of the Galerkin method. In mathematical language, the process is to construct an integral of the dot product of the residual and weight functions and set the integral to zero. In simple terms, it is a procedure that minimizes approximation error by fitting trial functions into the PDE. The residual is the error caused by the trial functions, and the weight functions are the polynomial approximation functions that reflect the residual. The process removes all spatial derivatives from the PDE, thus approximating the PDE locally.

- A set of algebraic equations for steady-state problems,
- A set of ordinary differential equations for transient problems,

In numerical analysis, finite difference methods (FDM) are a class of numerical techniques for solving differential equations with derivatives with respect to approximating finite differences. Both the spatial domain and the time interval (if any) are discretized or divided into a finite number of steps, and the value of the solution at these discrete points is estimated by solving algebraic equations containing finite differences and values from nearby points. Finite difference methods transform nonlinear ordinary differential equations (ODE) or partial differential equations (PDE) into a system of linear equations that can be solved by matrix algebra techniques. Modern computers can perform these linear algebraic calculations efficiently, and this, together with their relative ease of implementation, has led to the widespread use of FDM in

modern numerical analysis. Today, FDM is one of the most common approaches to numerical solution of PDE, along with finite element methods. First, assuming that the function to be approximated behaves properly, we can construct a Taylor series expansion according to Taylor's theorem.

$$f(x_o + h) = f(x_o) + \frac{f'(x_o)}{1!} + \frac{f^{(2)}(x_o)}{2!}h^2 + \cdots + \frac{f^{(n)}(x_o)}{n!}h^n + R_n(x) \qquad (3.1)$$

n! represents the factorial of n and $R'_n(x)$ where is a remainder term denoting the difference between the degree Taylor polynomial n and the original function. We will first cut the Taylor polynomial to get an approximation for the first derivative of the function "f":

$$f(x_o + h) = f(x_o) + f'(x_o)h + R_1(x) \qquad (3.2)$$

x_o=a

$$f(a + h) = f(a) + f'(a)h + R_1(x) \qquad (3.3)$$

$$\frac{f(a+h)}{h} = \frac{f(a)}{h} + f'(a) + \frac{R_1(x)}{h} \qquad (3.4)$$

$$f'(a) = \lim_{h\to 0} \frac{f(a+h)-f(a)}{h} \qquad (3.5)$$

The error in solving a method is defined as the difference between the approximation and the exact analytical solution. Two sources of error in finite difference methods are rounding error, loss of precision due to computer rounding in decimal quantities, and truncation error or discretization error, assuming the difference between the first solution of the differential equation plant and the exact quantity in perfect arithmetic (i.e. assuming no rounding). The finite difference method is based on discretizing a function on a grid. To use a finite difference method to approximate the solution to a problem, it is first necessary to separate the domain of the problem. This is usually done by dividing the area into a uniform grid. This means that finite difference

methods produce a different set of numerical approximations to the derivative, often in a "time-stepped" manner.

3.2.1. Lagrangian Analysis

Incremental displacements are assigned to coordinates so that the grid moves and deforms with the material it represents. This process is termed a Lagrangian formulation, in contrast to an Eulerian formulation, in which the material moves and deforms relative to a fixed grid. The constitutive formulation at each step is a slight strain but is equivalent to a large-strain formulation over many steps (ITASCA, FLAC Basics 2015). The model is integrated into the dynamic coupled stress flow finite difference program FLAC (Continua's Fast Lagrange Analysis) to capture the plastic deformations at all loading stages. Several researchers (Beaty & Byrne, 1998; Byrne et al., 2004; Puebla, Byrne, & Phillips, 1997; Ziotopoulou, Boulanger, & Kramer, 2012) have reported the successful validation of the UBCSand model for predicting the behavior of liquefiable soil measured in laboratory tests or field case histories. Puebla et al. (1997) and Byrne et al. (2004) noted that UBCSand and FLAC successfully predicted deformation and pore water pressure measurements in a dynamic model test used to design the field program.

3.3. Soil Model in FLAC

FLAC, which contains twelve different models formed by the arrangement of open, elastic, and plastic model groups, is a particular program that enables numerical modeling according to soil behavior characteristics (ITASCA, FLAC Basics 2015). That is a certain finite-difference program for geotechnical engineering program calculations, as explained before; it simulates the behavior of the duration, which could be structures, soil, rock, or other materials.

3.3.1. Elastic - Isotropic model

Soil is not homogeneous and, at the same time, has discontinuous structures. Various assumptions must be made since it is difficult to express these properties precisely. The soil has the same properties at every point and is considered a material that exhibits linear behavior. This concept, which is accepted to exhibit behavior according to the theory of soil elasticity, is called the concept of elastic soil. According to the elastic-isotropic theory, the behavior of the soil is investigated under the stress-strain relationship (Braja M.Das, 2010). According to the elastic isotropic soil model, the stress-strain equations and assumptions are as follows. Figure 3.2. shows the elastic isotropic coordinate axis.

$$E_1 = E_3 \qquad (E_x = E_z) \tag{3.6}$$

$$U_{13} = U_{31} \qquad (U_{xz} = U_{zx}) \tag{3.7}$$

$$U_{21} = U_{23} \qquad (U_{yx} = U_{yz}) \tag{3.8}$$

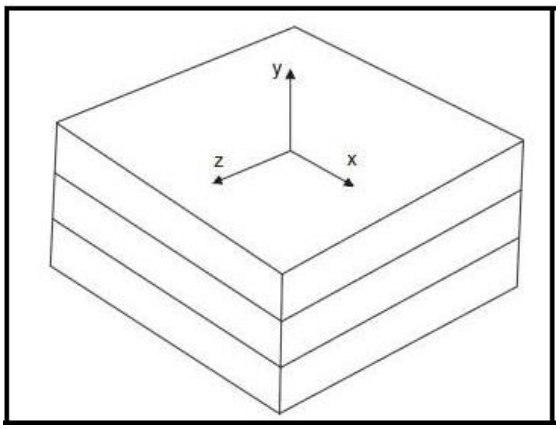

Figure 3.2. Elastic Isotropic Coordinate Axis
(Source: ITASCA, FLAC Basics 2015).

$$\Delta e_{11} = S11\ \Delta\sigma_{11} + S12\ \Delta\sigma_{22} + S13\ \Delta\sigma_{33} + S16\ \Delta\sigma_{12} \tag{3.9}$$

$$\Delta e_{22} = S12\ \Delta\sigma_{11} + S22\ \Delta\sigma_{22} + S23\ \Delta\sigma_{33} + S26\ \Delta\sigma_{12} \tag{3.10}$$

$$\Delta e_{33} = S13\,\Delta\sigma_{11} + S23\,\Delta\sigma_{22} + S33\,\Delta\sigma_{33} + S36\,\Delta\sigma_{12} \quad (3.11)$$

$$s_{11} = \frac{\cos^4\emptyset}{E_1} + \left[\frac{1}{G_{12}} - \frac{2U_{12}}{E_1}\right]\sin^2\emptyset\cos^2\emptyset + \frac{\sin^4\emptyset}{E_2} \quad (3.12)$$

$$s_{22} = \frac{\sin^4\emptyset}{E_1} + \left[\frac{1}{G_{12}} - \frac{2U_{12}}{E_1}\right]\sin^2\emptyset\cos^2\emptyset + \frac{\cos^4\emptyset}{E_2} \quad (3.13)$$

Poisson's ratio: It is the name given to the ratio of transverse contraction to longitudinal elongation. The Poisson's ratio, defined as geometric strain, is not a stress-strain measure. The voids and cracks in the ground affect this ratio. The Poisson's ratio ranges from 0 to 0.5. For elastic solids, this value is about 0.25. Different deformation forces depend on compression (pressure) or tensile forces resulting from external impact (Desai and Christian 1977).

$$\boldsymbol{\nu} = -\frac{\boldsymbol{\varepsilon}_{trans}}{\boldsymbol{\varepsilon}_{axial}} \quad (3.14)$$

Modulus of Elasticity (Young's Modulus): It is obtained from the ratio of the soil's transverse contraction due to the soil's compression and expansion forces under external force to the longitudinal elongation. The linear relationship between tensile or compressive stress and strain is defined by formulas (Braja M.Das, 2010).

$$\mathbf{E} = \frac{\sigma}{\boldsymbol{\varepsilon}} \quad (3.15)$$

E= Elasticity Modulus, σ = stress and $\boldsymbol{\varepsilon}$ = strain

Bulk Modulus: It measures the strength of the material against volume change. The literature explains it as a measure of stress - deformation in a rock under hydrostatic pressure.

$$\mathbf{K} = -V\frac{\partial \mathbf{P}}{\partial \mathbf{V}} \tag{3.16}$$

Bulk Modulus: Shear is the force tangential to the displaced surface in figure.3.3. It is a measure of the Stress-Strain ratio that occurs under the effect of force. The displacements that occur without any volume change represent shear deformation. Since liquid substances do not have any shear resistance, the shear value for liquids is zero.

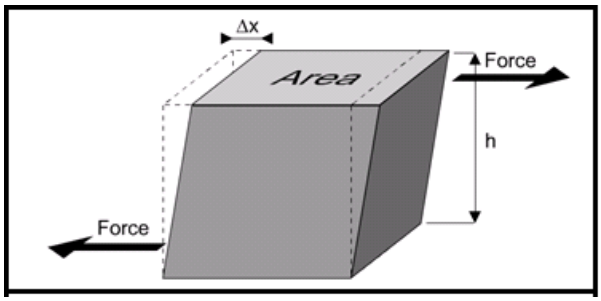

Figure 3.3. Shear Modulus

(Source: N. Benmebarek, 2018)

$$\mathbf{G} = \frac{\mathbf{F/A}}{\Delta_x/L} = \frac{FL}{A\Delta_x} \tag{3.17}$$

F= Force, A = region and Δ x= deformation

3.3.2. Mohr-Coulomb Model

In this model, principal stresses σ_1, σ_2, and σ_3 are used. Principal stresses and principal directions are evaluated according to stress tensors. Figure 3.4 show the details of the Mohr-Coulomb failure criteria.

$$\sigma_1 \leq \sigma_2 \leq \sigma_3 \tag{3.18}$$

The principal strain increments Δe_1, Δe_2, and Δe_3 are calculated according to the following formula;

$$\Delta e_i = \Delta e_i^e + \Delta e_i^p \tag{3.19}$$

Here e and p denote the elastic and plastic parts, respectively. According to the basic Hooke's law, the principal stresses and strains are expressed as follows;

$$\Delta\sigma_1 = \boldsymbol{\alpha_1}\Delta e_1^e + \boldsymbol{\alpha_2}(\Delta e_2^e + \Delta e_3^e) \tag{3.20}$$

$$\Delta\sigma_2 = \boldsymbol{\alpha_1}\Delta e_2^e + \boldsymbol{\alpha_2}(\Delta e_1^e + \Delta e_3^e \tag{3.21}$$

$$\Delta\sigma_3 = \boldsymbol{\alpha_1}\Delta e_3^e + \boldsymbol{\alpha_2}(\Delta e_1^e + \Delta e_3^e \tag{3.22}$$

$\boldsymbol{\alpha_1} = \mathrm{K} + \frac{4G}{3}$ and $\boldsymbol{\alpha_2} = \mathrm{K} - \frac{2G}{3}$

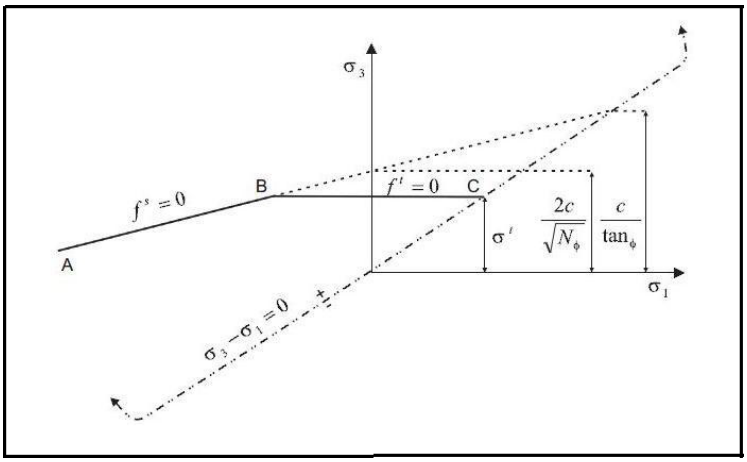

Figure 3.4. Mohr Coulomb Failure Criteria
(Source: ITASCA, FLAC Basics 2015)

3.3.3. UBCSand Model

In this thesis, UBCSand Constitutive Model version 904aR is used. It is an effective stress plasticity model for improved stress-deformation analyses of geotechnical structures (ITASCA, FLAC Basics 2015). FLAC is within the scope to calculate pore water pressure increase by performing stress-strain analyses in the dynamic operating model. This model was first used to predict Canadian liquefaction experiments (Canadian Liquefaction Experiment – CANLEX). The first version was developed and presented as UBCSand 904 in 2002. The model predicts the behavior of the soil under load increases, the response of pore water pressure is expressed together with the volumetric deformation and the behavior of the soil skeleton in figure 3.5. The elastic components of the UBCSand model are shear modulus (G^e) and Bulk modulus (B^e).

$$G^e = K_G^e \, Pa \left[\frac{\sigma'}{p\alpha_a}\right]^{ne} \tag{3.23}$$

It is a density-dependent shear modulus; the value starts from 500 in loose sands and reaches 2000 in dense sands. P_a = atmospheric pressure, $\sigma' = (\sigma'_x + \sigma'_y)/2$

The plastic shear strain increment, $d\gamma^p$ is related to the change in shear stress ratio.

$$d\gamma^p = \frac{1}{G^P/\sigma'} dn \tag{3.24}$$

Where G^p is the plastic shear modulus and, assuming a hyperbolic relationship between n and γ^p is given by:

$$G^p = G_i^P (1 - \frac{n}{n_f} R_f)^2 \tag{3.25}$$

Where;

G^p_i is the plastic modulus at a low level of stress ratio (n=0),

N_f is the stress ratio at failure and equals sin φ_f ,

φ_f is the peak friction angle and

R_f is the failure ratio used to truncate the fit hyperbolic relationship and prevent the over-prediction of strength at failure. R_f generally varies between 0.7 and 0.98 and decreases with increasing relative density.

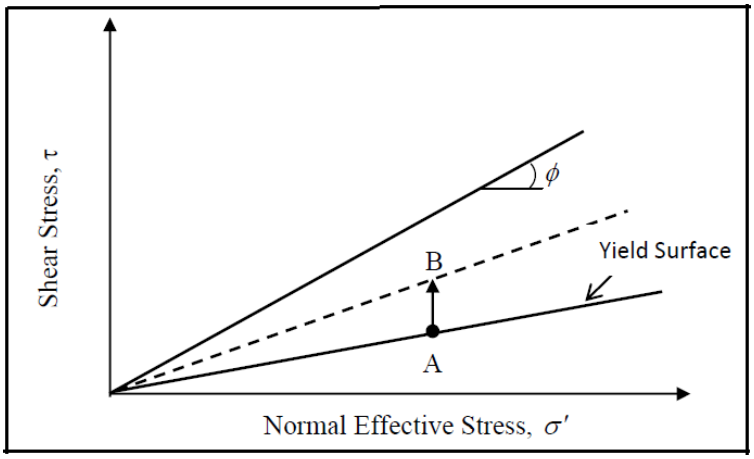

Figure 3. 5.Yield Surface in UBCSand Model

(Source: ITASCA, FLAC Basics 2015)

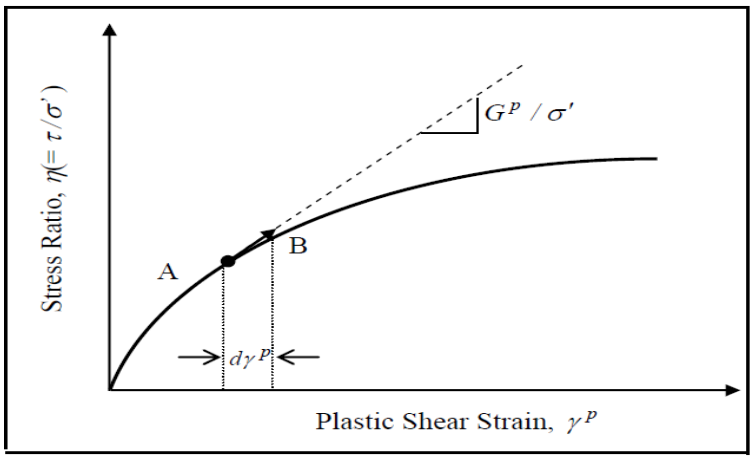

Figure 3. 6.Plastic strain increment and plastic modulus

(Source: ITASCA, FLAC Basics 2015)

As systems that can change shape with the infrastructure and superstructure, the ground environment moves with the effect of static and dynamic loads coming from outside. As it can be understood, the infrastructure and superstructure in the ground area should be considered as a part of the system.

In order to describe the energy lost in the semi-infinite environment of the ground and emitted into the system, viscous dampers, which are equivalent to the boundaries of the region, are called geometric damping (Radiation damping), a damping mechanism that has nothing to do with material damping and prevent wave reflections, are used. Figure 3.6. shows strain increment and plastic modulus. Table 3.1. describes UBCSand parameters and abbreviation name.

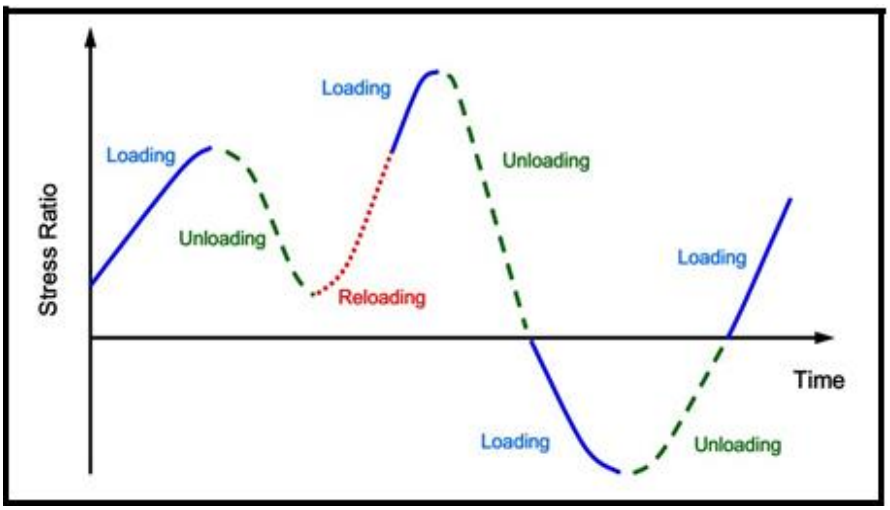

Figure 3.7.Stress ratio history showing loading, unloading, and reloading

(Source: Byrne and Beaty 2011)

Table 3.1. Main input parameters of UBCSand Model version 904aR

(Source: Braja M.Das, 2010)

Parameter	Description
General:	
m_n160	Relative density index defined as characteristic value of (N1)60cs
m_pa	Atmospheric pressure in model units
Elastic stiffness:	
m_kge	Value of Gmax/m_pa at mean effective pressure (σ'm)=1 atm
m_ne	Stress dependence of Gmax defined by (σ'm/m_pa)^m_ne
m_kb	Value of B/m_pa at σ'm=1 atm where B= bulk modulus of soil skeleton
m_me	Stress dependence of B defined by (σ'm/m_pa)^m_me
Plastic shear stiffness and flow rule:	
m_kgp	Plastic shear modulus number. Defines initial slope of hyperbolic relationship
m_np	Stress dependence of plastic shear modulus defined by (σ'm/m_pa)^m_np
m_rf	Hyperbolic fitting coefficient
m_hfac1	User-controlled factor applied to plastic stiffness. Typically used to modify Kσ behavior.
m_phicv	Constant volume friction angle to defined boundary between dilative and contractibe stres states
Strength:	
m_phif	Maximum friction angle that can be mobilized
Model control variables:	
m_sat	Average saturation of element (usually set by FISH function)
m_static	Set=1 for static analysis or initial setup. Set= 0 for earthquake analysis
m_ratmax	Set=0 to reinitialize stress history. Typically use at start of earthquake.

3.4. How to Perform Dynamic Analysis

The dynamic analysis is repeated in this study with different soil properties and acceleration. The liquefaction triggering conditions are compared with different conditions. For this analysis, the acceleration is applied to the bottom boundary of the

model. The acceleration given in the bottom is transmitted and performed along with the model. An artificial sinusoidal motion is applied in a horizontal direction. The equation of motion is given,

$$a = A \times \sin(\omega t) \tag{3.26}$$

Where a is acceleration, A is amplitude, ω is the angular frequency, and t is dynamic time.

3.5. Boundary Conditions

Due to the damping feature of the ground, working with a large-size model prevents problems that may arise from boundary conditions. The solution of large model systems takes time and complicates numerical working conditions. In studies with numerical modeling, the solution to prevent problems in boundary conditions should be provided. To avoid these problems, the fading boundary conditions of FLAC 2D can be used. These boundary conditions are called viscous boundary conditions. There are different formulations suggested by Lysmer and Kuhmeyer, 1973 for the boundary conditions.

Studies in the literature show that free-field reflections can be prevented in dynamic analysis. It is envisaged to avoid reflections due to keeping the required distance. In our model, free-field boundary conditions ensure the ground's continuity and prevent wave reflections at the boundaries. Wave reflections can be seen in the numerical analysis due to boundary conditions. The working principle of free-field boundary conditions is shown in Figure 3.8 (Das, 2010). In this study, the free-field boundary condition was used in the dynamic analysis of the numerical model.

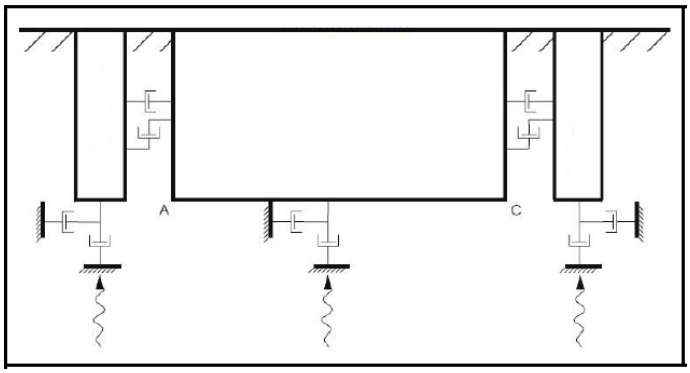

Figure 3.8. Free-field boundary conditions principle in model

(Source: Das, 2010)

3.6. Local Damping and Damping Ratio

It is possible to group loads acting on soils. Depending on the property of the material and external influence, we can examine it as stress-strain and strength properties. FLAC 2D contains three different damping modules. Local damping is also used in dynamic and characteristic simulations developed for equivalent static analysis. In addition, the damping module is added and subtracted at mass nodes following the law of conservation of mass. Rayleigh damping is controlled by two parameters that express the critical damping value of the ground and the ground's natural frequency. Depending on the soil's behavior, the damping ratio parameters are updated and changed in the analyzes made with FLAC 2D. Hysterical Damping is a supplementary addition in nonlinear models with linear scope. In this method, which is used in the seismic analysis of soils to calculate wave propagation, the damping ratio-strain relationship is applied to the numerical model.

CHAPTER 4

FLAC-2D LIQUEFACTION SIMULATION VERIFICATION WITH CDSS TEST

4.1. Introduction

This chapter presents the parametric studies conducted using the explicit finite differences methods to explore the influence of the fine content and ground acceleration on liquefaction resistance of the soil. Moreover, the duration of seismic load on the soil model was studied. The UBCSand model is used to represent the soil behavior. The finite-difference codes of the FLAC program enable the program to work in a phased manner.

The dynamic analysis model can analyze data such as displacements, pore water pressures, shear stresses, and stresses in the model under dynamic effect. Besides, dynamic analysis can also analyze liquefaction problems in soils with liquefaction potential. The displacement, pore water pressures, shear stresses in the model due to the liquefaction data was analyzed with the damping analysis.

4.2. Geometry of the Model

One of the critical factors when performing numerical analysis is model sizing. The dimensions of the model change the reality ratio of the analyses made. Wave reflections occur in boundary conditions in the analyses made with models with small dimensions. Analyses made with models with large dimensions take long periods and affect the researcher negatively.

In this thesis, an ideal ground size, which was determined due to the dimensioning studies carried out in the same ground conditions, was used in the model. The primary objective of this study is to carry out two-dimensional finite-difference modeling of the

different fines content. Another critical discussion is different acceleration and its effect on the liquefaction mechanism.

The liquefaction phenomenon is studied on the same geometries, where fine content and ground acceleration vary. The model had a single one soil profile, and each run model had different fine content and ground acceleration. The cross-section of the model along a representative mean geometry in the latitudinal direction is shown in Figure 4.1. Seismic load applied at the bottom of the model with lateral direction. Figure shows the points where data were received from the middle side of the model. The model dimensions are 30 m in the x-direction and 18 m in the y-direction.

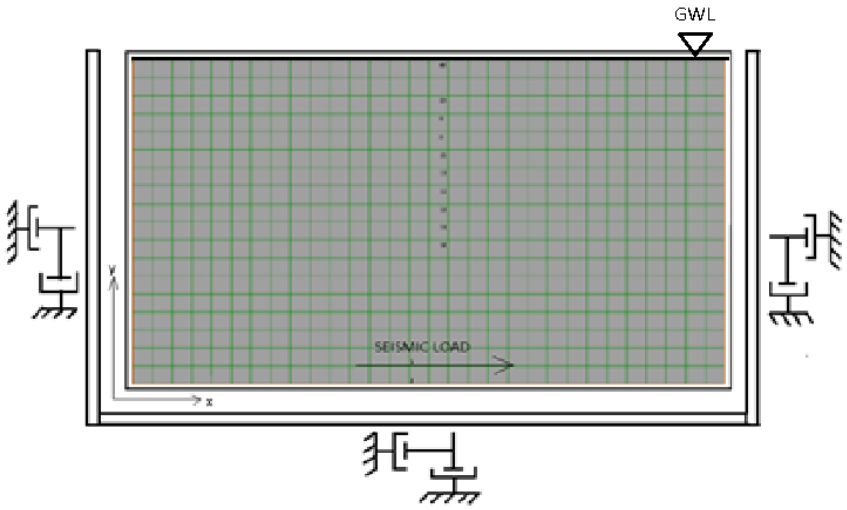

Figure 4.1. Geometry, boundary, and soil profile

4.2.1. Mesh in Numerical Model

Mesh intervals have an essential place in numerical analysis. Mesh intervals play a role in defining the soil properties in the numerical model and examining the analysis results. The frequency of mesh intervals affects the precision of the analysis results. However, the frequency of mesh intervals extends the numerical analysis times. In such cases, researchers can make precise analyzes in a shorter time by tightening the mesh intervals in the region where the effects they want to examine in the numerical model they have established. Figure 4.1. shows the mesh size. All mesh in the model had the same size as each other. The most appropriate mesh size was selected. There are 540 meshes in the model, and they have the same size. The size of one mesh is 1 m by 1 m.

4.2.2. Construction Phase in the Numerical Model

The construction phase is essential in numerical analysis while the model is set up. This study modeled the soil layer and mesh intervals were determined while creating the numerical model. After the ground layer, the underground water level was entered into the model. The ground water entered at the surface. Hence, the whole model is analyzed as fully saturated. Once the model construction was completed, the dynamic effect was applied to the model, and liquefaction analysis was performed. Data records at the dynamic analysis period were taken from the examination points shown in Figure 4.1.

4.3. Dynamic and Static Parameters from Previous Laboratory Tests

4.3.1. CDSS Tests

Simple shear (CDSS) tests, including a series of constant volume cyclic direct, were performed on mixtures of two basic sand grains and four non-plastic silts at different fine contents, allowing the authors to observe the liquefaction response of silty sands of different grades (Tutuncu, 2021 and Monkul, 2021). The base sand was used in the testing program. It was obtained from the Urla region of Izmir and named Silica sand. All soils are deposited in a dry condition into a cylindrical simple shear divided mold using the automatic dry cone deposition technique (Tutuncu,2021 and Monkul, 2021). Saturated simple shear specimens typically had 64 mm diameter and 20 mm initial height. Before cyclic loading, all samples were consolidated to vertical stresses of 100 kPa (i.e., $\sigma'vc$ = 100 kPa). It was accepted that liquefaction occurred when the samples' estimated pore water pressure reached the first vertical practical stress value of 100 kPa. Soil parameters that are determined by Arik (2021) were used in the numerical analysis. The sample was the same as the samples used in the dynamic tests at Yeditepe University.

In Yeditepe University, a total of 260 CDSS tests were performed. 7 CDSS test results were verified with numerical results in this thesis. CDSS tests in this study were done on several different Dr values on various silty sand specimens having different fines contents (Monkul, 2021).

4.3.2. CPTu, SCPT and DPPT Tests

Arik (2021) carried out Piezo Cone Penetration Test (CPTu), Seismic Cone Penetration Test (SCPT), and Direct push permeability test (DPPT) tests in box to investigate the effect of different fines content and relative density on cone penetration resistance and excessive pore water pressure in clean sand and silty sands of 5%, 15%, and 35%. Soil parameters that are determined by Arik (2021) were used in the numerical analysis. The sample was the same as the samples used in the dynamic tests at Yeditepe University. Silty sand samples have been prepared at the silt content of 5%, 15%, and 35% by dry weight. Experiments were performed inside the box at 150 cm length, 40 cm wide, and 160 cm in depth. 13 tests were carried out on clean sand and 5%, 15%, and 35% silty sand. The sample was the same as the samples used in the dynamic tests at Yeditepe University (Tutuncu, 2021).

CPTu, SCPT, and DPPT are applied with different fine content soils. Soil samples were densified. The loose soil obtained by the dry fill method in soils filled with layers was quickly changed into the desired medium dense and dense soils. SCPT application is made with the SCPT probe, which is obtained by adding a seismic detector to a standard CPT conical tip. Recording of seismic measurement as numerical data; It is provided by transferring the seismic signal detected by the seismometer to the digital environment from the depth at which the application is made utilizing a seismic cable passed through the rods. The seismic energy was created by hitting a 10 kg sledgehammer on the metal plate placed horizontally on the surface. Figure 4.2. shows the system of the SCPT.

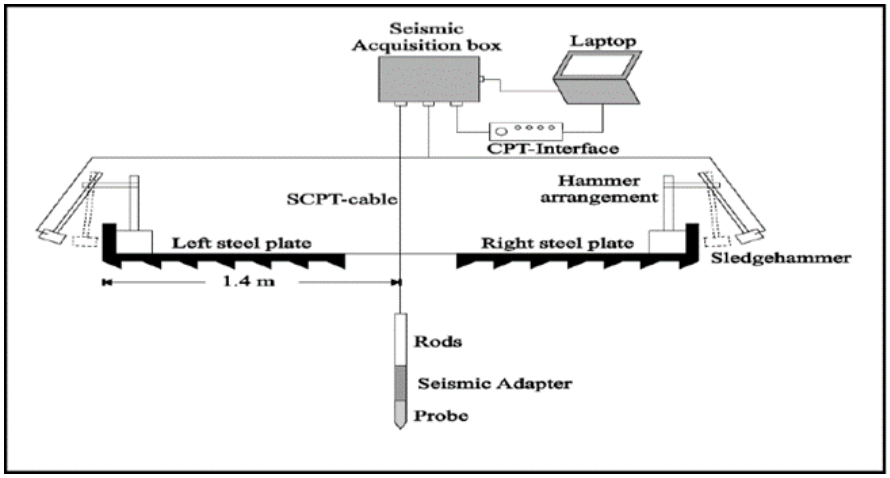

Figure 4.2. The SCPT system and equipment
(Source: Holmsgaard et al., 2016)

4.4. Soil Parameters in Numeric Model

This numerical study was verified with the laboratory work performed at Yeditepe University (Monkul et al., 2021). Table 4.1. show the soil models that are used in the numerical analysis. As shown in the table, the parameters are;

Void ratio (e) is calculated by Equation 4.1.

$$S * e = w * G_s \tag{4.1}$$

where S is the degree of saturation and w is the water content. The degree of saturation of the sample is taken as 1.0 since the sample is fully saturated with water. Thus, Equation 5.1 has turned into Equation 4.2.

$$e = w * G_s \tag{4.2}$$

Relative density (D_r) is calculated by Equation 4.3.

$$D_r = \frac{e_{max} - e}{e_{max} - e_{min}} \tag{4.3}$$

The laminar box consists of 160 cm length, 40 cm width and 150 cm depth. Since the samples are loaded from bottom to top, the total volume depends only on the height of the loaded sample. Each sample was loaded at different heights (Arık, 2021).

Total volumes are calculated by Equation 4.4.

$$Total\ Volume = Box\ Lenght * Box\ Width * Depth\ of\ The\ Sample \tag{4.4}$$

Water content is calculated by Equation 4.5.

$$Water\ content = \frac{Weight\ of\ water}{Weight\ of\ solid} \tag{4.5}$$

Density is calculated by Equation 4.6.

$$Density = \frac{Weight\ of\ solid + Weight\ of\ water}{Total\ volume} \tag{4.6}$$

Shear modulus (G), often called stiffness or torsional modulus, measures the solid or rigid nature of different types of solid materials. It is an elastic parameter. It is obtained from the ratio of the shear stress value of the material to the shear strain. Shear stress is a value of how much force is applied to the square area of a material, usually measured at pressure values of pascals. The stiffer a substance is, the higher the shear modulus value depending on the measured ambient temperature. As the value of the shear modulus increases, this indicates that a much greater force or strain is required to stretch or deform it along the force direction plane.

$$G = V_s^2 p \tag{4.7}$$

The Poisson's ratio is the negative sign of the ratio of lateral stress to axial stress for a uniaxial stress state. The Poisson ratio is sometimes expressed as the ratio of the absolute values of the axial and lateral strains. Since both strain values are unitless, the Poisson ratio is also unitless. The Poisson ratio is assumed to be 0.25 in the thesis.

Modulus of Elasticity (E) is the ratio of the stress within elastic limits (Hooke's Law) to the unit elongation (deformation per unit length) due to this stress for any material. This ratio is constant up to the yield point within the limits of Hooke's Law. It is the elastic parameter.

$$E = 2G(1 + v) \tag{4.8}$$

For the body under hydrostatic stresses, the volumetric stress ratio to volumetric strain is called bulk or compression modulus (K). Permeability (k) is the capacity of porous rock or soil to transmit liquid and gas. It measures how easily a liquid can flow under conditions of unequal pressure. It is a dynamic parameter. Permeability is calculated using the equations below (Lee et al., 2001):

$$k = \frac{Q}{4\pi \Delta h a_s} \tag{4.9}$$

$$a_s = \sqrt{\frac{1}{2} al} \tag{4.10}$$

where k is permeability, Q is volumetric flow, Δh is the excess head, as is the effective radius of the spherical injection zone, a is the radius of the screen, and l is the pitch's length.

Soil friction angle is the shear strength parameter of soils. Its definition is derived from the Mohr-Coulomb failure criterion and is utilized to describe the friction shear resistance of soils and the expected effective stress (Braja M.Das, 2010).

Table 4.1. Material Models and short description

FC %	MATERIAL	MATERIAL MODEL	DESCRIPTION
0	LOOSE SILTY SAND	UBCSand	EFFECTIVE STRESS PLASTICITY MODEL
	MEDIUM SILTY SAND	UBCSand	EFFECTIVE STRESS PLASTICITY MODEL
	DENSE SILTY SAND	UBCSand	EFFECTIVE STRESS PLASTICITY MODEL
5	LOOSE SILTY SAND	UBCSand	EFFECTIVE STRESS PLASTICITY MODEL
	MEDIUM SILTY SAND	UBCSand	EFFECTIVE STRESS PLASTICITY MODEL
	DENSE SILTY SAND	UBCSand	EFFECTIVE STRESS PLASTICITY MODEL
15	LOOSE SILTY SAND	UBCSand	EFFECTIVE STRESS PLASTICITY MODEL
	MEDIUM SILTY SAND	UBCSand	EFFECTIVE STRESS PLASTICITY MODEL
	DENSE SILTY SAND	UBCSand	EFFECTIVE STRESS PLASTICITY MODEL
35	LOOSE SILTY SAND	UBCSand	EFFECTIVE STRESS PLASTICITY MODEL
	MEDIUM SILTY SAND	UBCSand	EFFECTIVE STRESS PLASTICITY MODEL
	DENSE SILTY SAND	UBCSand	EFFECTIVE STRESS PLASTICITY MODEL

1 cm^3 of a unit volume of substances is defined as the density of substances. In other words, the ratio of the mass of a substance to its volume expresses the density. Shear wave velocity is a measure of the mechanical property of soil. Table 4.1. shows UBCSand soil models. Table 4.3 shows the description of the UBCSand model parameters. Physical and mechanical soil input parameters are obtained from Arık (2021).

Within the framework of these corrections, depending on the soil type and groundwater level, geological load correction (C_N), groundwater level correction and driving speed correction (C_{BF}) variables, instrumental details and energy correction (C_E), rod length correction depending on the test application method. (C_R), bore diameter correction (C_B), sampler sheath correction (C_S), hammer head correction (CA), and ram pad correction (C_C) factors need to be used. The following expressions give corrections shown as N_a (site), N_{60}, or $N_{1,60}$:

$$N_{60} = C_E * C_R * C_B * C_S * C_A * C_{BF} * C_C * N_A \quad (4.11)$$

$$N_{1,60} = C_N * N_{60} \quad (4.12)$$

$$m\_n160 = N_{1,60} \quad (4.13)$$

$$\text{m\_pa} = 100 \text{ kPa approximately (atmospheric pressure)} \quad (4.14)$$

The first step in using very complex or simple liquefaction models with finite element analysis is to determine the model parameters for different soil types and loading conditions. As mentioned before, this stage should be calibrated for that project before being applied to any project in the use of liquefaction models. Because most of these models contain parameters that are dependent on the stress state and cannot be determined directly by laboratory tests. Many laboratory experiments have been used in the literature for the calibration of liquefaction models. Because of the dependency of stress states. For dynamic analysis proposed by a few researchers Finn et al. (1995), Marcuson (2007), Beaty and Perlea (2011) calibration can be performed using cyclic loading tests such as simple shear and triaxial torsion shear test. Determining the model parameters by using appropriate laboratory tests for the current loading conditions in that field is important for the sensitivity of the analysis parameters. Table 4.4. shows the material parameters used in the numerical model are given. As in many liquefaction models, model parameters in the UBCSand model can be determined by cyclic undrained simple shear tests (CDSS). However, in many cases such test results may not always be available. Available data can only be test data from field experiments such as SPT (Standard Penetration Test) or CPT (Cone Penetration Test). For this reason, some correlations were suggested for clean and silty sands to obtain the model parameters (Table 4.2) used in the UBCSand model by utilizing the validated equivalent SPT impact number $(N_1)_{60}$ measurements (Beaty and Perlea, 2011).

Table 4.2. UBCSand model soil parameters

(Source: UBCSand V.904aR, 2011)

UBCSand model parameters	
Elastic Shear Stiffness Number (m_kge)	m_kge=21.7*15$((N_1)_{60})^{0.333}$
Maximum Shear Modulus (G_{max})	G_{max}=m_kge*P_{atm} $(\frac{\sigma'_m}{P_{atm}})^{m\_ne}$
Bulk Stiffness Number (m_kb)	M_kb=m_kge*0,916
Bulk Modulus (K)	K=m_kb*P_{atm} $*$ $(\frac{\sigma'_m}{P_{atm}})^{m\_me}$
Stress Exponents (m_ne, m_me)	m_ne=0.5 , m_me=0.5
Elastic Shear Stiffness (m_kge)	M_kge=21.7*15*$((N_1)_{60})^{0.333}$
Stress Exponents (m_ne=0.5 and m_me=0.5)	
Plastic Shear Modulus Number (m_kgp)	m_kgp=(m_kge*$((N_1)_{60})^2$*0.003+100
Plastic Shear Modulus (G)	G=m_kgp*P_{atm} $(\frac{\sigma'_m}{P_{atm}})^{m\_np}$
Plastic Shear Modulus Stress Exponent (m_np)	M_rf=1.0- $\frac{m\_n160}{100}$ Where 0.5 <m_rf<0.99
Anisotropy Parameter (m_anisofac)	M_anisofac =0.0166* $(N_1)_{60}$ Where 0.333<m_anisofac<1.0
Constant Volume Friction Angle (m_phicv)	
Peak Friction Angle (m_phif)	m_phif=m_phicv+$\frac{(N_1)_{60}}{5}$
Failure Ratio (m_rf)	m_rf=1.0+$\frac{m\_n160}{100}$ Where 0.5<m_rf<0.99
Saturation (m_sat)	0<m_sat<1

Table 4.3. Soil parameters used in the Mohr-Coulomb model

SOIL PARAMETERS														
Test No:	FC	Density	Vs	G (Shear Modulus)		Poison Ratio	E (Young's Modulus)		K (Bulk Modulus)		k (Permability)	Friction Angle	e (Void Ratio)	n (Porosity)	Dilatation Angle
-	%	kg/m^3	m/sec	Pa	Mpa	-	Pa	Mpa	Pa	Mpa	m/sec	°	-	-	°
T1 Loose	0	1899	74	10398924	10,40	0,25	25997310	26,00	17331540	17,33	0,000443	36	0,95	0,487179487	8
T2 Medium	0	1933	90	15657300	15,66	0,25	39143250	39,14	26095500	26,10	0,000362	36	0,85	0,459459459	10
T3 Dense	0	2059	100	20590000	20,59	0,25	51475000	51,48	34316667	34,32	0,000332	36	0,77	0,435028249	15
T4 Loose	5	1828	71	9214948	9,21	0,25	23037370	23,04	15358247	15,36	0,000404	34	0,89	0,470899471	7
T5 Medium	5	1889	83	13013321	13,01	0,25	32533303	32,53	21688868	21,69	0,000368	34	0,86	0,462365591	9
T6 Dense	5	1960	91	16230760	16,23	0,25	40576900	40,58	27051267	27,05	0,000188	34	0,74	0,425287356	14
T7 Loose	15	2052	67	9211428	9,21	0,25	23028570	23,03	15352380	15,35	0,00000331	29	0,82	0,450549451	6
T8 Medium	15	1955	88	15139520	15,14	0,25	37848800	37,85	25232533	25,23	0,00000295	29	0,77	0,435028249	8
T9 Dense	15	1935	100	19350000	19,35	0,25	48375000	48,38	32250000	32,25	0,00000235	29	0,74	0,425287356	8
T10 Loose	35	1943	67	8722127	8,72	0,25	21805318	21,81	14536878	14,54	0,000000444	25	0,7	0,411764706	5
T11 Medium	35	2206	83	15197134	15,20	0,25	37992835	37,99	25328557	25,33	0,000000384	25	0,64	0,390243902	5
T12 Dense	35	2083	86	15405868	15,41	0,25	38514670	38,51	25676447	25,68	0,00000027	25	0,51	0,337748344	5

Note: FC=Fine content, V_s = Shear wave velocity, G= Shear modulus, E =Young's modulus, K = Bulk Modulus, k=Permeability, e = Void ratio ,and n =Porosity

Table 4.4. Soil parameters used in the UBCSand mod

SOIL PARAMETERS UBCSAND MODEL IN FLAC 2D																			
Test No:	FC:	m_n160	m_pa	fi	m_kge	m_kgp	m_phif	m_rf	m_ne	m_np	m_static	m_hfac1	m_hfac2	m_hfac3	m_anisofac	m_sat	porosity	qc	Dr
-	%	-	Pa	deg	-	-	-	-	-	-	-	-	-	-	-	-	-	kPa	%
T1 Loose	0,00	11,50	10000,00	36,00	734,11	391,26	38,30	0,89	0,50	0,50	1,00	1,00	1,00	1,00	1,00	1,00	0,49	250,00	18,00
T2 Medium	0,00	16,00	10000,00	36,00	819,45	729,34	39,20	0,84	0,50	0,50	1,00	1,00	1,00	1,00	1,00	1,00	0,46	1297,00	55,00
T3 Dense	0,00	23,00	10000,00	36,00	924,71	1567,52	40,60	0,77	0,50	0,50	1,00	1,00	1,00	1,00	1,00	1,00	0,44	1857,00	83,00
T4 Loose	5,00	10,50	10000,00	34,00	712,21	335,56	36,10	0,90	0,50	0,50	1,00	1,00	1,00	1,00	1,00	1,00	0,47	177,00	18,00
T5 Medium	5,00	15,00	10000,00	34,00	802,03	641,37	37,00	0,85	0,50	0,50	1,00	1,00	1,00	1,00	1,00	1,00	0,46	518,00	31,00
T6 Dense	5,00	22,00	10000,00	34,00	911,12	1422,95	38,40	0,78	0,50	0,50	1,00	1,00	1,00	1,00	1,00	1,00	0,43	2324,00	77,00
T7 Loose	15,00	9,00	10000,00	29,00	676,57	264,41	30,80	0,91	0,50	0,50	1,00	1,00	1,00	1,00	1,00	1,00	0,45	111,00	21,00
T8 Medium	15,00	13,00	10000,00	29,00	764,71	487,71	31,60	0,87	0,50	0,50	1,00	1,00	1,00	1,00	1,00	1,00	0,44	412,00	38,00
T9 Dense	15,00	20,00	10000,00	29,00	882,66	1159,19	33,00	0,80	0,50	0,50	1,00	1,00	1,00	1,00	1,00	1,00	0,43	544,00	46,00
T10 Loose	35,00	6,00	10000,00	25,00	591,12	163,84	26,20	0,94	0,50	0,50	1,00	1,00	1,00	1,00	1,00	1,00	0,41	247,00	26,00
T11 Medium	35,00	10,50	10000,00	25,00	712,21	335,56	27,10	0,90	0,50	0,50	1,00	1,00	1,00	1,00	1,00	1,00	0,40	439,00	32,00
T12 Dense	35,00	17,50	10000,00	25,00	844,27	875,68	28,50	0,83	0,50	0,50	1,00	1,00	1,00	1,00	1,00	1,00	0,34	439,00	36,00

4.5. Dynamic Loading in Numeric Model

During an earthquake, seismic waves cause displacement of soil particles by creating shear forces relative to each other, primarily as they propagate in undrained, saturated, and loose soils, especially with shear waves. Under these conditions, saturated and loose soil particles tend to converge. The tension at the contact points of the particles in this state is transmitted to the surrounding water. Since seismic waves cause sudden and short-term movements during the earthquake, they do not allow sufficient time for the antiparticle water to drain. Therefore, the pore water pressure suddenly increases, which cannot move away from the environment. The earthquake load is simulated with a sinusoidal load in the model. The loads are varied with different amplitudes with 0.2 g, 0.3 g, 0.4 g, and 0.5 g. The frequency of the dynamic loads is the same as 2 Hz. Dynamic loads are applied from the bottom of the numeric model. Figure 4.3. and figure 4.4. show the dynamic loads in the model.

The thesis presents the parametric studies conducted using the explicit finite differences method to explore the influence of the fine content of soil and ground acceleration liquefiable of the soil and the significant duration of seismic load on the model.

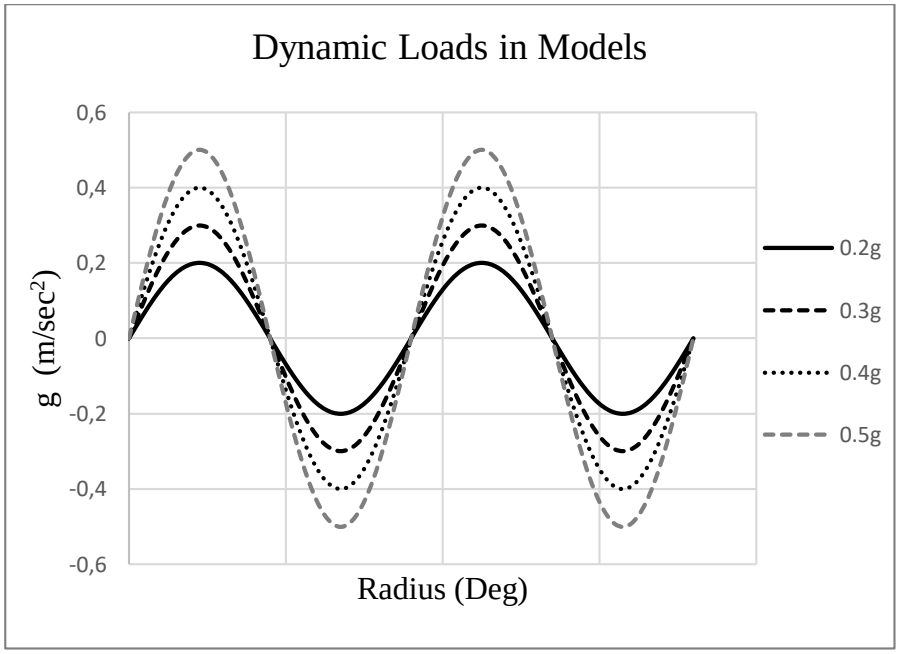

Figure 4.3. Seismic load in model with 0.2g, 0.3g, 0.4g, 0.5g amplitude and 2 Hz frequency

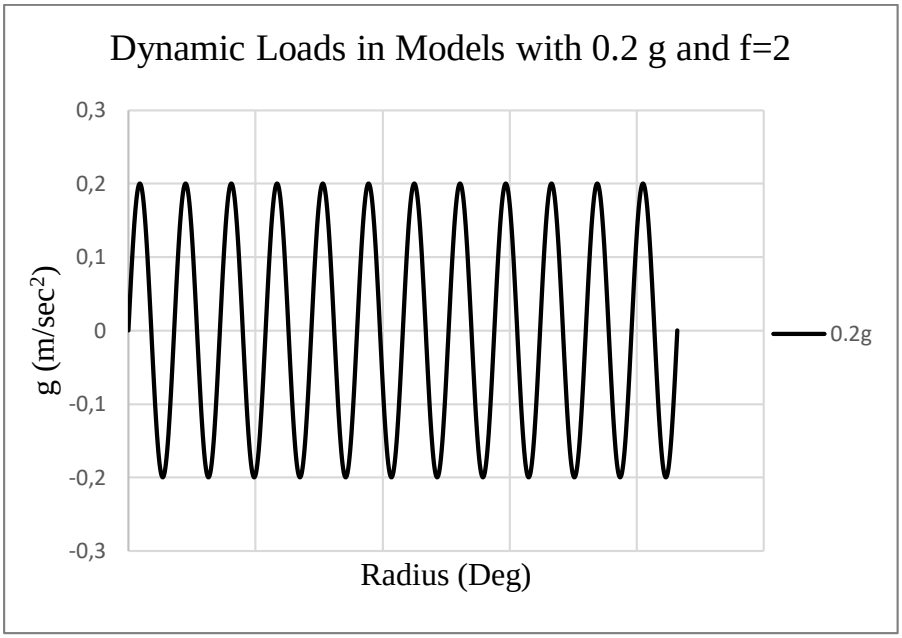

Figure 4.4. Seismic load in model with 0.2g amplitude and 2 Hz frequency

4.6. Numerical Analysis Results

The loads are varied with different amplitudes with 0.2 g, 0.3 g, 0.4 g, and 0.5 g. The frequency of the dynamic loads is the same as 2 Hz. Dynamic loads are applied from the bottom of the numeric model. Figure 4.3. and figure 4.4. show the dynamic loads in the model. There is no explicit agreement on what affects the liquefaction resistance of sands and silty sands. The results investigate the liquefaction phenomenon in different conditions, such as different fine content and relative density. Pore Water Pressure, Pore Water Pressure ratio, Vertical Displacement (Y_{disp}), Shear Stress, Shear Strain, Cyclic Stress Ratio, Number of Cycles to Liquefaction, and Cyclic Resistance Ratio (CRR) results are determined by liquefaction. These results help evaluate the effects of soil properties and acceleration on liquefaction. Also, these numerical results were verified with the laboratory work of Tutuncu (2021) and Monkul (2021).

The beginning of liquefaction studies was analyzed considering cohesion less soil, but many numerical and experimental studies indicated that liquefaction was also observed in silty sand. It was also observed that based on ground acceleration and environmental factors, almost all soils, including sands, silts, clays, and gravels, and their mixtures could liquefy. The purpose is to describe the effect of liquefaction on the

dynamic behavior of silty sand and to investigate whether the liquefaction resistance of silt sand is related to different accelerations.

4.6.1. Pore Water Pressure Ratio (r_u)

To examination the triggering of liquefaction, the ratio of excess pore pressure to initial effective stress ($r_u=\Delta u/\sigma_{v0}'$) is obtained. When excess pore pressure value is equal to or close to effective stress ($r_u=1$), liquefaction said to be triggered. The criterion required for liquefaction to occur and the experiment was determined by when the ru reaches one or peak to peak shear strain reaches 10 % in this study. However, in some cases, even if the excess pore pressure ratio reaches 1, the experiment continues until peak to peak shear strain reaches 10 %. In this case, after the experiment was completed, the value at which the excess pore pressure ratio is equal to one was used as the required number of cycles to occur liquefaction.

Four different FC are examined in this thesis. At each FC, different D_r of soil was modeled. Results are taken from the middle of the model at 9 m depth ($\gamma'z$= ((20.5-9,81)kg/m^3 x 9m) = 96.21 kPa approximately 100 kPa differences 4%). All models are consolidated to vertical stresses of 100 kPa (σ'_{vc} = 100 kPa). When the FC and relative density of the soil are increased, liquefaction triggered potential is decreased. Figure 4.5. shows the pore water pressure ratio change by time in FC 0% soil with three relative densities (18%, 55%, and 83%) and ground acceleration of 0.2g. Figure 4.6. shows the pore water pressure ratio change by time in FC 5% soil with three relative densities (18%, 31%, and 77%) and ground acceleration of 0.2g. Figure 4.7. shows the pore water pressure ratio change by time in FC 15% soil with three relative densities (21%, 38%, and 46%) and ground acceleration of 0.2g. Figure 4.8. shows the pore water pressure ratio change by time in FC 35% soil with three relative densities (23%, 32%, and 79%) and ground acceleration of 0.2g. When relative density increases, liquefaction resistance increased. Table 4.5. shows the liquefaction triggered cycles (N_L) of each test from r_u. Appendix A, B and C are showed results of 0.3g, 0.4g, and 0.5g ground acceleration.

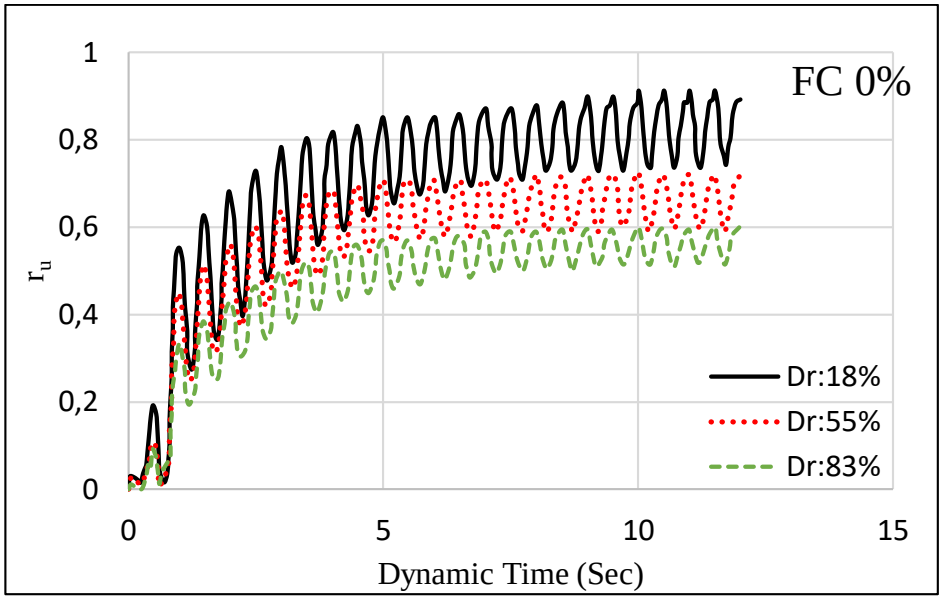

Figure 4.5. r_u vs time in FC 0% soil with three different relative densities, ground acceleration 0.2g and frequency 2 Hz

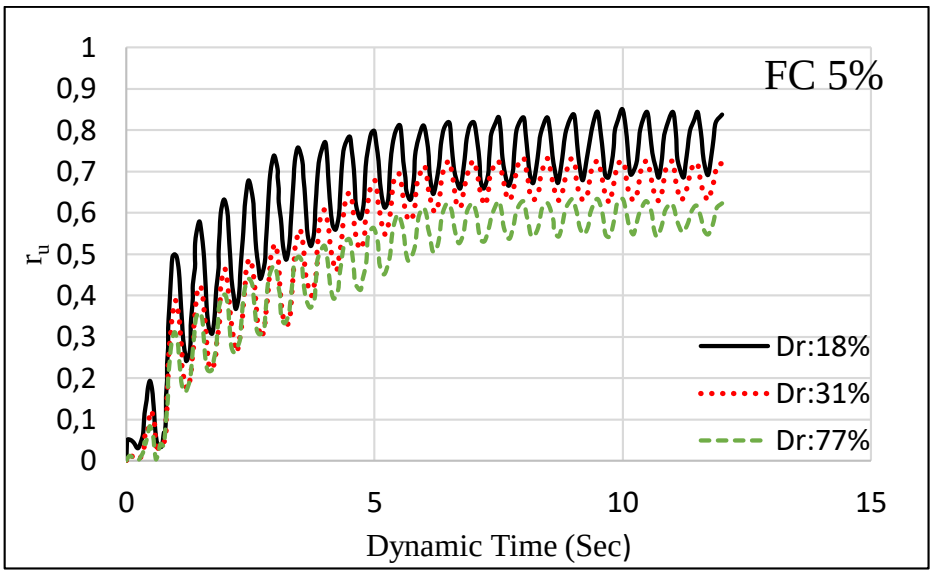

Figure 4.6. r_u vs time in FC 5% soil with three different relative densities, ground acceleration 0.2g and frequency 2 Hz

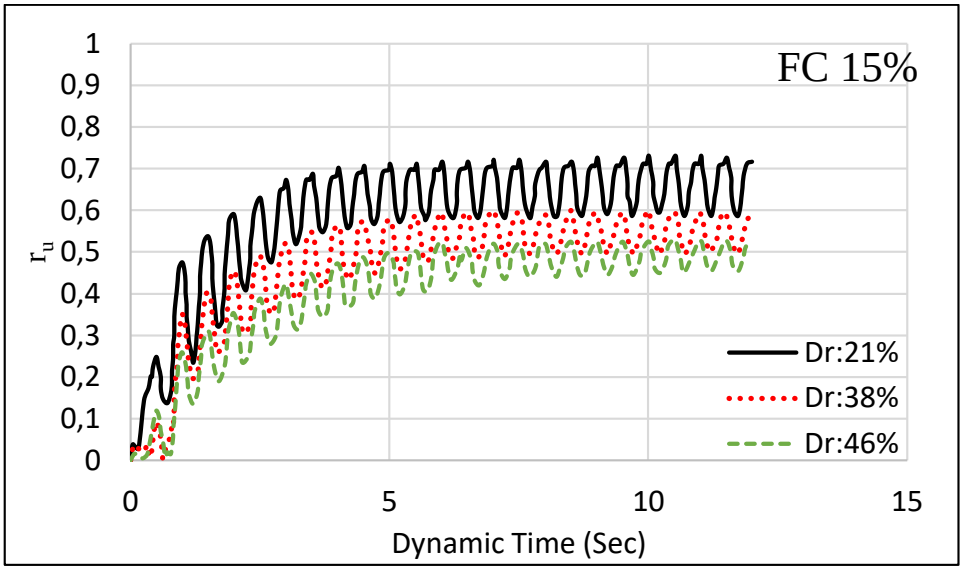

Figure 4.7. r_u vs time in FC 15% soil with three different relative densities, ground acceleration 0.2g and frequency 2 Hz

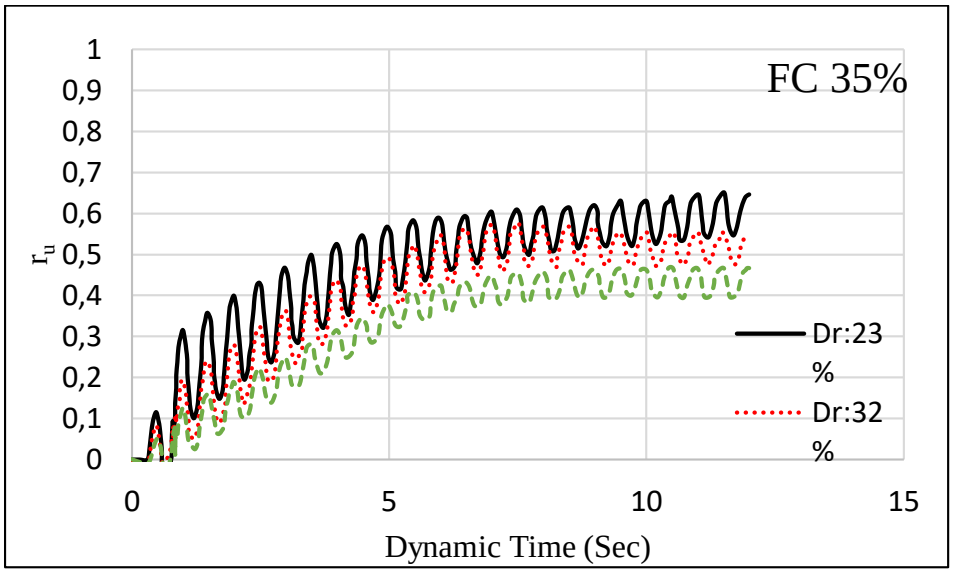

Figure 4.8. r_u vs time in FC 35% soil with three different relative densities, ground acceleration 0.2g and frequency 2 Hz

Table 4.5. Liquefaction triggered cycle (N_L) summary from r_u for 0.2g

FC (%)	**D_r% (%)**	**Liquefaction triggered cycle (N_L)**
0	18	11
	55	14
	83	15
5	18	10
	31	14
	77	15
15	21	10
	38	11
	46	16
35	23	15
	32	16
	79	17

4.6.2. Vertical Direction Displacement

Vertical displacement in the middle of soils with four different fine contents is examined in this thesis. At each fine content, different relative density soil was modeled. When the soil's fine content and relative density are increased, liquefaction triggered potential is decreased. Therefore, displacement results are varied. Displacements are directly related to the liquefaction potential. When liquefaction impacts are decreased, displacements are decreased as well. Figure 4.9. shows the change of vertical displacement by time in FC 0% soil with three different relative densities (18%, 55%, and 83%) and ground acceleration of 0.2g. Figure 4.10. shows the vertical displacement by time in FC 5% soil with three relative densities (18%, 31%, and 77%) and ground acceleration of 0.2g. Figure 4.11. shows the vertical displacement by time in FC 15% soil with three relative densities (21%, 38%, and 46%) and ground acceleration of 0.2g. Figure 4.12. shows the change of vertical displacement by time in FC 35% soil with three different relative densities (23%, 32%, and 79%) and ground acceleration of 0.2g Table

4.6. shows summary results of vertical displacement at liquefaction triggered. When FC and D_r are increased, vertical displacement is decreased. Generally, minimum vertical displacement is obtained in maximum FC of 35%.

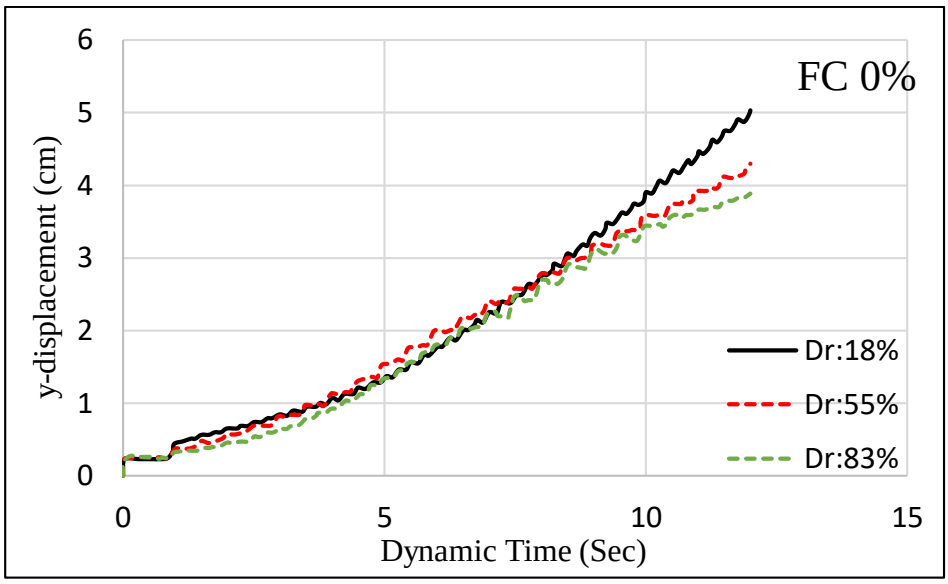

Figure 4.9.Vertical displacement vs time in FC 0 % soil with three different relative densities, ground acceleration 0.2g and frequency 2 Hz

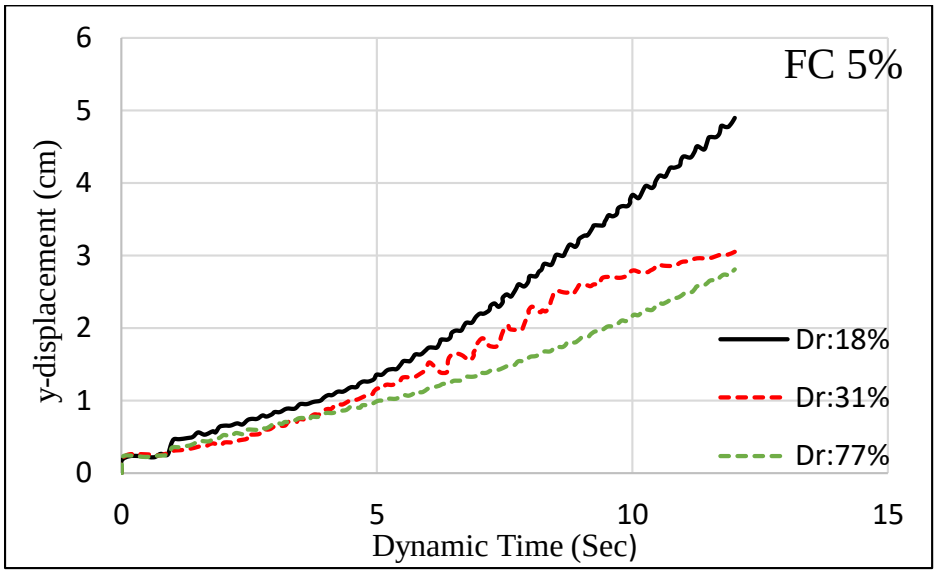

Figure 4.10. Vertical displacement vs time in FC 5 % soil with three different relative densities, ground acceleration 0.2g and frequency 2 Hz

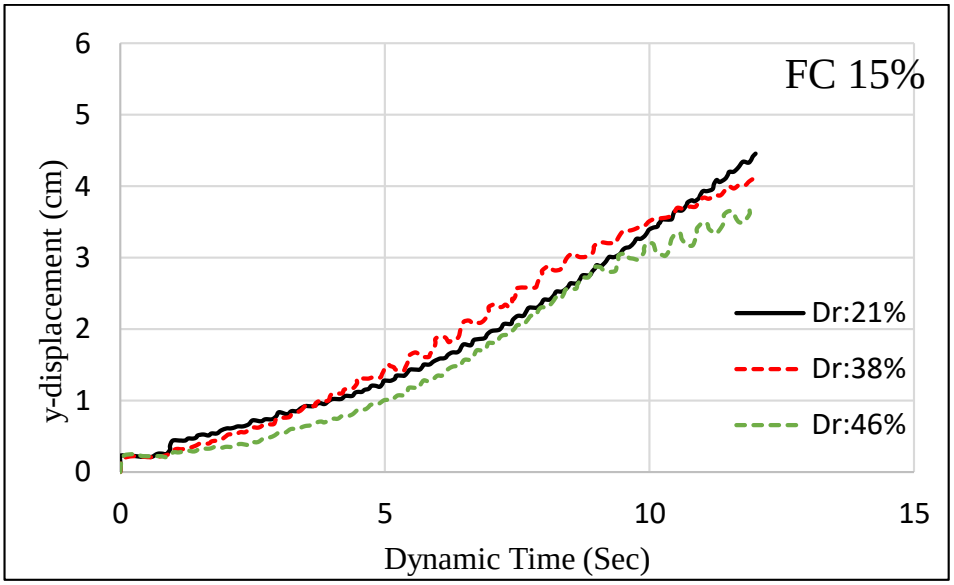

Figure 4. 11. Vertical displacement vs time in FC 15 % soil with three different relative densities, ground acceleration 0.2g and frequency 2 Hz

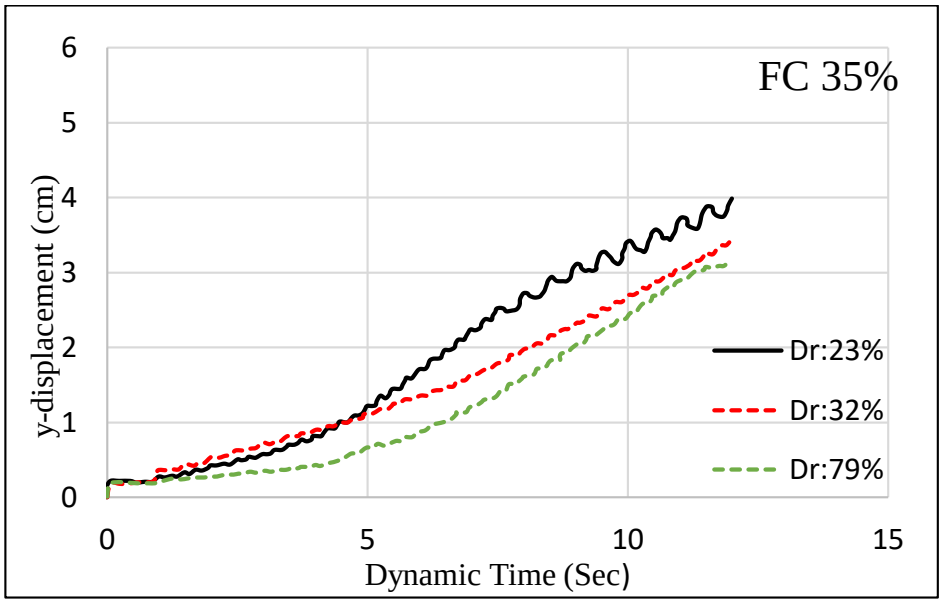

Figure 4.12. Vertical displacement vs time in FC 35 % soil with three different relative densities, ground acceleration 0.2g and frequency 2 Hz

Table 4.6. Liquefaction triggered cycle (N_L) summary from r_u for 0.2g

FC (%)	D_r (%)	Vertical displacement (cm)
0	18	5.00
	55	4.20
	83	3.95
5	18	4.96
	31	3.00
	77	2.85
15	21	4.50
	38	4.10
	46	3.75
35	23	4.00
	32	3.40
	79	3.20

4.6.3. Number of Cycles to Liquefaction

Figure 4.13. shows N_L and D_r with four different FC, ground acceleration of 0.2g and frequency of 2 Hz. Figure 4.14. shows N_L and D_r with four different FC, ground acceleration of 0.3g, and frequency 2 Hz. Figure 4.15. shows N_L and D_r with four different FC, ground acceleration of 0.4g and frequency 2 Hz. Figure 4.16. shows N_L and D_r with four different FC, ground acceleration of 0.5g, and frequency 2 Hz. Results were done on several different D_r values on various silty sand specimens having different fines contents. Where the change in the number of cycles to liquefaction (N_L) with relative density at different CSRs can be observed in the figures. They show that NL increases with increasing relative density at a given CSR, which is an expected trend. However, the exponential trend of increase in N_L seems to be more appropriate as the magnitude of CSR decreases. A similar trend was consistently observed for the other sands and silty sands (with different FC and relative density) modeled in this thesis.

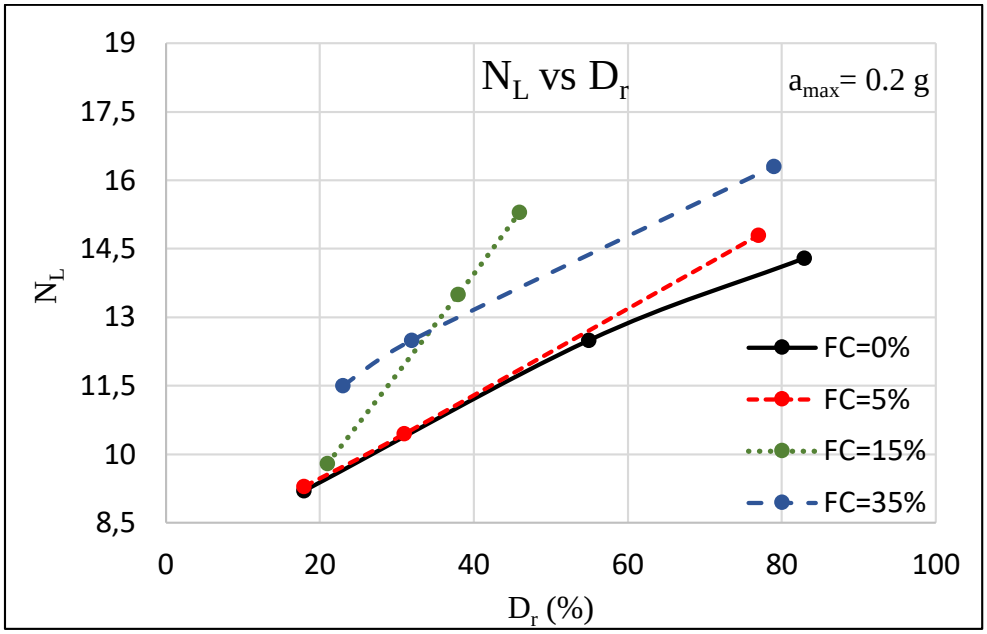

Figure 4.13. N_L with D_r at four different fine content, ground acceleration 0.2g and frequency 2 Hz

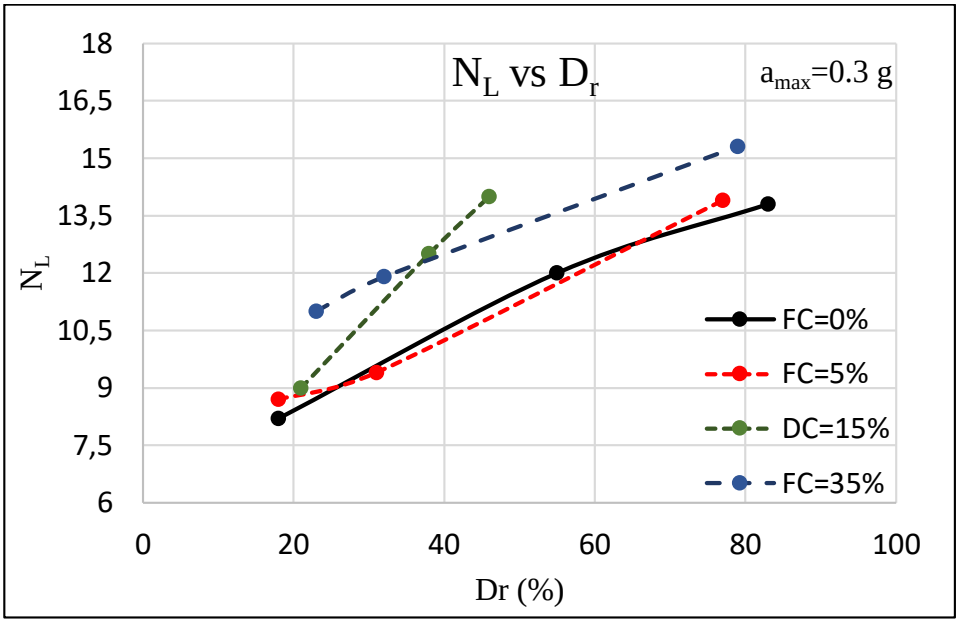

Figure 4.14. N_L with D_r at four different fine content, ground acceleration 0.3g and frequency 2 Hz

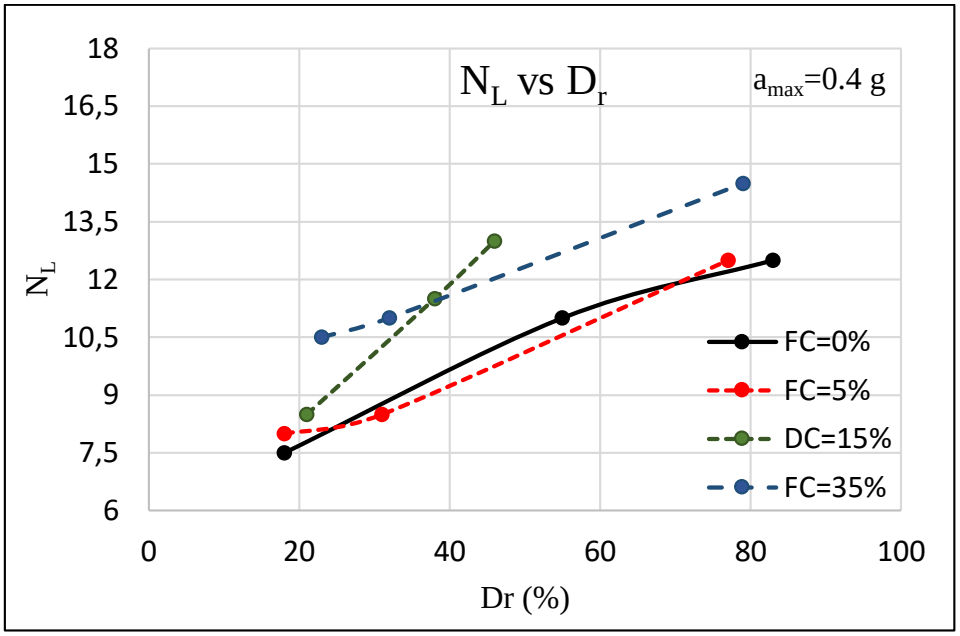

Figure 4.15. N_L with D_r at four different fine content, ground acceleration 0.4g and frequency 2 Hz

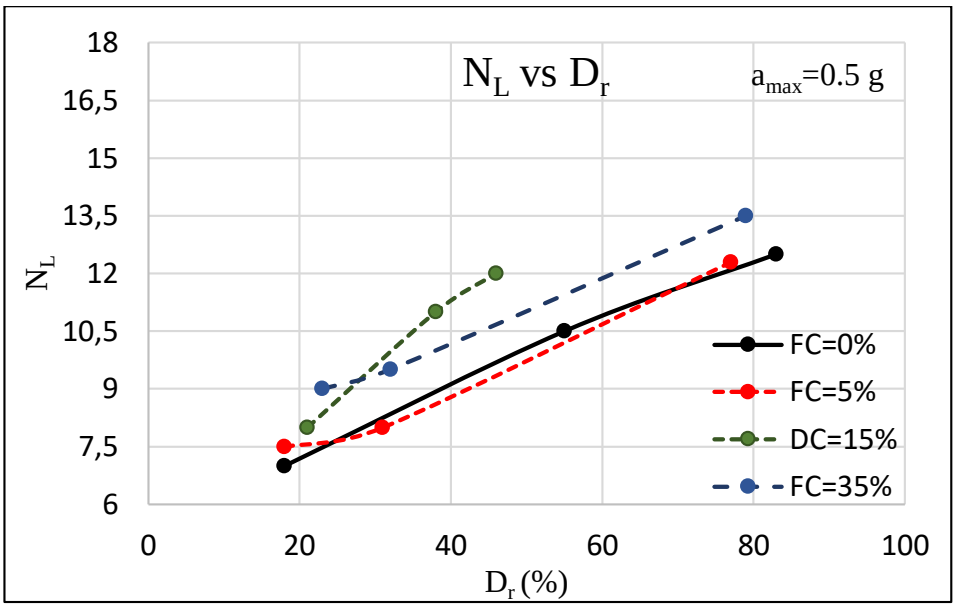

Figure 4.16. N_L with D_r at four different fine content, ground acceleration 0.5g and frequency 2 Hz

Figure 4.17. shows CSR and N_L in FC 0% soil with three different D_r, ground acceleration of 0.2g, and frequency 2 Hz. Figure 4.18. shows CSR and N_L in FC 5% soil with three different D_r, ground acceleration of 0.2g, and frequency 2 Hz. Figure 4.19. shows CSR and N_L in FC 15% soil with three different D_r and ground acceleration of 0.2g

and frequency 2 Hz. Figure 4.20. shows CSR and N_L in FC 35% soil with three different D_r, ground acceleration of 0.2g, and frequency 2 Hz. Figure 4.21. shows numerical and test results of N_L and D_r with different FC and ground acceleration of 0.2g. N_L required for liquefaction of silty sands with 5%. FC increased faster than clean sands as CSR decreased. This shows that silty sands with 5%. FC are more resistant than clean sands. N_L required for liquefaction of silty sands with 35%. FC increased less than the sands as CSR decreased. Therefore, clean sands are more resistant compared to silty sands with 35% FC. This condition is different for silty sands with 15% FC. In cases where the D_r is lower than 35%, N_L required for liquefaction of clean sands is higher than silty sands with 15% FC as CSR decreases.

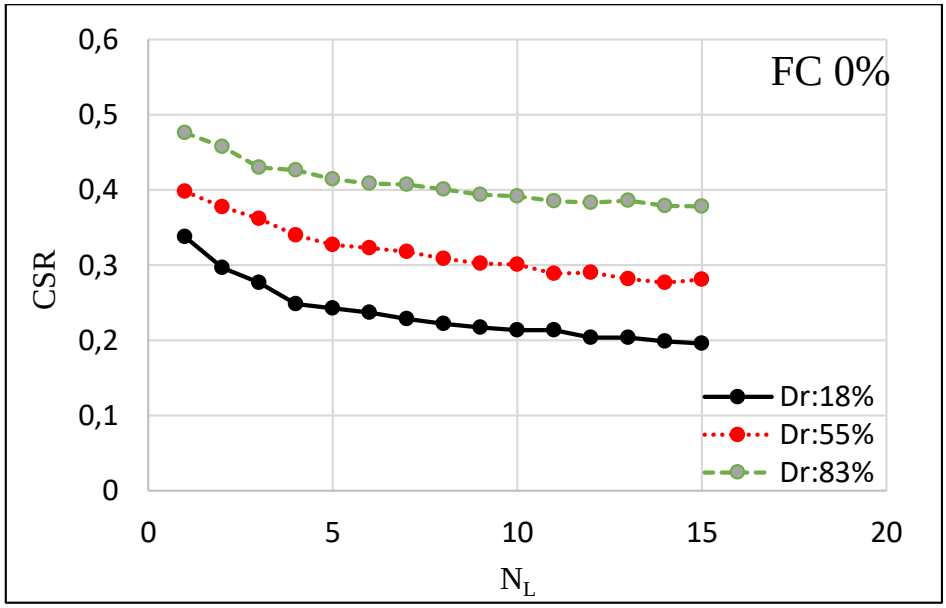

Figure 4.17. CSR vs N_L in FC 0% with three different relative densities, ground acceleration 0.2g and frequency 2 Hz

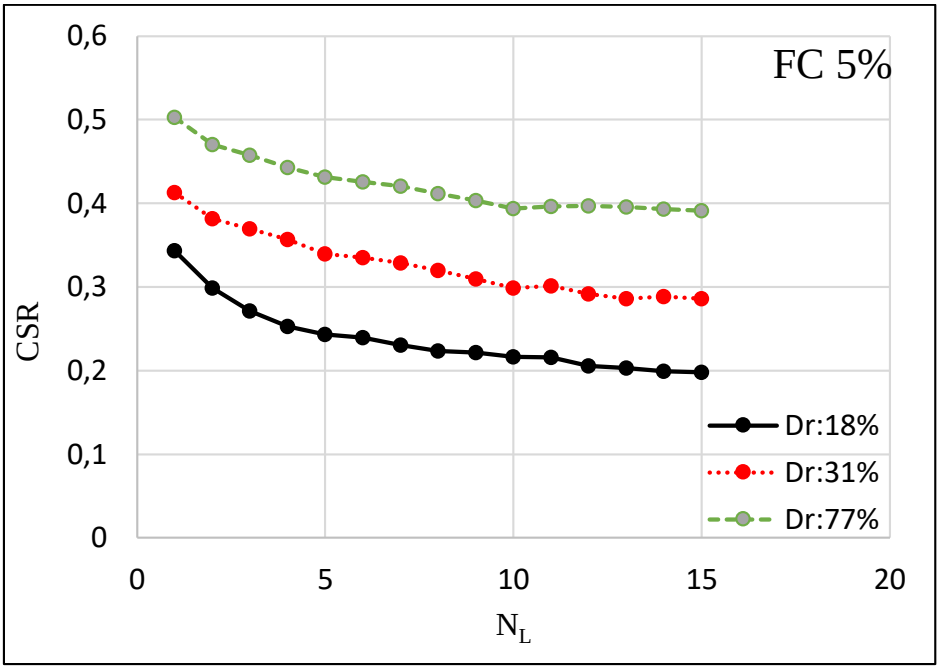

Figure 4.18. CSR vs N_L in FC 5% with three different relative densities, ground acceleration 0.2g and frequency 2 Hz

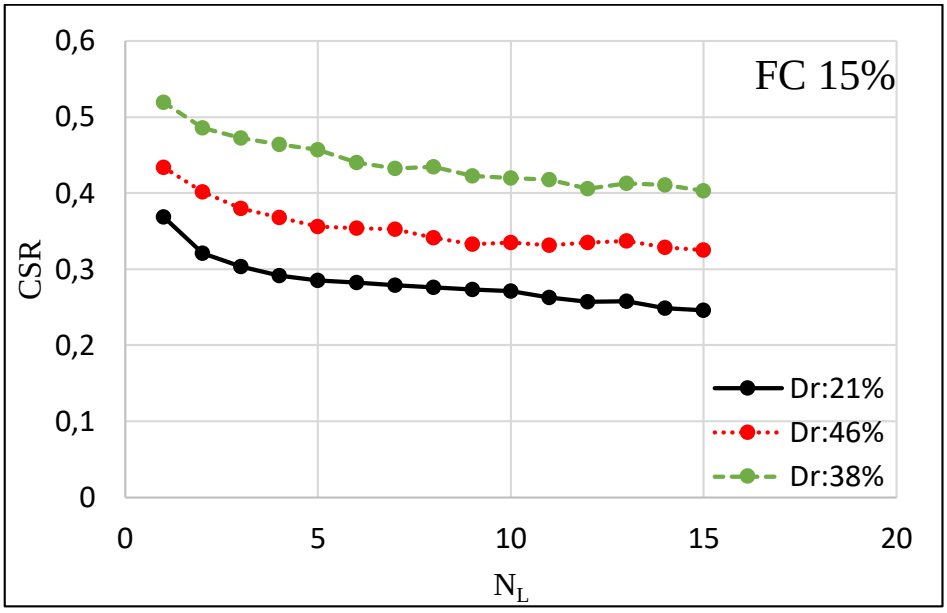

Figure 4.19. CSR vs N_L in FC 15% with three different relative densities, ground acceleration 0.2g and frequency 2 Hz

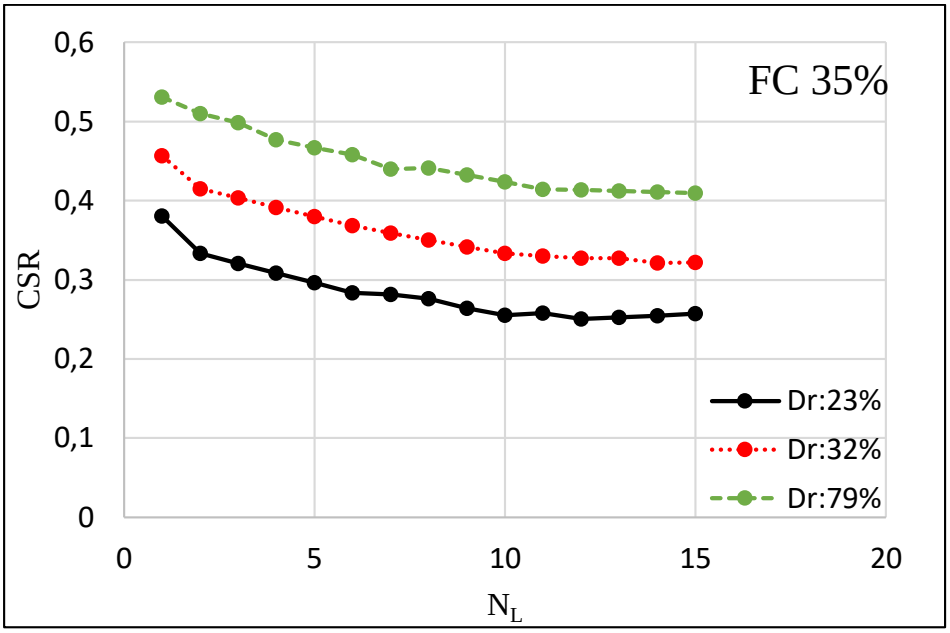

Figure 4.20. CSR vs N_L in FC 35% with three different relative densities, ground acceleration 0.2g and frequency 2 Hz

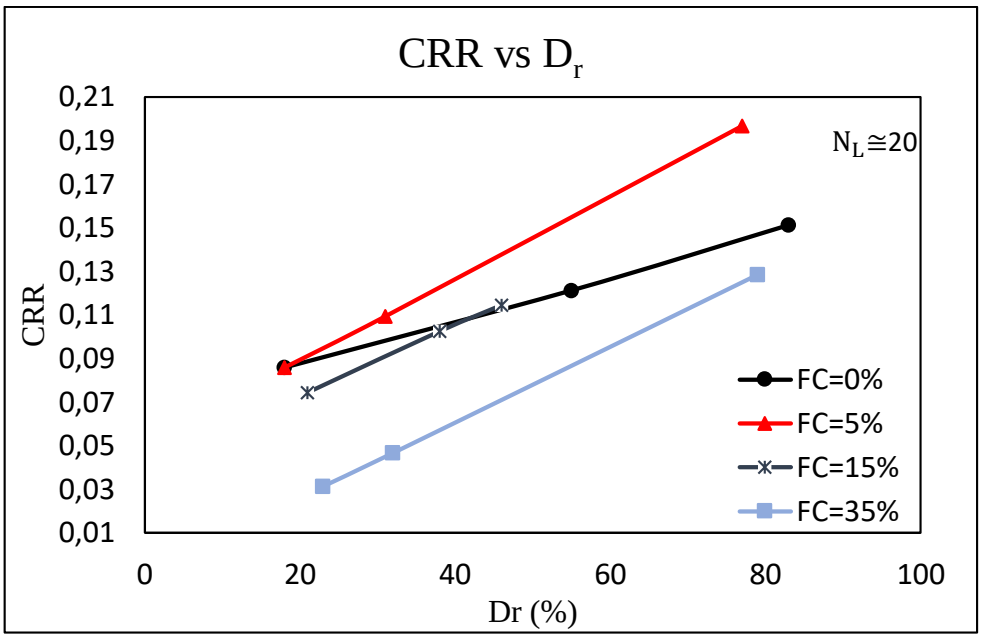

Figure 4.21. CRR vs D_r with four different fine content, ground acceleration 0.2g and frequency 2 Hz

4.6.4. Shear Stress Versus Shear Strain

The numerical model tests are made on several different D_r values on different silty sand specimens having different fines contents and ground acceleration. Shear stress and strain results are shown in Figures 4.22, 4.23, 4.24, and 4.25. The change in relative density and fine content at the same ground acceleration 0.2g can be observed in effect on liquefaction. When the soil's relative density and fine content increase, liquefaction effects are decreased. Results show the same shear stress and less shear strain with different relative density and fine content.

Figure 4.22. shows numerical shear stress versus shear strain results in FC 0% soil with three relative densities (18%, 55%, and 83%) and ground acceleration of 0.2g. Figure 4.23. shows numerical shear stress and shear strain results in FC 5% soil with three relative densities (18%, 31%, and 77%) and ground acceleration of 0.2g. Figure 5.24. shows numerical shear stress and shear strain results in FC 15% soil with three relative densities (21%, 38%, and 46%) and ground acceleration of 0.2g. Figure 4.25. shows numerical shear stress and shear strain results in FC 35% soil with three relative densities (23%, 32%, and 79%) and ground acceleration of 0.2g.

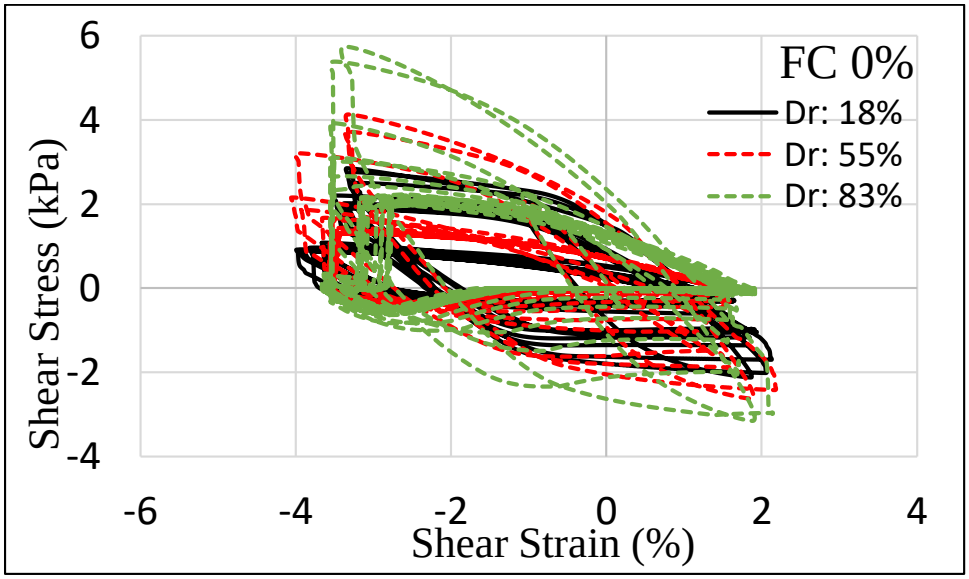

Figure 4.22. Shear stress vs shear strain in FC 0% soil with three different relative densities, ground acceleration 0.2g and frequency 2 Hz

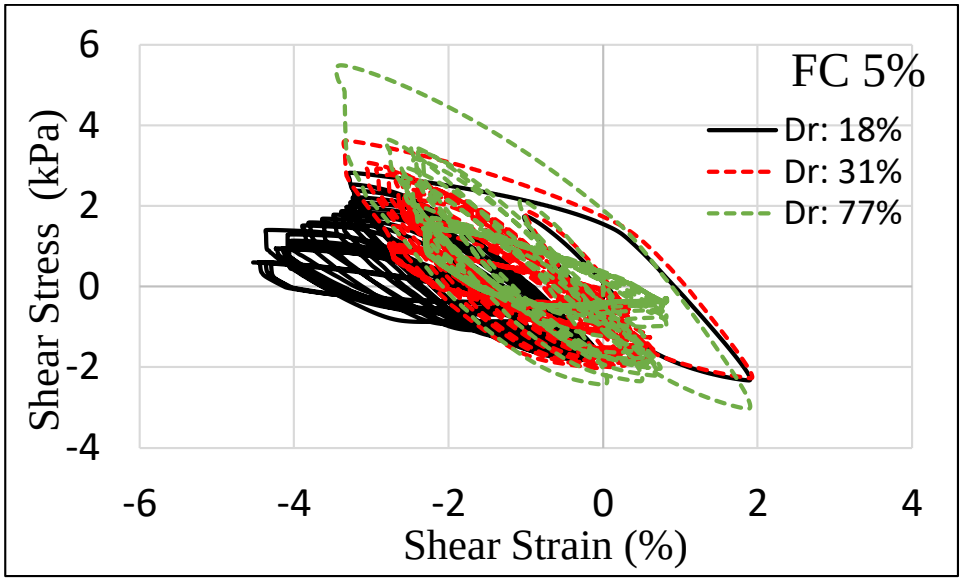

Figure 4.23. Shear stress vs shear strain in FC 5% soil with three different relative densities, ground acceleration 0.2g and frequency 2 Hz

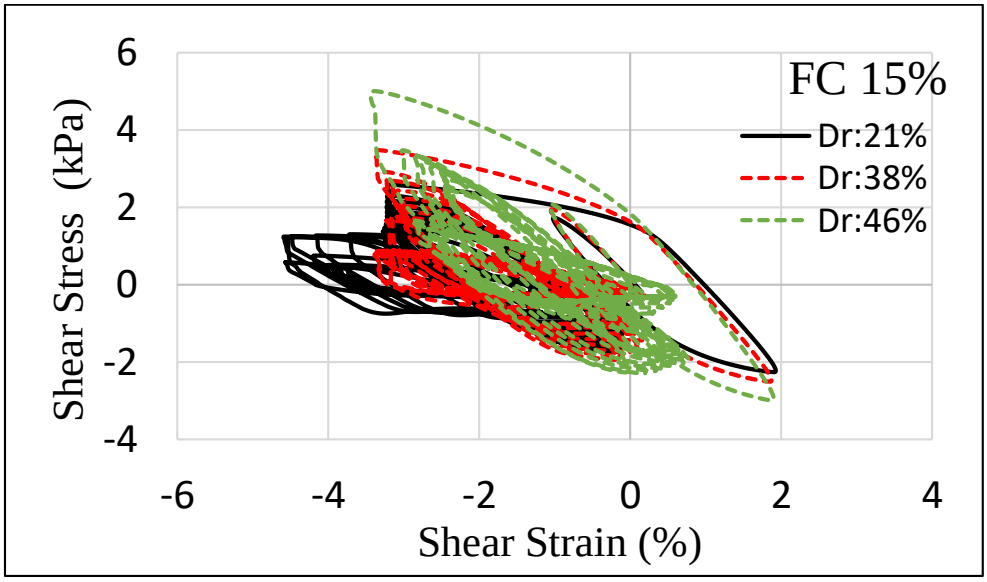

Figure 4.24. Shear stress vs shear strain in FC 15% soil with three different relative densities, ground acceleration 0.2g and frequency 2 Hz

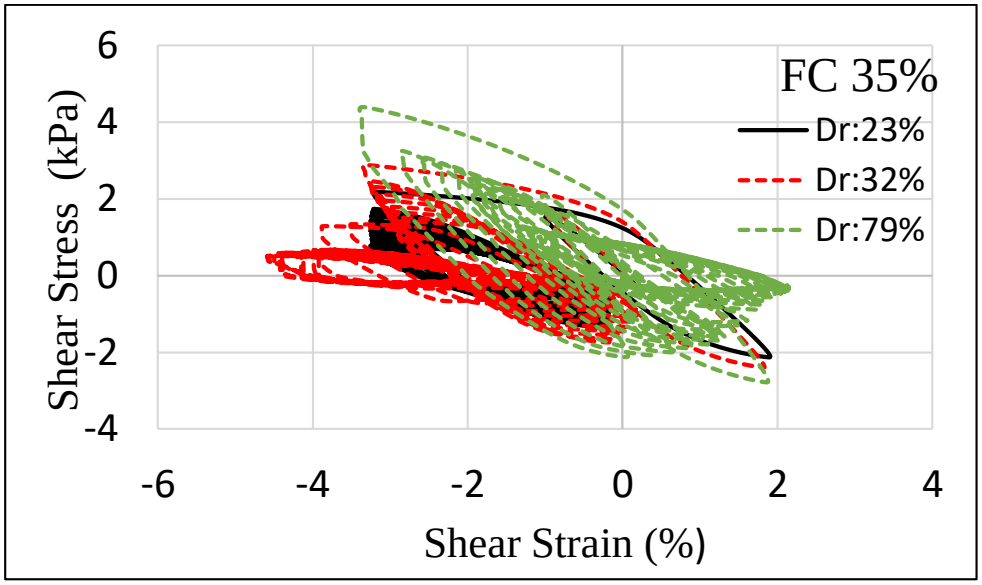

Figure 4.25. Shear stress vs shear strain in FC 35% soil with three different relative densities, ground acceleration 0.2g and frequency 2 Hz

4.6.5. Comparison of the Numerical and the CDSS Test Results

4.6.5.1 Shear Stress Versus Shear Strain

Figure 4.26. compares the numerical and CDSS test results of shear stress and shear strain in FC 0% soil with 55% Dr and ground acceleration of 0.2g. Figure 4.27. compares numerical and CDSS test of shear stress and shear strain in FC 0% soil with 83% and 73% Dr and ground acceleration of 0.2g. Hysteresis loop obtained in the shear stress and strain graph from numerical and CDSS test results.

Figure 4.28. compares numerical and CDSS test results of shear stress and shear strain in FC 5% soil with 77% and 67% D_r and ground acceleration of 0.2g.

Figure 4.29. compares numerical and CDSS test of shear stress and shear strain in FC 15% soil with 38% and 46% Dr and ground acceleration of 0.2g Figure 4.30. compares numerical and CDSS test results of shear stress and shear strain in FC 15% soil with 46% and 57% D_r and ground acceleration of 0.2g.

Figure 4.31. compares numerical and CDSS test of shear stress and shear strain in FC 35% soil with 23% and 32% D_r and ground acceleration of 0.2g. Figure 4.32.

compares numerical and CDSS test results of shear stress and shear strain in FC 35% soil with 79% and 82% D_r and ground acceleration of 0.2g. CDSS test results are obtained from Tutuncu's thesis (2021). 123 CDSS tests are performed in total and seven CDSS tests are compared with the numerical results performed in this study. The reason to compare only seven CDSS results is D_r values are close. In this thesis, close D_r values are used for comparison with CDSS test. In this study, applied dynamic load to the base of the model was amax 0.2g and frequency 2 Hz. The CDSS test results obtained from the CSR of 0.14 approximately 0.2g and 0.1 Hz frequency. Therefore, CDSS tests have a bigger loop and greater value of shear stress and strain than the numeric study performed in this study.

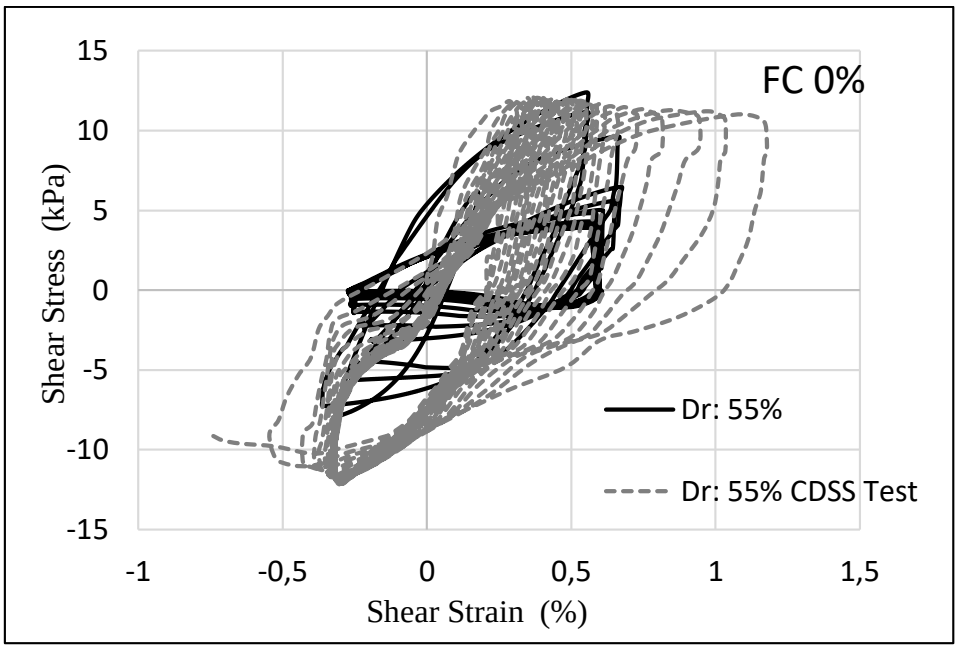

Figure 4.26. Shear stress vs shear strain in FC 0%, D_r 55 % and D_r 55 % soil with CDSS test results and ground acceleration 0.2g and frequency 2 Hz

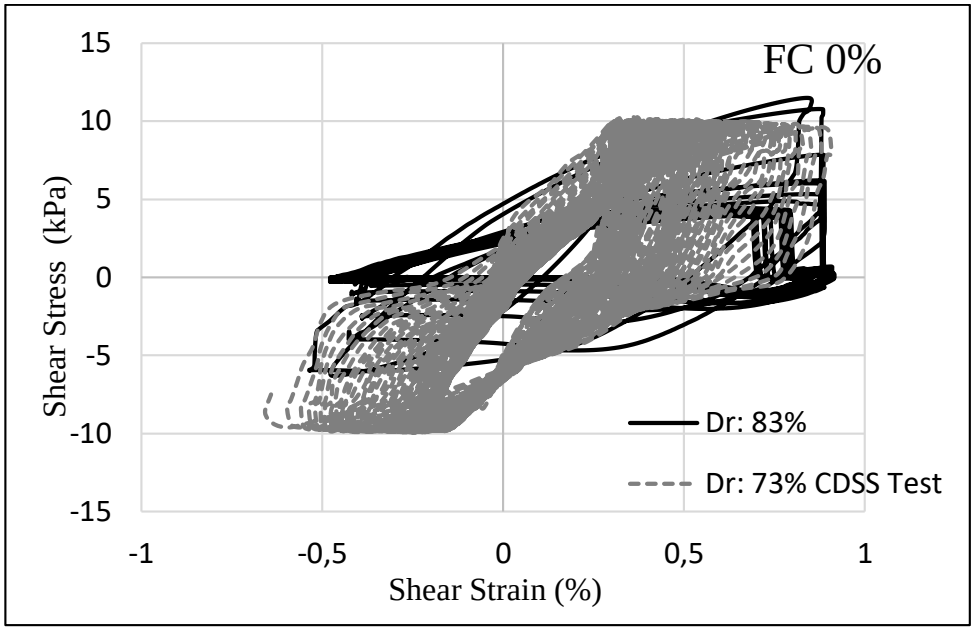

Figure 4.27. Shear stress vs shear strain in FC 0%, D_r: 83 % and D_r: 73 % soil with CDSS test results and ground acceleration 0.2g and frequency 2 Hz

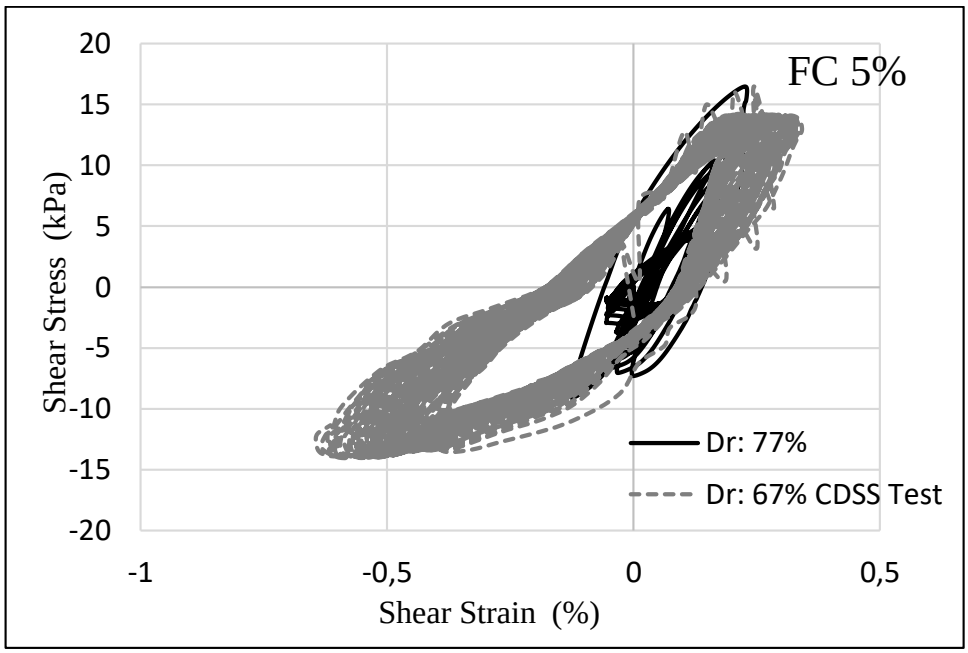

Figure 4.28. Shear stress vs shear strain in FC 5%, D_r: 77 % and D_r: 67 % soil with CDSS test results and ground acceleration 0.2g and frequency 2 Hz

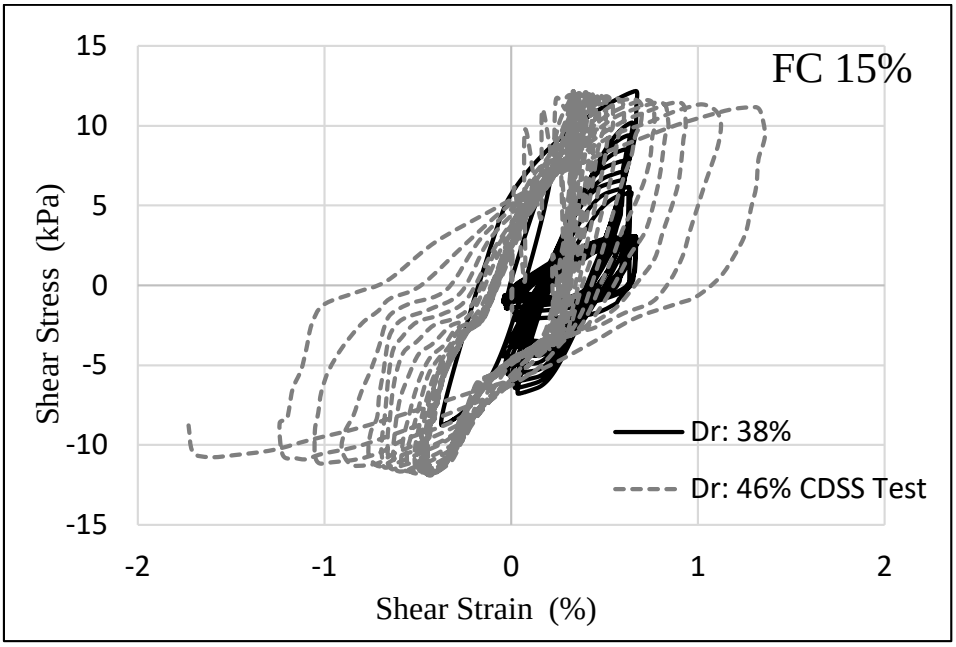

Figure 4.29. Shear stress vs shear strain in FC%15, D_r: 36 % and D_r: 46 % soil with CDSS test results and ground acceleration 0.2g and frequency 2 Hz

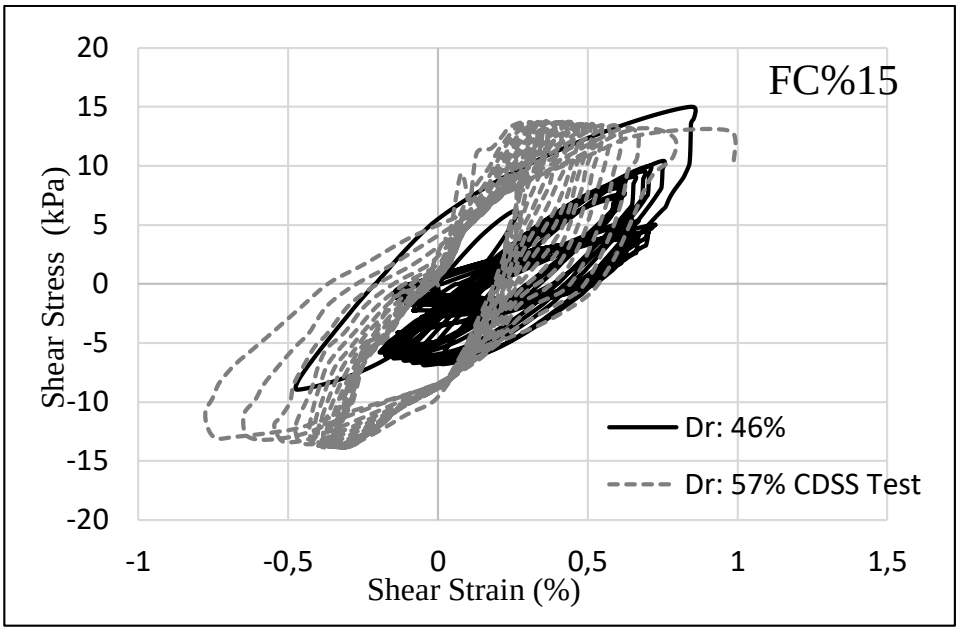

Figure 4.30. Shear stress vs shear strain in FC%15, D_r: 46 % and D_r: 57 % soil with CDSS test results and ground acceleration 0.2g and frequency 2 Hz

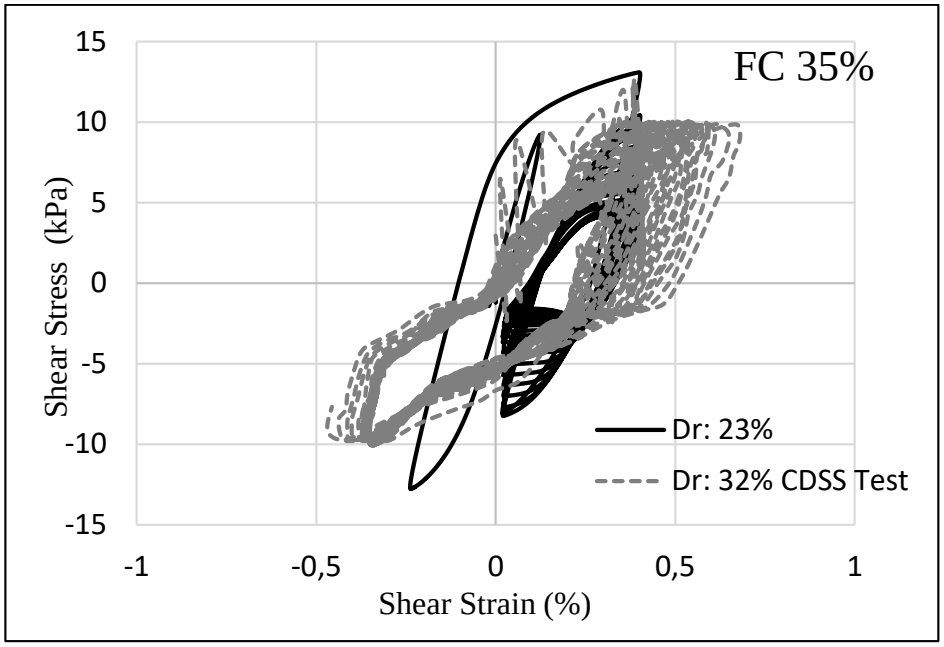

Figure 4.31. Shear stress vs shear strain in FC 35%, D_r: 23 % and D_r: 32 % soil with CDSS test results and ground acceleration 0.2g and frequency 2 Hz

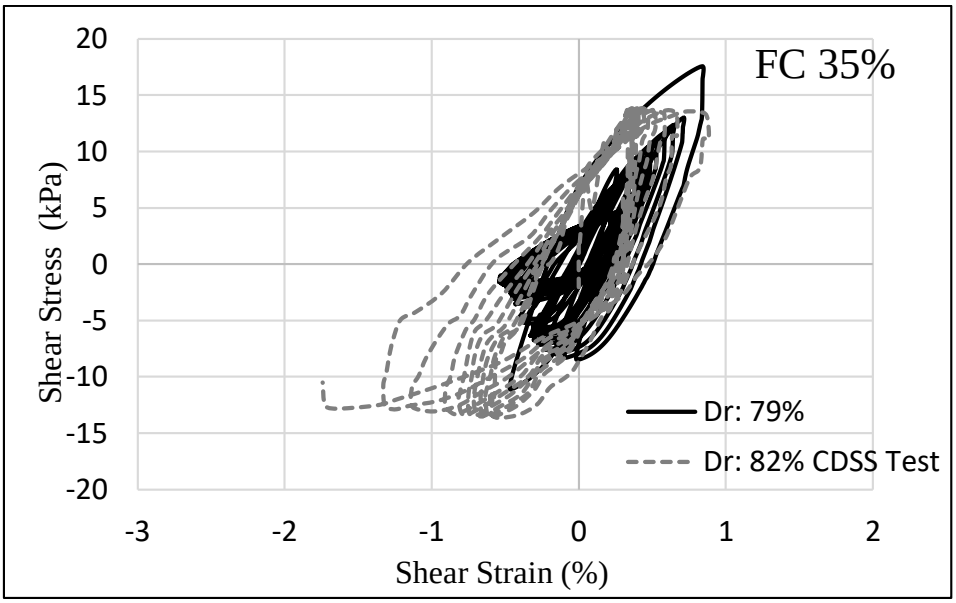

Figure 4.32. Shear stress vs shear strain in FC 35 %, D_r: 79 % and D_r: 82 % soil with CDSS test results, ground acceleration 0.2g and frequency 2 Hz

4.6.5.2 Pore Water Pressure

The numerical CRR-D_r results given above (Figure 4.33) were compared with the CDSS test results of Tutuncu (2021) and Monkul et al. (2021). The numerical results obtained from this study and the laboratory experiments conducted at Yeditepe University gave similar results. Similarly, different failure criteria used in different studies could influence the absolute values of CRR for silty sands. For instance, some of them used r_u = 1 as the liquefaction criterion (Oka, 2008). Others used 5% double amplitude axial strain (Carraro, 2003), while this thesis adopted a dual criterion (either r_u = 1 or 10% shear strain). The 10% shear strain corresponds to approximately 6.75% axial strain in triaxial conditions, more significant than many previous triaxial studies employing the strain criterion.

However, some of them considered 15 cycles of uniform loading (Polito, 2001), while others considered 20 cycles of uniform loading (Carraro, 2003) to obtain the CRR of different silty sands. In CDSS tests, twenty cycles of uniform loading (N_L=20) are preferred. The numerical analysis gave accurate results and provided time and cost savings at this rate. Figure 4.33. shows numerical and test results of N_L and D_r with different FC and ground acceleration of 0.2g from Monkul, 2021. The results are similar. Hence, the numerical model and element test model gave relevant results.

Figure 4.33. shows the comparison of the numerical and test results. It gives the relationship with fine content and relative density on liquefaction resistance. When the CRR of soils are affected by both FC and the D_r. As the Dr increased, the CRR increased as expected. First of all, the liquefaction resistance of clean sand and silty sands with 5% fine contents are close to the silty sand with 15 % FC. Secondly, the silty sands with 15 % FC have lower liquefaction resistance compared to the liquefaction resistance of clean sand and silty sands with 5 % FC for less than about 40 % D_r. Lastly, although the Dr range of silty sands with 35 % FC is between 40 % and 80 %, it is clear that the liquefaction resistance of silty sands with 35 % FC is less than the liquefaction resistance of clean sand. When the Figure 4.33 is carefully analyzed, the positive effect of the D_r on liquefaction resistance of the silty sand, especially for FC 5 %, has become much clear as the relative density increases. Another point is that the CRR has the maximum value in 5 % FC, and then it started to decrease with increasing FC. As a result of thesis performed under different FC and D_r, it was observed that the number of cycles increased with

increasing relative density. They performed at various relative densities, it was observed that the N_L increased as the CSR decreased. Results show that liquefaction resistance of silty sands with 5 % FC increases compared to the resistance of clean sands and liquefaction resistance of silty sands with 35 % FC decreases compared to the resistance of clean sands. Also, results show that liquefaction resistance of silty sands with 15 % FC decreases on soil model where the D_r is less than 40 % compared to the resistance of clean sands and liquefaction resistance of silty sands with 15 % FC increases on soil models where the D_r is higher than 40 % compared to the resistance of clean sands. Figure 4.33 is analyzed. For 4 different FC for, CSR reached a maximum value when the silt content increased up to 5%, then the cyclic resistance began to decrease as the FC increased. As the D_r increased, the increase of the cyclic resistance became reasonable for especially silty sand with 5% FC.

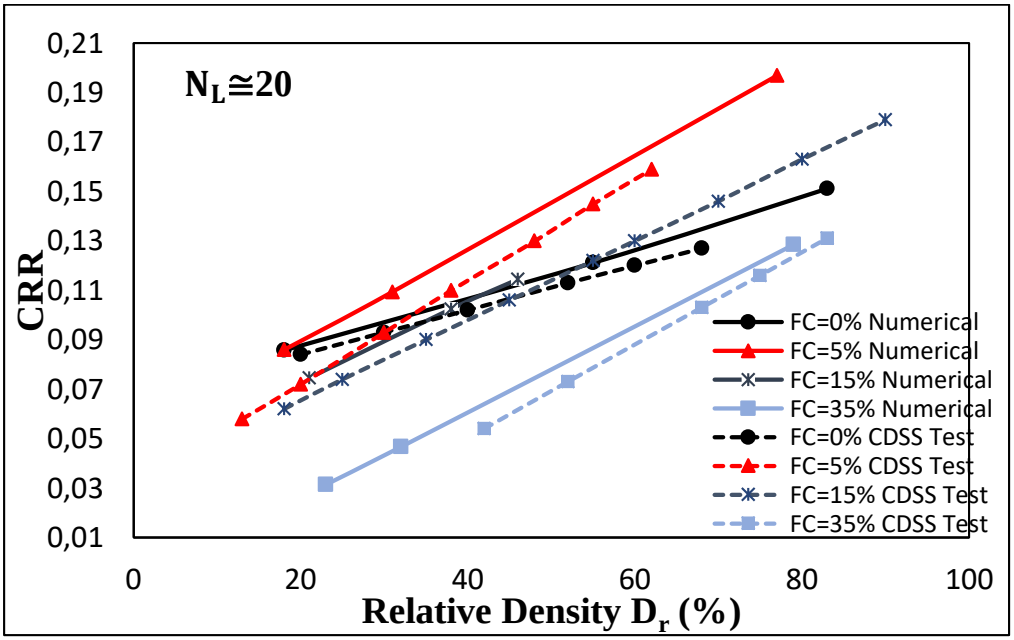

Figure 4.33. Comparison of liquefaction resistance versus relative density obtained from the numerical analysis and CDSS test

CHAPTER 5

CONCLUSION

5.1. Summary of Findings

In this thesis, the liquefaction triggering phenomena and a method for liquefaction palliation were examined based on the FDM numerical analysis. FLAC 2D geotechnical software program was used for the numerical calculations. Static and dynamic soil parameters were obtained from the laboratory test results of Arık (2021). The numerical liquefaction study was verified by using the CDSS test results of Tutuncu (2021).

The data from all these experiments were used to analyze the soil conditions prone to liquefaction. Then, CDSS test results performed for the same silty sands were used to verify the numerical study (Tutuncu, 2021 and Monkul, 2021). The effects of FC, a_{max} and D_r on liquefaction resistance of soil were obtained. It is found that CDSS test and numerical results are significantly similar. The CRR-D_r and shear stress and shear strain numerical results were compared with the CDSS test results. To consider the triggering of liquefaction, the ratio of pore pressure to initial effective stress ($r_u=\Delta u/\sigma_{v0}'$) is calculated. When pore pressure value is equal to or close to effective stress ($r_u=1$), liquefaction said to be triggered in the CDSS test and numerical results. CRR is the ratio of resistance of shear stress to liquefaction to the vertical effective stress.

The developed numerical model can be used in different studies for evaluating liquefaction phenomena. The response law of the effects of the fines content on the characteristics of the liquefaction resistance of silt sand soil is verified. These research results are consistent with the variation tendency of the Dr with the increase of FC. With a different Dr, the liquefaction resistance decreases with the increase of the FC. Fine content, relative density, and maximum ground acceleration are directly related to liquefaction resistance.

- When the D_r and FC increases, liquefaction resistance is increased.
- There is an inverse relationship between a_{max} and liquefaction resistance. When the a_{max} increases, liquefaction resistance is decreased.

- a_{max} and frequency are taken 0.2g and 2 Hz in this thesis. CDSS test results are calculated with 0.14 CSR approximately 0.2g and 0.1 Hz. Therefore, the difference between shear stress and strain loops is based on the different applied loading parameters.
- When the FC increases, shear stress and strain loops become smaller. So, the shear strain is decreased because of liquefaction resistance.
- As a result of the CDSS test and numerical model, it was observed that the liquefaction resistance increased with increasing relative density.
- It was discovered that several important factors including, FC, a_{max}, and D_r have coupled effects on liquefaction resistance. Therefore, when liquefaction resistance is investigated, their effects should be considered coupled, rather than individually.

Pore water pressure, r_u, Y_{disp}, σ, τ, CSR, N_L, CRR are determined with different soil properties and acceleration in FLAC-2D. The liquefaction phenomenon is compared with different FC, a_{max} and Dr with the CDSS test. These results proved the relationship between these conditions in liquefaction resistance. The validated numerical model can examine different model sizes, soil parameters, and dynamic loads (ground acceleration and frequency) in other studies. In the light of all these results, the effects of silty sands on clean sands have been compared with element CDSS tests and numerical analyses.

5.2. Suggestions for Future Research

Field surveys and full-scale laboratory experiments are not always applicable due to their high costs. Numerical solutions developed as an alternative to these, the field is modeled by numerical modeling in the computer environment, and the studies can be done more economically and realistically. There are several suggestions for future research.

1. The analysis can also be repeated by three-dimensional software (such as FLAC-3D). These analyses can be repeated with different conditions, such as in combination with dynamic and static loads.

2. In the thesis, the UBCSand model is used. Different soil models can be used as well.

3. SCPT can be modeled with the same conditions performed in the laboratory, and results can be compared.

4. The dynamic analysis can be repeated by changing the sinusoidal motion to a suitable earthquake loads. After the analysis, the effect of different earthquake motions can be analyzed and compared.

5. The model can be used in other parametric studies for investigating different conditions of liquefaction phenomena.

REFERENCES

Andrews, D. C., & Martin, G. R. 2000, January. Criteria for liquefaction of silty soils. In Proc., 12th World Conf. on Earthquake Engineering (pp. 1-8). Upper Hutt, New Zealand: NZ Soc. for EQ Engrg.

Andrus, R. D., & Stokoe II, K. H. 2000. Liquefaction resistance of soils from shear-wave velocity. Journal of geotechnical and geoenvironmental engineering, 126(11), 1015-1025. Andrus, R. D., Stokoe, K. H., Chung, R. M., & Bay, J. A. (1998). Liquefaction evaluation of densified sand at approach to Pier 1 on Treasure Island, California, using SASW method.

Arab, A., & Belkhatir, M. 2012. Fines content and cyclic preloading effect on liquefaction potential of silty sand: a laboratory study. Acta Polytechnica Hungarica, 9(4), 47-64.

Arık, M. S. 2021. Effect of fines content on CPT resistance in silty sands (Master's thesis, Izmir Institute of Technology).

Astm, C. 1958. ASTM standards. Philadelphia: American Society for Testing Materials.

Bahadori, H., Farzalizadeh, R., Barghi, A., & Hasheminezhad, A. 2018. A comparative study between gravel and rubber drainage columns for mitigation of liquefaction hazards. Journal of Rock Mechanics and Geotechnical Engineering, 10(5), 924-934.

Beaty, M. H., & Byrne, P. M. 2011. UBCSAND constitutive model version 904aR. Itasca UDM Web Site, 69.

Beaty, M., & Byrne, P. M. 1998, August. An effective stress model for pedicting liquefaction behaviour of sand. In Geotechnical Earthquake Engineering and Soil Dynamics III (pp. 766-777). ASCE.

Beaty, M.H., Perlea, V.G., 2011. “Several observations on advanced analyses with liquefiable materials”, 21st Century Dam Design - Advances and Adaptations, 31st Annual USSD Conference, 11-15 April, San Diego, California.

Benmebarek, S., Djeridi, S., Benmebarek, N., & Belounar, L. 2018. Improvement of bearing capacity of strip footing on reinforced sand. International Journal of Geotechnical Engineering, 12(6), 537-545.

Bolton Seed, H., Tokimatsu, K., Harder, L. F., & Chung, R. M. 1985. Influence of SPT procedures in soil liquefaction resistance evaluations. Journal of geotechnical engineering, 111(12), 1425-1445.

Boulanger, R. W., & Idriss, I. M. 2014. CPT and SPT based liquefaction triggering procedures. Report No. UCD/CGM.-14, 1.

Boulanger, R. W., & Idriss, I. M. 2016. CPT-based liquefaction triggering procedure. Journal of Geotechnical and Geoenvironmental Engineering, 142(2), 04015065.

Bray, J. D., & Rodriguez-Marek, A. 2004. Characterization of forward-directivity ground motions in the near-fault region. Soil dynamics and earthquake engineering, 24(11), 815-828.

Bray, J. D., & Sancio, R. B. 2006. Assessment of the liquefaction susceptibility of fine-grained soils. Journal of geotechnical and geoenvironmental engineering, 132(9), 1165-1177.

Carraro, J. A. H., Bandini, P., & Salgado, R. 2003. Liquefaction resistance of clean and nonplastic silty sands based on cone penetration resistance. Journal of geotechnical and geoenvironmental engineering, 129(11), 965-976.

Carraro, J. A. H., Prezzi, M., & Salgado, R. 2009. Shear strength and stiffness of sands containing plastic or nonplastic fines. Journal of geotechnical and geoenvironmental engineering, 135(9), 1167-1178.

Celep Z., Kumbasar N. 2004: “Deprem Mühendisliğine Giriş ve Depreme Dayanıklı Yapı Tasarımı”, İstanbul, Beta Dağıtım.

Chen, S. G., Zhao, J., Makurat, A., & Madshus, C. 2000. Mesh size influence on dynamic modeling. Fragblast, 4(2), 164-174.

Das, B. M. (Ed.). 2010. Geotechnical engineering handbook. J. Ross publishing.

Dash, H. K., & Sitharam, T. G. 2009. Undrained cyclic pore pressure response of sand–silt mixtures: effect of nonplastic fines and other parameters. Geotechnical and Geological Engineering, 27(4), 501-517.

De Alba, P. A., Chan, C. K., & Seed, H. B. 1976. Sand liquefaction in large-scale simple shear tests. Journal of the Geotechnical Engineering Division, 102(9), 909-927.

Dobry, R., Ladd, R. S., Yokel, F. Y., Chung, R. M., & Powell, D. 1982. Prediction of pore water pressure buildup and liquefaction of sands during earthquakes by the cyclic strain method (Vol. 138, p. 150). Gaithersburg, MD: National Bureau of Standards.

Finn, W.D., Ledbetter, R.H., Marcuson, W.F. III, 1995. “Modern practice in the seismic response analysis of embankment dams”, Scientia Iranica, 2(2):145-164.

Georgiannou, V. N. 2006. The undrained response of sands with additions of particles of various shapes and sizes. Géotechnique, 56(9), 639-649.

Green, R. A., & Terri, G. A. 2005. Number of equivalent cycles concept for liquefaction evaluations—Revisited. Journal of Geotechnical and Geoenvironmental Engineering, 131(4), 477-488.

Hazirbaba, K., & Rathje, E. M. 2009. Pore pressure generation of silty sands due to induced cyclic shear strains. Journal of geotechnical and geoenvironmental engineering, 135(12), 1892-1905.

Huang, Y. T., Huang, A. B., Kuo, Y. C., & Tsai, M. D. 2004. A laboratory study on the undrained strength of a silty sand from Central Western Taiwan. Soil Dynamics and Earthquake Engineering, 24(9-10), 733-743.

Idriss, I. M., & Boulanger, R. W. 2006. Semi-empirical procedures for evaluating liquefaction potential during earthquakes. Soil dynamics and earthquake engineering, 26(2-4), 115-130.

Ishihara, K. 1993. Liquefaction and flow failure during earthquakes. Geotechnique, 43(3), 351-451.

Ishihara, K., Tatsuoka, F., & Yasuda, S. 1975. Undrained deformation and liquefaction of sand under cyclic stresses. Soils and foundations, 15(1), 29-44.

Itasca 2015. FLAC – Fast Lagrangian Analysis of Continua, Version, Itasca ConsultingbGroup, Inc., Minneapolis, Minnesota.

Kramer, S. L., Mayfield, R. T., & Huang, Y. M. 2008. Performance-Based Liquefaction Potential Evaluation.

Kuerbis, R., Negussey, D., & Vaid, Y. P. 1988. Effect of gradation and fines content on the undrained response of sand. Geotechnical special publication, (21), 330-345.

Lee, C. T., Cheng, C. T., Liao, C. W., & Tsai, Y. B. 2001. Site classification of Taiwan free-field strong-motion stations. Bulletin of the Seismological Society of America, 91(5), 1283-1297.

Magee, J., & Kramer, J. 1996. Dynamic structure in software architectures. ACM SIGSOFT Software Engineering Notes, 21(6), 3-14.

Marcuson, W.F. III, Hynes, M.E., Franklin, A.G., 2007.“Seismic Design and Analysis of Embankment Dams”, The State of Practice, The Donald M. Burmister Lecture, Department of Civil engineering Mechanics, Columbia University.

Mayne, P. W. 2007. Cone penetration testing (Vol. 368). Transportation Research Board.

MLIT, 2015: http://www.mlit.go.jp/road/census/h22-1/ (Accessed 15 February 2015)

Monkul, M. M. 2010. Influence of silt size and content on static liquefaction potential of sand. Oregon State University.

Monkul, M. M., Kendir, S. B., & Tutuncu, Y. E. 2021. Combined effect of fines content and uniformity coefficient on cyclic liquefaction resistance of silty sands. Soil Dynamics and Earthquake Engineering, 151, 106999.

Naranjo, C. A., Sellers, E. M., Sullivan, J. T., Woodley, D. V., Kadlec, K., & Sykora, K. 1987. The serotonin uptake inhibitor citalopram attenuates ethanol intake. Clinical Pharmacology & Therapeutics, 41(3), 266-274.

Nemat-Nasser, S., & Shokooh, A. 1979. A unified approach to densification and liquefaction of cohesionless sand in cyclic shearing. Canadian Geotechnical Journal, 16(4), 659-678.

Özener, P. T., Greenfield, M. W., Sideras, S. S., & Kramer, S. L. 2020. Identification of time of liquefaction triggering. Soil Dynamics and Earthquake Engineering, 128, 105895.

Polito, C. P., & Martin II, J. R. 2001. Effects of nonplastic fines on the liquefaction resistance of sands. Journal of geotechnical and geoenvironmental engineering, 127(5), 408-415.

Poulos, S. J., Castro, G., & France, J. W. 1985. Liquefaction evaluation procedure. Journal of Geotechnical Engineering, 111(6), 772-792.

Puebla, H., Byrne, P. M., & Phillips, R. 1997. Analysis of CANLEX liquefaction embankments: prototype and centrifuge models. Canadian Geotechnical Journal, 34(5), 641-657.

Robertson, P. K., & Wride, C. E. 1998. Evaluating cyclic liquefaction potential using the cone penetration test. Canadian geotechnical journal, 35(3), 442-459.

Seed, H. B., & Idriss, I. M. 1971. Simplified procedure for evaluating soil liquefaction potential. Journal of the Soil Mechanics and Foundations division, 97(9), 1249-1273.

Seed, H. B., & Lee, K. L. 1966. Liquefaction of saturated sands during cyclic loading. Journal of the Soil Mechanics and Foundations Division, 92(6), 105-134.

Seed, R. B., Cetin, K. O., Moss, R. E., Kammerer, A. M., Wu, J., Pestana, J. M., ... & Faris, A. 2003. Recent advances in soil liquefaction engineering: a unified and consistent framework. In Proceedings of the 26th Annual ASCE Los Angeles Geotechnical Spring Seminar: Long Beach, CA.

Terzaghi, K., & Peck, R. B., 1948. Soil mechanics in engineering practice (2nd Edition). John Wiley and Sons, Inc.

Terzaghi, K., Peck, R., & Mesri, G., 1996. Soil mechanics in engineering practice (3rd Edition). New York: Wiley.

Tutuncu, 2021, Influence of non-plastic silt content on seismic liquefaction of sands. Degree of Master of Science in Civil Engineering Yeditepe University

Vaid, Y. P., & Thomas, J. 1995. Liquefaction and postliquefaction behavior of sand. Journal of Geotechnical Engineering, 121(2), 163-173.

Xenaki, V. C., & Athanasopoulos, G. A. 2003. Liquefaction resistance of sand–silt mixtures: an experimental investigation of the effect of fines. Soil Dynamics and Earthquake Engineering, 23(3), 1-12.

Yamamuro, J. A., & Lade, P. V. 1997. Static liquefaction of very loose sands. Canadian Geotechnical Journal, 34(6), 905-917.

Yamamuro, J. A., & Lade, P. V. 1998. Steady-state concepts and static liquefaction of silty sands. Journal of geotechnical and geoenvironmental engineering, 124(9), 868-877.

Yassine, B., Ghali, K., Ghaddar, N., Chehab, G., & Srour, I. 2014. Effectiveness of the earth tube heat exchanger system coupled to a space model in achieving thermal comfort in rural areas. International Journal of Sustainable Energy, 33(3), 567-586.

Youd, T. L. 1984. Geologic effects-liquefaction and associated ground failure. Proceedings of the Geologic and Hydraulic Hazards Training Program, 210-232.

Zlatović, S., & Ishihara, K. 1995, November. On the influence of nonplastic fines on residual strength. In First International Conference on Earthquake Geotechnical Engineering (Vol. 95, pp. 239-244).

APPENDICES

APPENDIX A: a_{max} = 0.3g

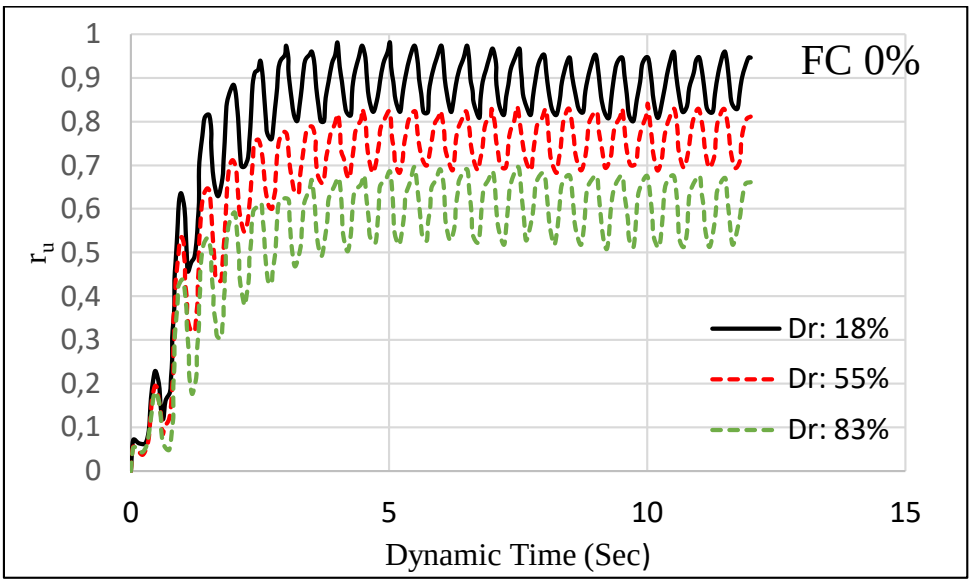

Figure A.1. r_u vs time in FC 0% soil with three different relative densities, ground acceleration 0.3g and frequency 2 Hz

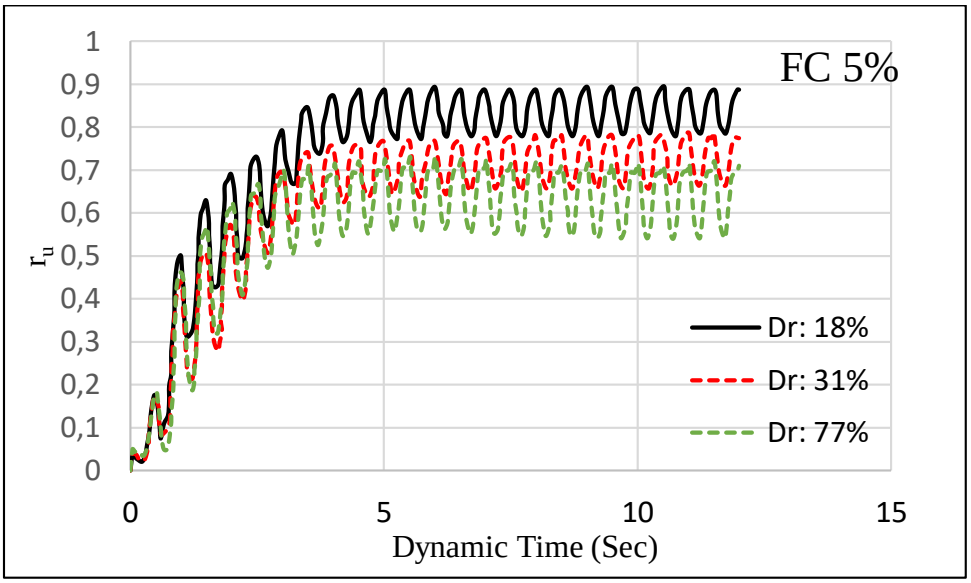

Figure A.2. r_u vs time in FC 5% soil with three different relative densities, ground acceleration 0.3g and frequency 2 Hz

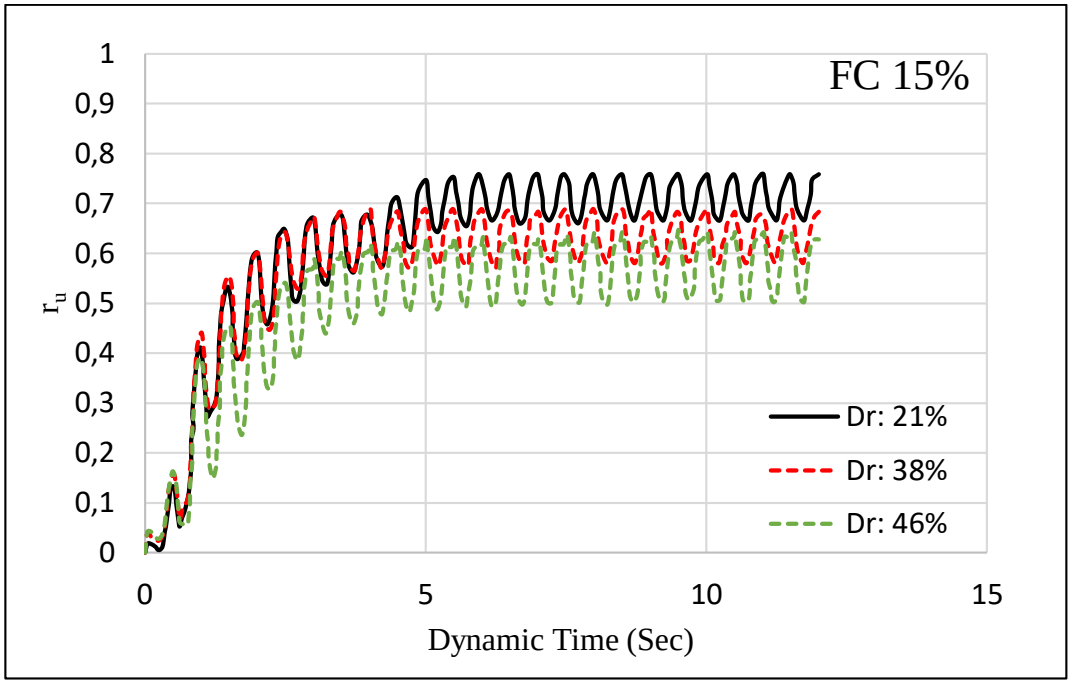

Figure A.3. r_u vs time in FC 15% soil with three different relative densities, ground acceleration 0.3g and frequency 2 Hz

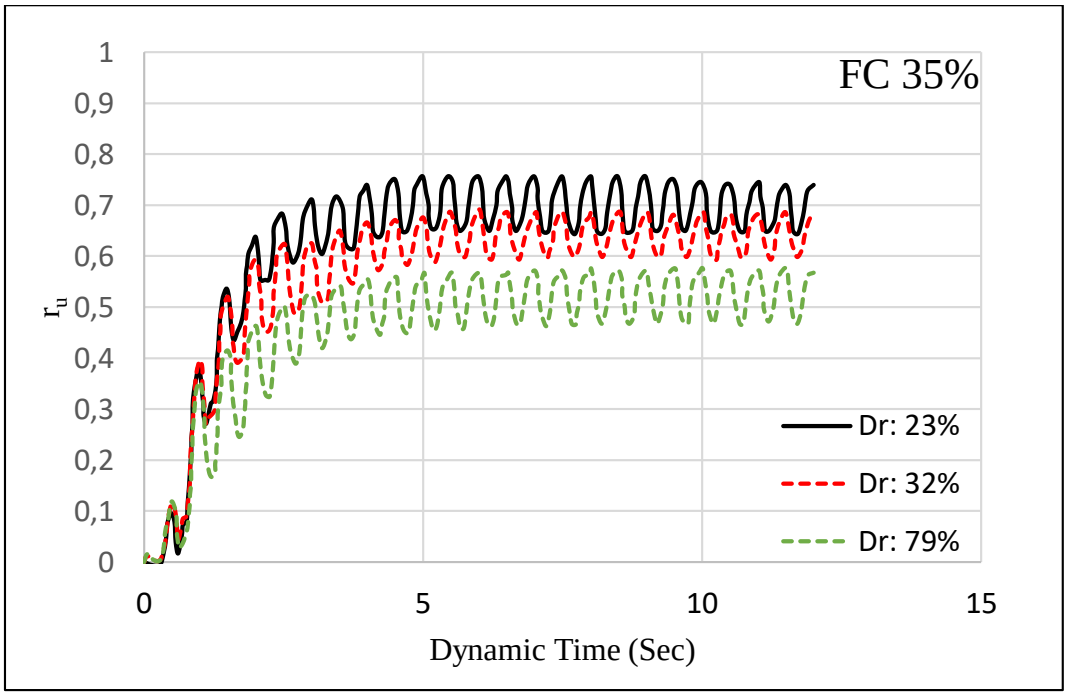

Figure A.4. r_u vs time in FC 35% soil with three different relative densities, ground acceleration 0.3g and frequency 2 Hz

Table A.1. Liquefaction triggered summary from r_u for 0.3g

FC%	D_r%	Liquefaction triggered cycle
0	18	7
0	55	9
0	83	9
5	18	9
5	31	8
5	77	8
15	21	11
15	38	11
15	46	12
35	23	10
35	32	11
35	79	11

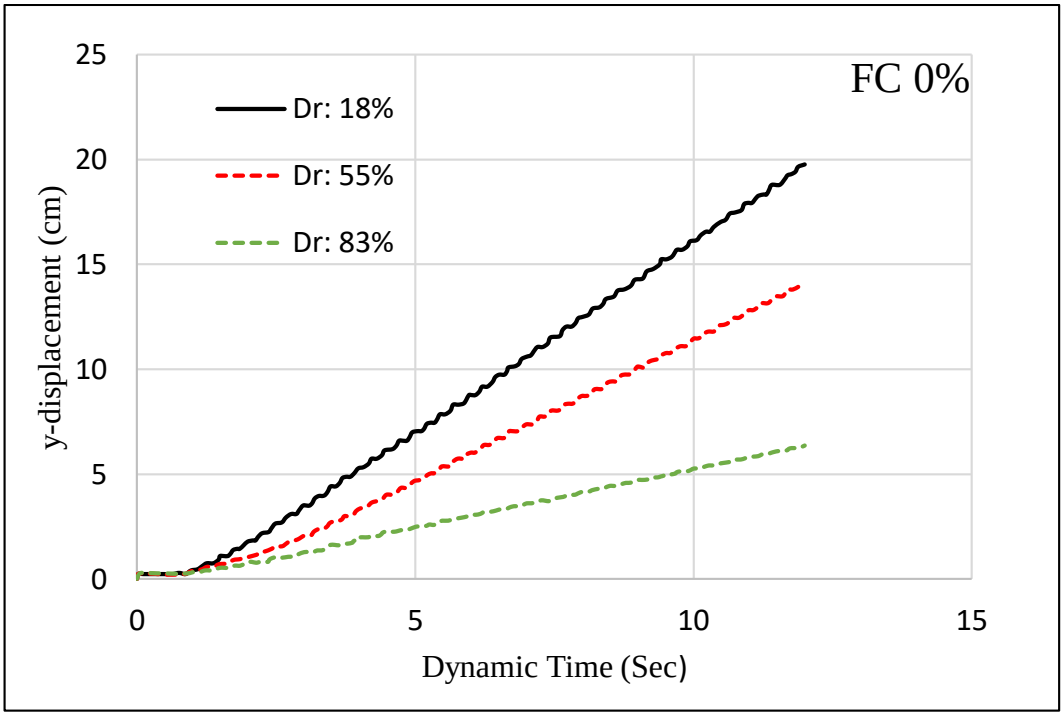

Figure A.5. Vertical displacement vs time in FC 0 % soil with three different relative densities, ground acceleration 0.3g and frequency 2 Hz

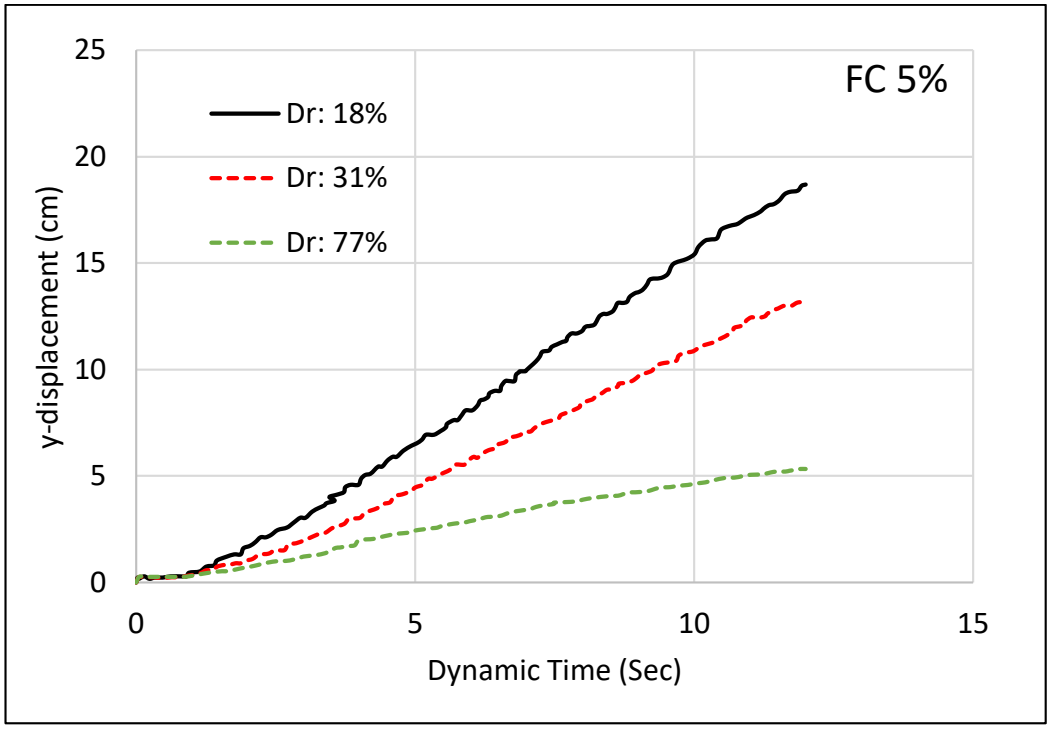

Figure A.6. Vertical displacement vs time in FC 5 % soil with three different relative densities, ground acceleration 0.3g and frequency 2 Hz

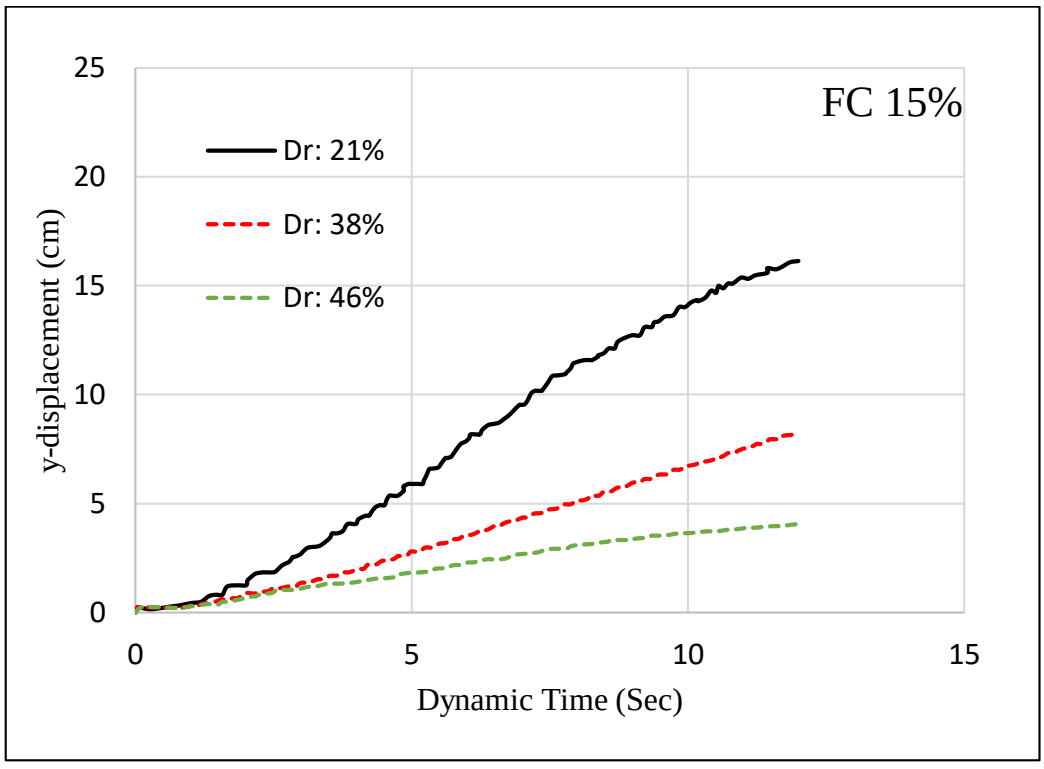

Figure A.7. Vertical displacement vs time in FC 15 % soil with three different relative densities, ground acceleration 0.3g and frequency 2 Hz

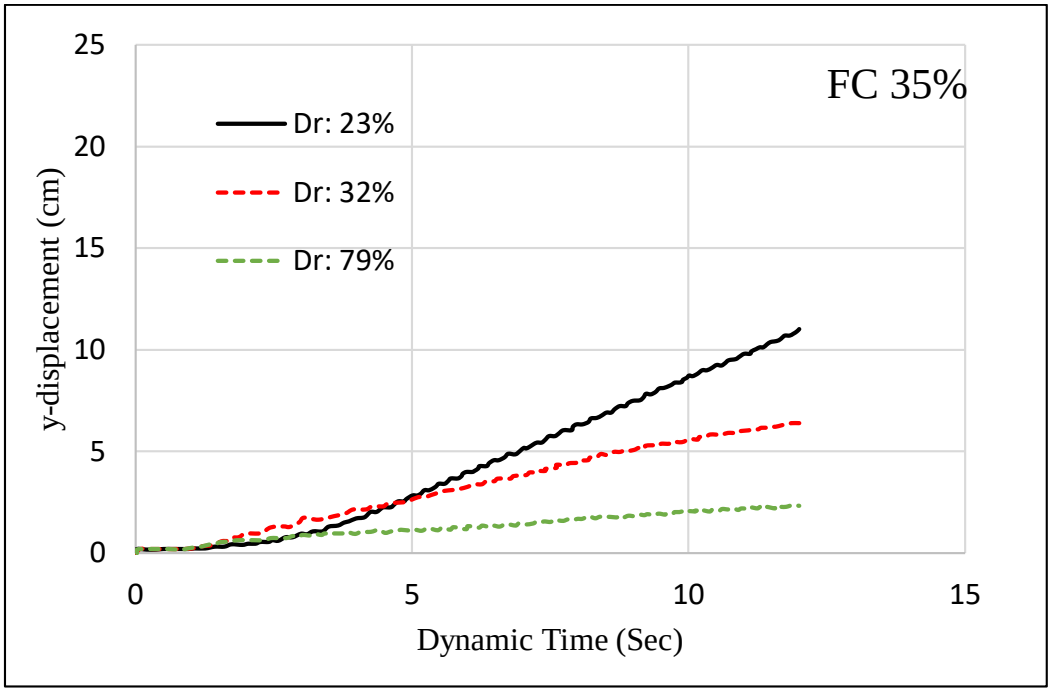

Figure A.8. Vertical displacement vs time in FC 35 % soil with three different relative densities, ground acceleration 0.3g and frequency 2 Hz

Table A.2. Vertical displacement liquefaction summary of each test for 0.3g

FC%	D_r%	Vertical displacement (cm)
0	18	20
0	55	14.2
0	83	8.35
5	18	17.2
5	31	13.3
5	77	6
15	21	16.1
15	38	8.5
15	46	4.4
35	23	11.2
35	32	6
35	79	3.3

APPENDIX B: a_{max} = 0.4g

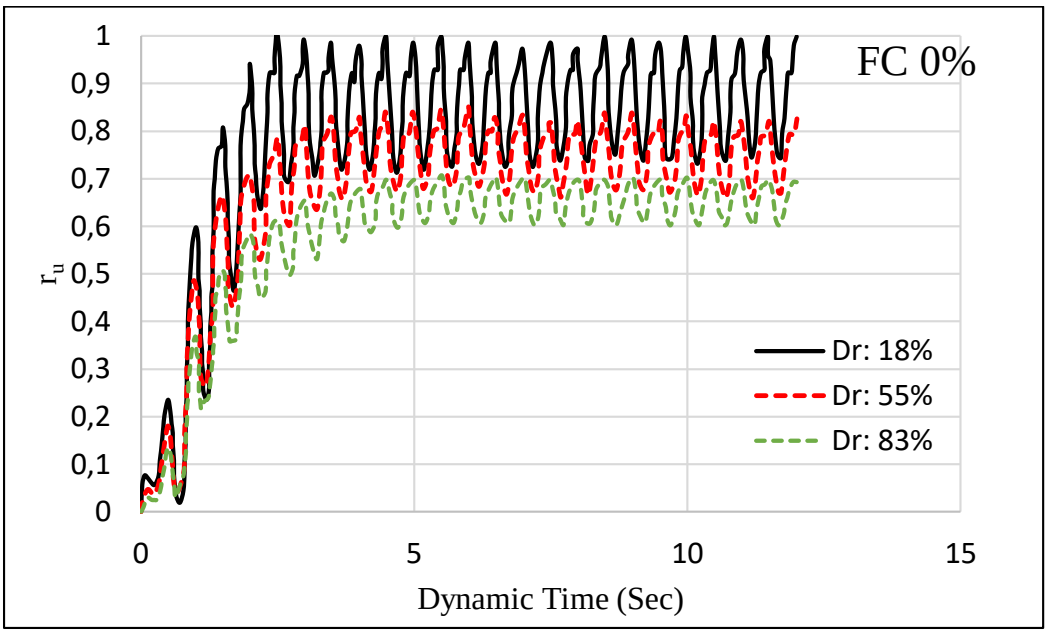

Figure B.1. r_u vs time in FC 0% soil with three different relative densities, ground acceleration 0.4g and frequency 2 Hz

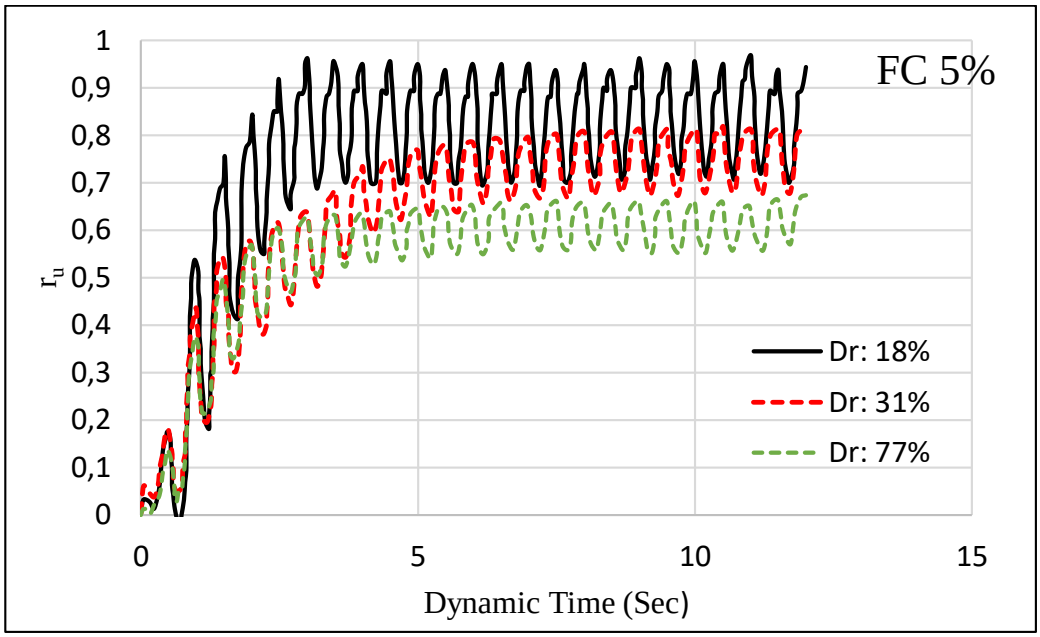

Figure B.2. r_u vs time in FC 5% soil with three different relative densities, ground acceleration 0.4g and frequency 2 Hz

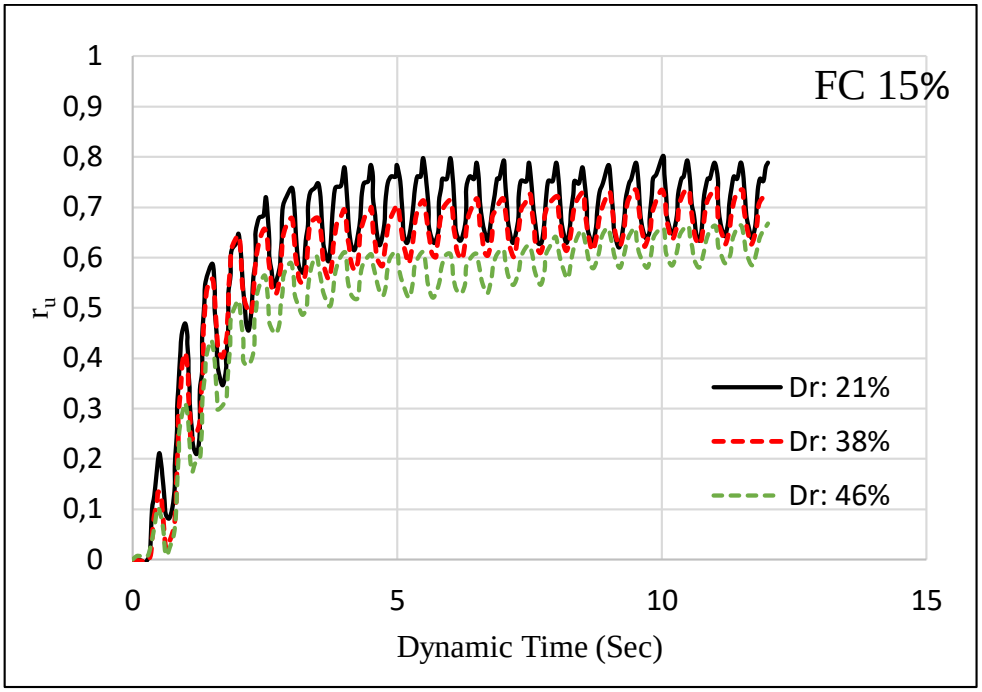

Figure B.3. r_u vs time in FC 15% soil with three different relative densities, ground acceleration 0.4g and frequency 2 Hz

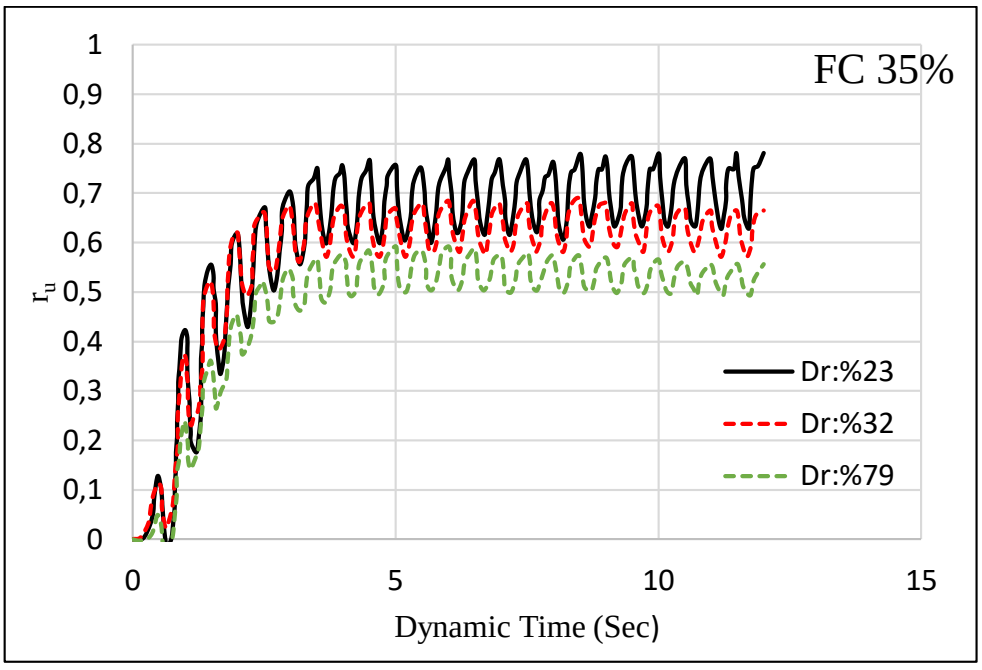

Figure B.4. r_u vs time in FC 35% soil with three different relative densities, ground acceleration 0.4g and frequency 2 Hz

Table B.1. Liquefaction triggered summary from r_u for 0.4g

FC%	D_r%	Liquefaction triggered cycle
0	18	6
0	55	8
0	83	8
5	18	7
5	31	11
5	77	9
15	21	9
15	38	10
15	46	10
35	23	7
35	32	8
35	79	10

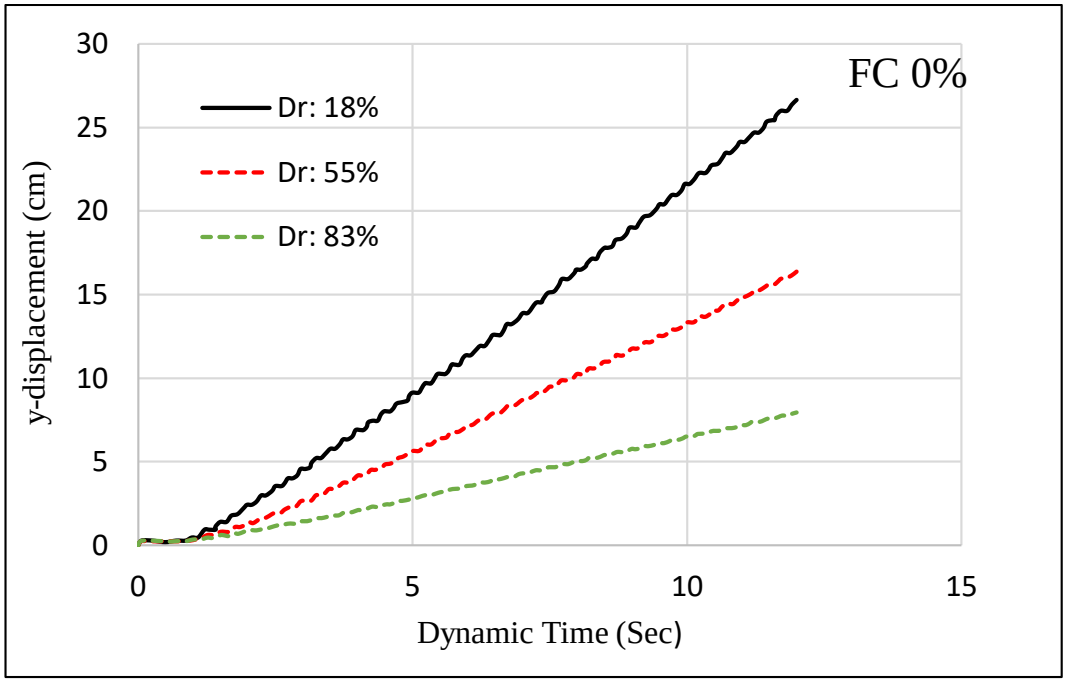

Figure B.5. Vertical displacement vs time in FC 0% soil with three different relative densities, ground acceleration 0.4g and frequency 2 Hz

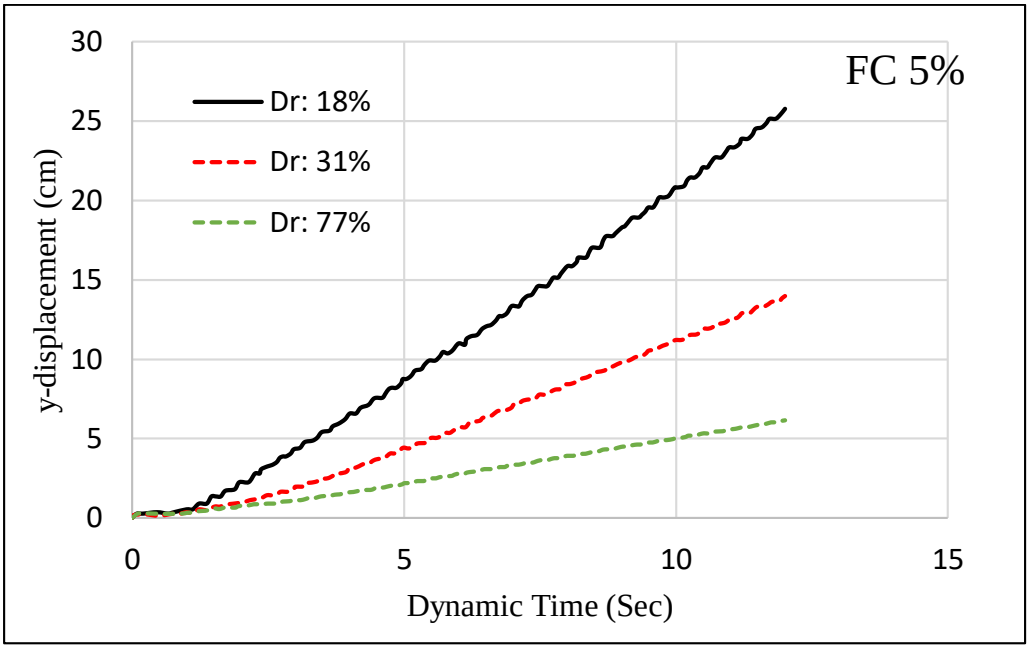

Figure B.6. Vertical displacement vs time in FC 5% soil with three different relative densities, ground acceleration 0.4g and frequency 2 Hz

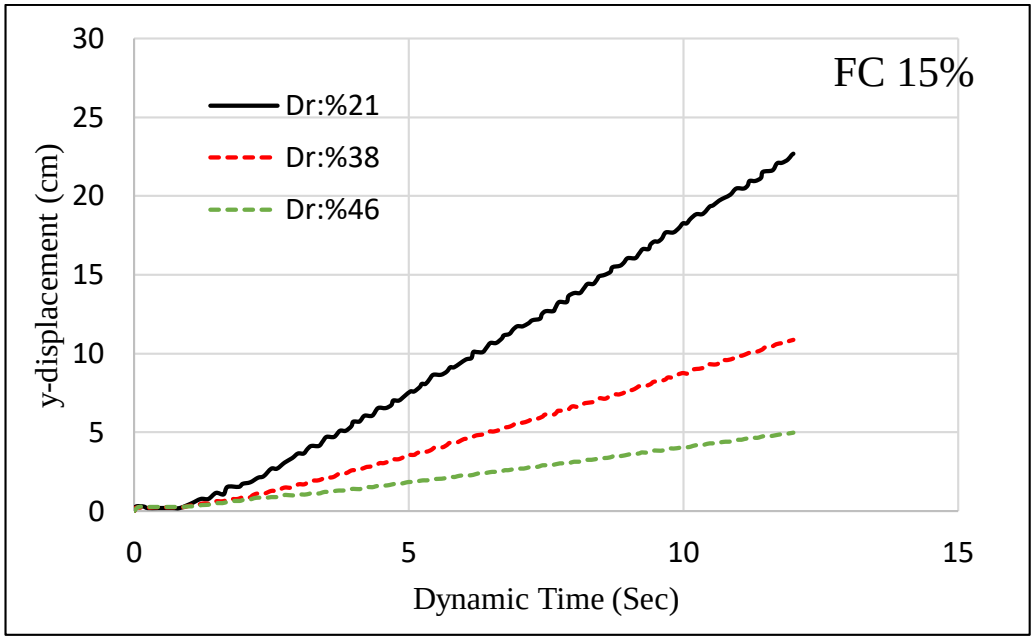

Figure B.7. Vertical displacement vs time in FC 15% soil with three different relative densities, ground acceleration 0.4g and frequency 2 Hz

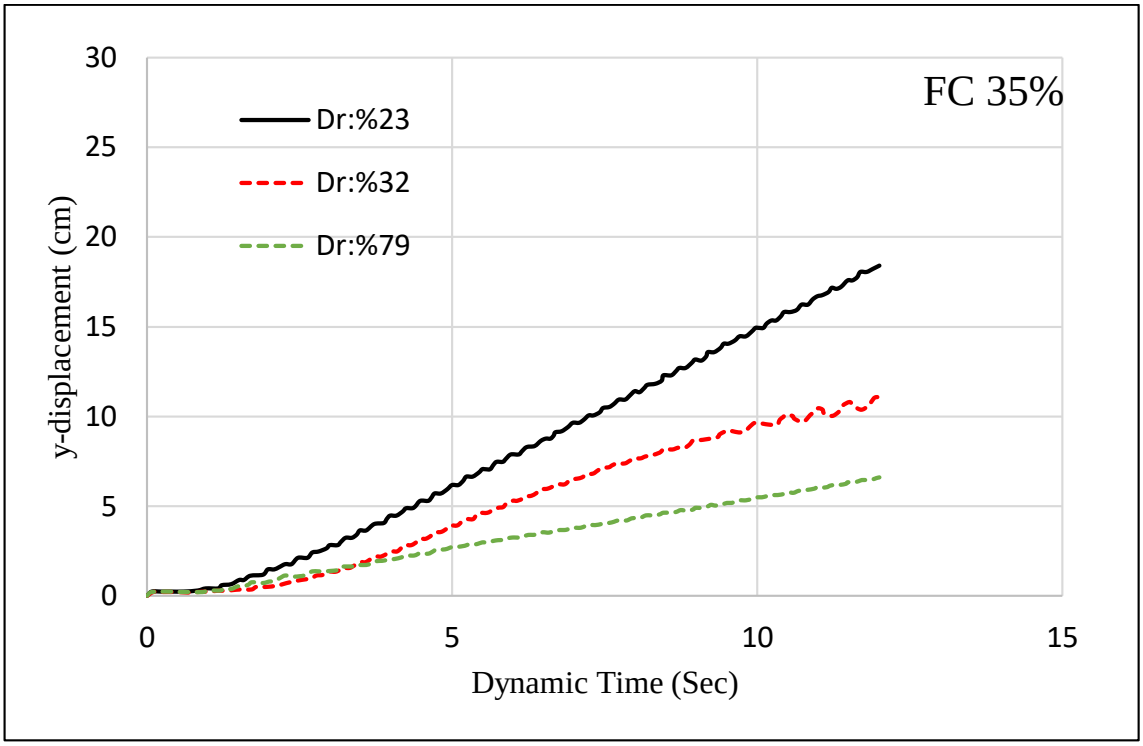

Figure B.8. Vertical displacement vs time in FC 35% soil with three different relative densities, ground acceleration 0.4g and frequency 2 Hz

Table B.2. Vertical displacement liquefaction summary of each test for 0.4g

FC%	D_r%	Vertical displacement (cm)
0	18	27
0	55	17.2
0	83	8.5
5	18	25.5
5	31	14
5	77	6.2
15	21	22.5
15	38	11.3
15	46	5
35	23	18.6
35	32	11.4
35	79	6.5

APPENDIX C: a_{max} = 0.5g

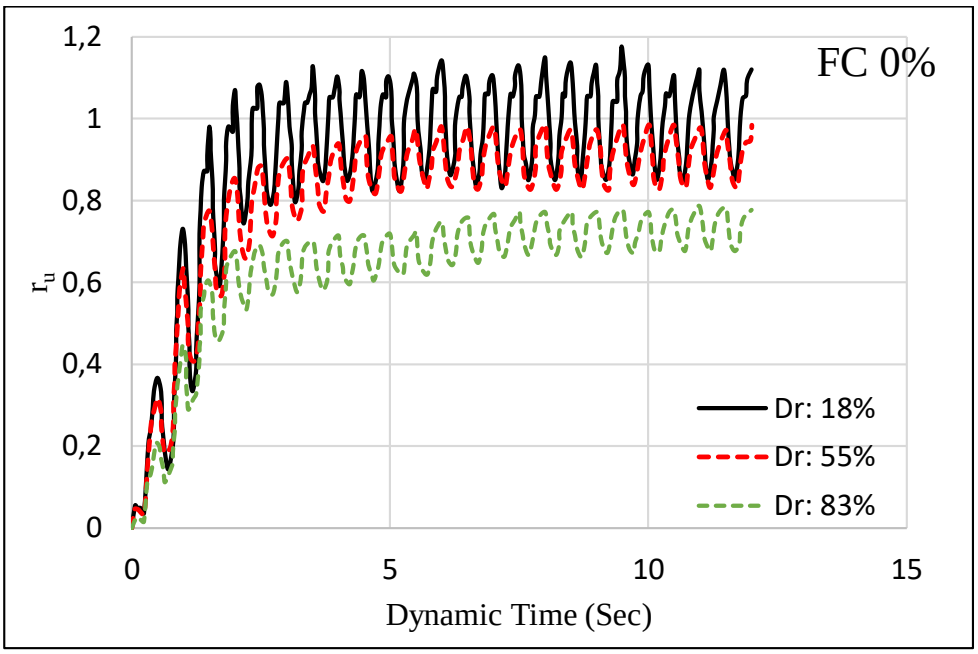

Figure C.1. r_u vs time in FC 0% soil with three different relative densities, ground acceleration 0.5g and frequency 2 Hz

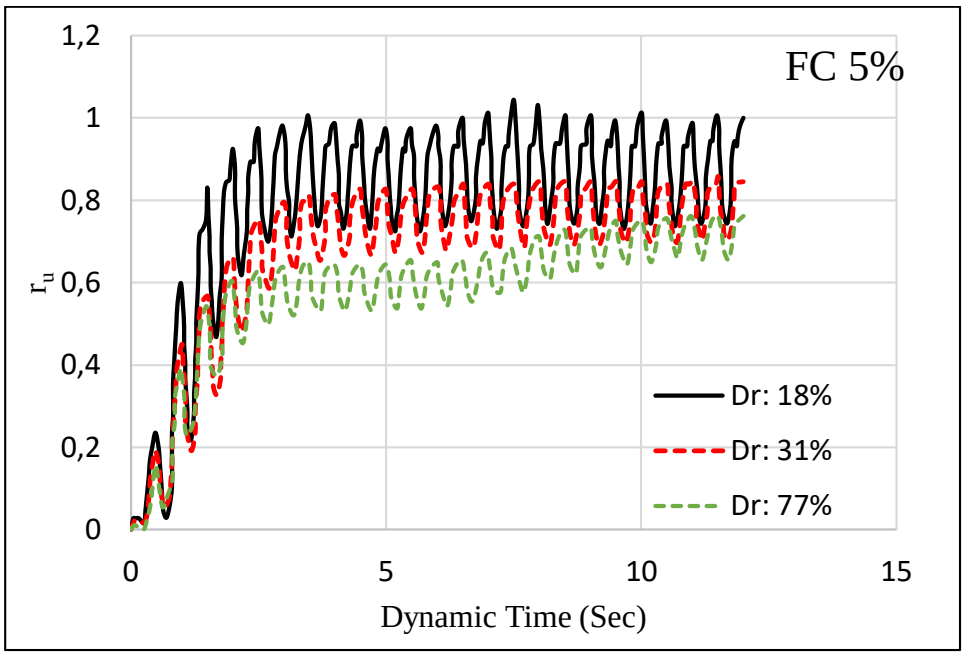

Figure C.2. r_u vs time in FC 5% soil with three different relative densities, ground acceleration 0.5g and frequency 2 Hz

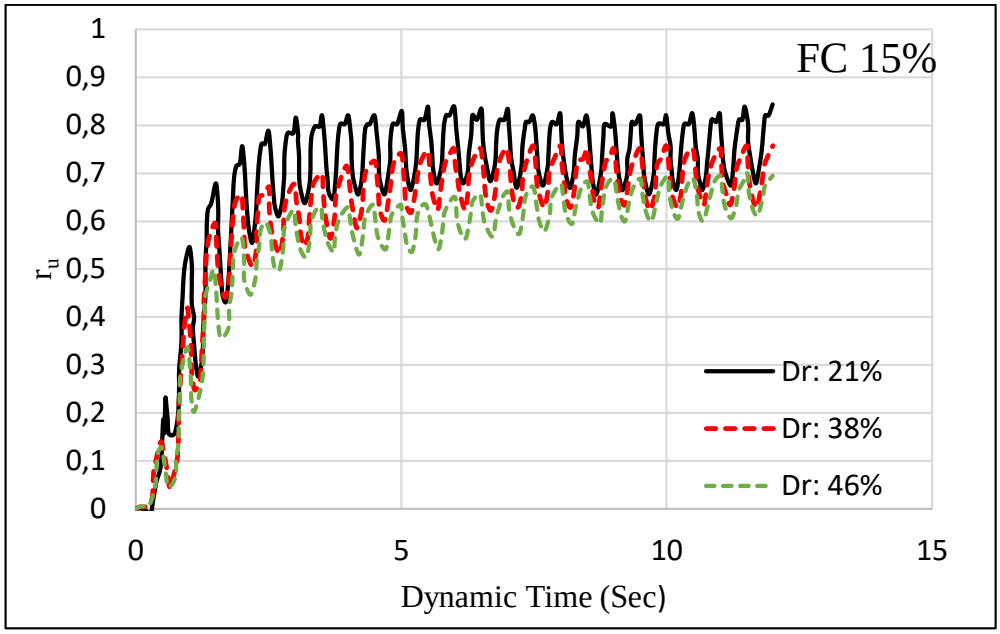

Figure C.3. r_u vs time in FC 15% soil with three different relative densities, ground acceleration 0.5g and frequency 2 Hz

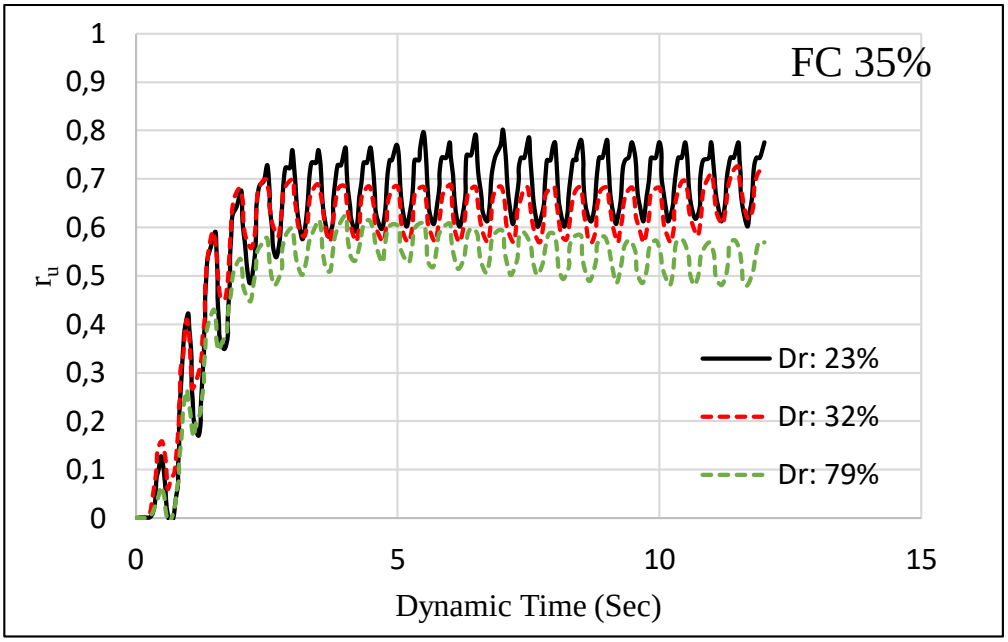

Figure C.4. r_u vs time in FC 35% soil with three different relative densities, ground acceleration 0.5g and frequency 2 Hz

Table C.1. Liquefaction triggered summary from r_u for 0.5g

FC%	D_r%	Liquefaction triggered cycle
0	18	6
0	55	7
0	83	9
5	18	8
5	31	8
5	77	10
15	21	7
15	38	10
15	46	11
35	23	6
35	32	7
35	79	8

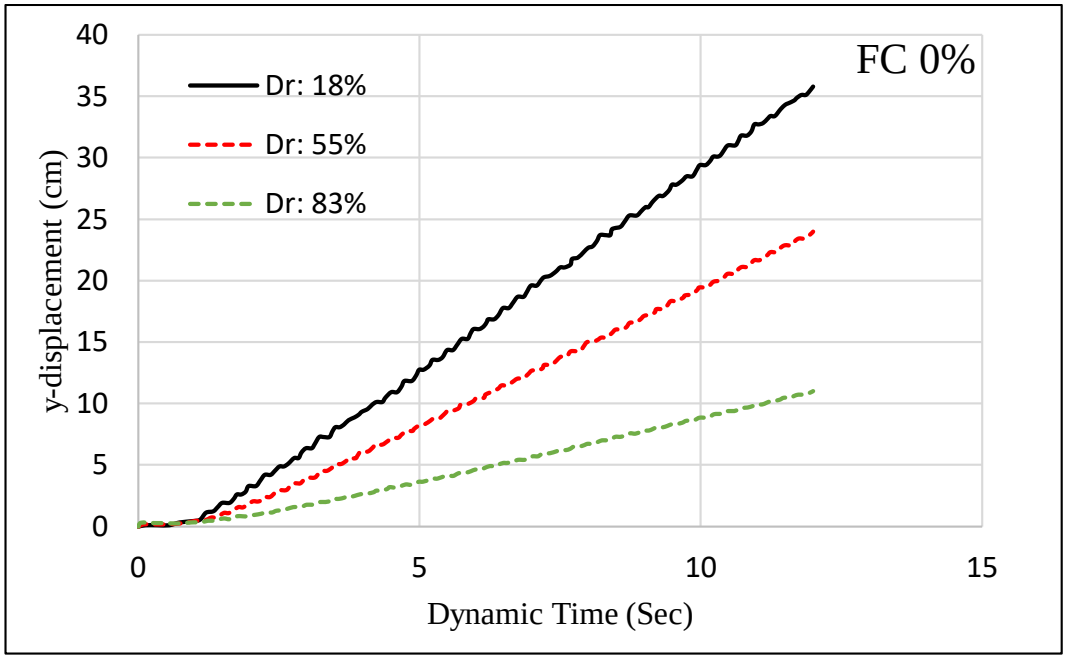

Figure C.5. Vertical displacement vs time in FC 0% soil with three different relative densities, ground acceleration 0.5g and frequency 2 Hz

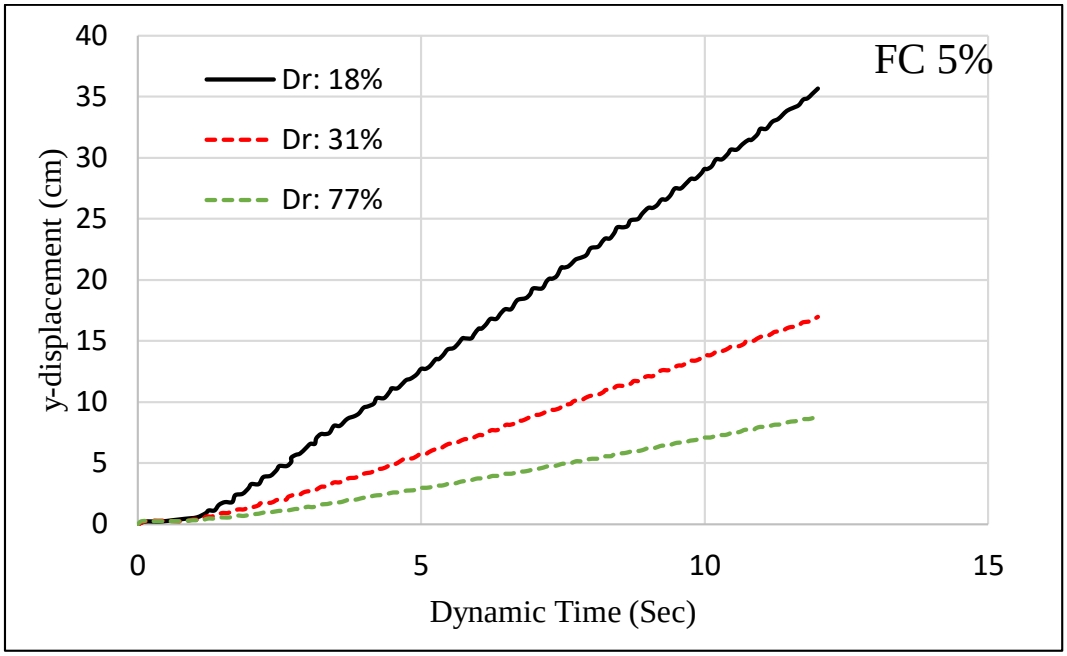

Figure C.6. Vertical displacement vs time in FC 5% soil with three different relative densities, ground acceleration 0.5g and frequency 2 Hz

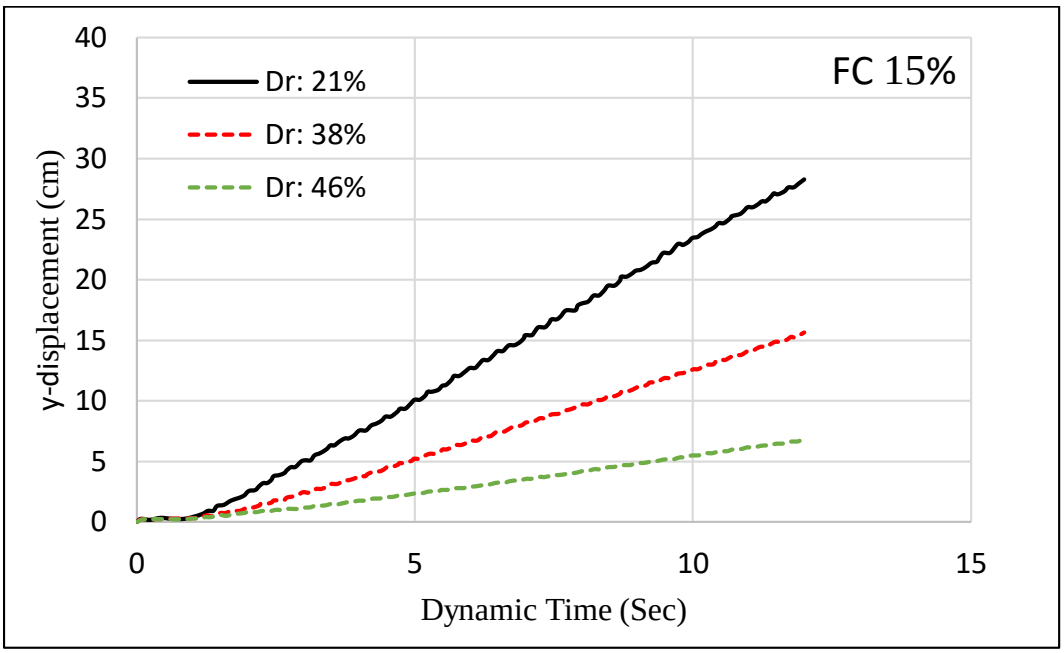

Figure C.7. Vertical displacement vs time in FC 15% soil with three different relative densities, ground acceleration 0.5g and frequency 2 Hz

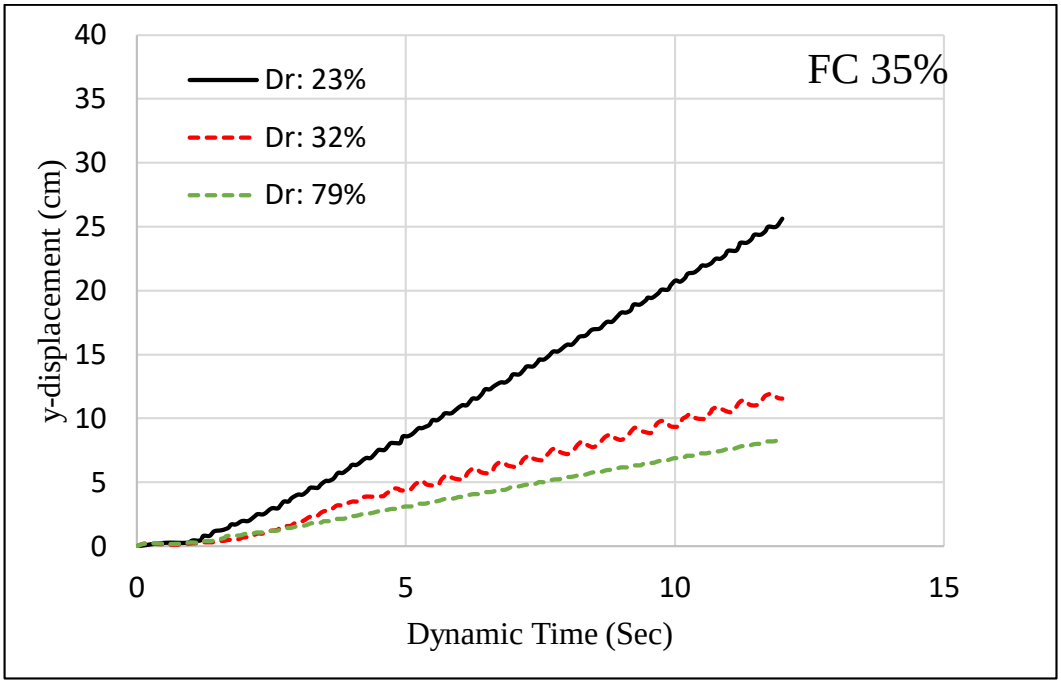

Figure C.8. Vertical displacement vs time in FC 35% soil with three different relative densities, ground acceleration 0.5g and frequency 2 Hz

Table C.2. Vertical displacement liquefaction summary of each test for 0.5g

FC%	D_r%	Vertical displacement (cm)
0	18	35.3
0	55	25
0	83	12.5
5	18	35.8
5	31	17
5	77	9.2
15	21	29
15	38	15
15	46	6
35	23	25.5
35	32	12.4
35	79	8